



## รายงานวิจัยฉบับสมบูรณ์

### โครงการ

การศึกษาเปรียบเทียบโครงสร้างดีเอ็นเอโอริกามิแบบสองมิติและ สามมิติในการทำหน้าที่เป็นตัวนำส่งยาระดับนาโนเมตร (Comparative functional studies on two- and three-dimensional DNA origami nanostructures as nanocarriers in a drug delivery system)

โดย นางสาวอนุตตรา อุดมประเสริฐ และคณะ

## รายงานวิจัยฉบับสมบูรณ์

โครงการ การศึกษาเปรียบเทียบโครงสร้างดีเอ็นเอโอริกามิแบบสองมิติและสาม มิติในการทำหน้าที่เป็นตัวนำส่งยาระดับนาโนเมตร

โดย อนุตตรา อุดมประเสริฐ และคณะ

สนับสนุนโดยสำนักงานคณะกรรมการการอุดมศึกษา และสำนักงานกองทุนสนับสนุนการวิจัย

(ความเห็นในรายงานนี้เป็นของผู้วิจัย สกอ. และ สกว. ไม่จำเป็นต้องเห็นด้วยเสมอไป)

#### บทคัดย่อ

**รหัสโครงการ:** MRG6080033

ชื่อโครงการ: การศึกษาเปรียบเทียบโครงสร้างดีเอ็นเอโอริกามิแบบสองมิติและสามมิติในการทำหน้าที่

เป็นตัวนำส่งยาระดับนาโนเมตร

(Comparative functional studies on two- and three-dimensional DNA origami

nanostructures as nanocarriers in a drug delivery system)

ชื่อนักวิจัย / สถาบัน: ผู้ช่วยศาสตราจารย์ ดร. อนุตตรา อุดมประเสริฐ / มหาวิทยาลัยบูรพา

อีเมลล์: anuttara@go.buu.ac.th

ระยะเวลาโครงการ: 3 เมษายน 2560 - 3 เมษายน 2562

บทคัดย่อ:

ดีเอ็นเอเป็นสารชีวโมเลกุลชนิดหนึ่งที่มีการนำเอามาใช้เป็นวัสดุเชิงโครงสร้างในงานทางด้านนาโน เทคโนโลยี การสังเคราะห์โครงสร้างที่มีขนาดเล็กระดับนาโนเมตรด้วยดีเอ็นเอสามารถทำได้โดยอาศัยเทคนิคที่ เรียกว่า ดีเอ็นเอโอริกามิ โดยพบว่ามีการนำเอาโครงสร้างขนาดนาโนเมตรที่สร้างขึ้นจากดีเอ็นเอไปประยุกต์ใช้ ทางด้านการแพทย์ จากงานวิจัยก่อนหน้าพบว่าโครงสร้างดีเอ็นเอโอริกามิสามารถนำไปใช้เป็นตัวนำส่งยาซึ่ง สามารถช่วยเพิ่มประสิทธิภาพของการรักษา ลดผลข้างเคียงที่เกิดการจากการใช้ยาเคมีบำบัด และยังสามารถ เอาชนะการดื้อยาได้ ในงานวิจัยนี้เป็นการศึกษาเปรียบเทียบเกี่ยวกับคุณสมบัติที่สำคัญต่าง ๆ ในการทำหน้าที่ เป็นตัวนำส่งยา ได้แก่ ความคงตัว ความสามารถในการบรรจุและปลดปล่อยยา ความสามารถในการเข้าสู่เซลล์ ประสิทธิภาพในการยับยั้งการเจริญของเซลล์มะเร็ง รวมถึงความจำเพาะต่อเซลล์เป้าหมายเมื่อมีการดัดแปลง โครงสร้างด้วย aptamer ของโครงสร้างดีเอ็นเอโอริกามิที่มีรูปร่างคล้ายกันแต่มีมิติที่แตกต่างกัน โดยใน งานวิจัยนี้ศึกษาโครงสร้างดีเอ็นเอโอริกามิรูปทรง DISC DONUT และ SPHERE เปรียบเทียบกัน หลังจากทำ การวิเคราะห์โครงสร้างดีเอ็นเอโอริกามิต่าง ๆ ที่สร้างขึ้นแล้วนำโครงสร้างที่ได้ไปทำการทดสอบคุณสมบัติต่าง ๆ จากผลการทดลองพบว่า SPHERE มีความคงตัวสูงที่สุดในบรรดาโครงสร้างทั้งสามแบบ และโครงสร้าง SPHERE ยังสามารถบรรจุและปลดปล่อยยา doxorubicin ได้มากที่สุด จากการทดสอบการเข้าสู่เซลล์ของ โครงสร้างดีเอ็นเอโอริกามิทั้งสามแบบ พบว่าสำหรับโครงสร้างที่ไม่มีการดัดแปลงด้วย aptamer นั้น โครงสร้าง DONUT สามารถที่จะเข้าสู่เซลล์ MCF-7 ได้มากที่สุด แต่เมื่อมีการดัดแปลงด้วย MUC-1 aptamer พบว่า โครงสร้าง DISC สามารถเข้าสู่เซลล์ MCF-7 ได้ดีกว่า ทั้งนี้จากผลการทดลองที่ได้พบว่ายา doxorubicin จะ สามารถเข้าสู่เซลล์ได้ดีกว่าเมื่อมีโครงสร้างดีเอ็นเอโอริกามิเป็นตัวนำส่ง และโครงสร้าง DISC ที่มีการดัดแปลง ด้วย MUC-1 aptamer พร้อมทั้งบรรจุยา doxorubicin มีประสิทธิภาพในการยับยั้งการเจริญของเซลล์มะเร็ง MCF-7 แบบจำเพาะได้ดีที่สุด

คำหลัก: ดีเอ็นเอนาโนเทคโนโลยี ดีเอ็นเอโอริกามิ ตัวนำส่งยาระดับนาโนเมตร ระบบตัวนำส่งยา

#### Abstract

Project Code: MRG6080033

Project Title: Comparative functional studies on two- and three-dimensional DNA origami

nanostructures as nanocarriers in a drug delivery system

Investigator / Institute: Assist. Prof. Anuttara Udomprasert / Burapha University

E-mail: anuttara@go.buu.ac.th

Project Period: 3 April 2017 – 3 April 2019

Abstract:

Structural DNA nanotechnology utilizes DNA molecules as building blocks for nanoscale construction. DNA Origami nanostructures have been widely used in nanomedicine applications. Previous results showed that DNA origami nanostructures are promising candidate as nanocarriers in the drug delivery system because they could enhance therapeutic efficacy, reduce the side effects of chemotherapy, and also circumvent drug resistance. In this study, DNA origami nanostructures in DISC, DONUT, and SPHERE shapes were used as representatives of 2D and 3D nanostructures for the examination of dimensional difference effects on stability, loading and releasing capabilities, internalization efficiency, and also the specificity after aptamer modification. After structural characterization, the stability was determined in different conditions and the results showed that SPHERE nanostructures exhibit the highest stability. For Dox-loading and release capacity, SPHERE nanostructures also have the highest capacity. Without any modification, the empty DONUT nanostructures show the highest cellular internalization into MCF-7 cells. MUC-1 aptamer was chosen to be modified onto DNA origami nanostructures to enhance specificity of the nanocarriers. With aptamer modification, DISC nanostructures show the highest cellular internalization into MCF-7 cells. Also, with DNA origami nanostructures as nanocarriers, much more Dox could be uptake into cells. For anticancer efficiency, the higher concentration of Dox-loaded DNA origami nanostructures, the lower the cell viability of both MCF-7 and MDA-MB-231 cells. Dox-loaded DISC nanostructures with MUC-1 aptamer modification have the highest efficiency against MCF-7 cells.

Keywords: structural DNA nanotechnology, DNA origami, nanocarriers, drug delivery system

#### **Executive Summary**

ข้าพเจ้า ผศ.ดร. อนุตตรา อุดมประเสริฐ ได้รับทุนสนับสนุนโครงการวิจัยจากสำนักงานคณะกรรมการ การอุดมศึกษาและสำนักงานกองทุนสนับสนุนการวิจัย โครงการวิจัยเรื่อง การศึกษาเปรียบเทียบโครงสร้างดี เอ็นเอโอริกามิแบบสองมิติและสามมิติในการทำหน้าที่เป็นตัวนำส่งยาระดับนาโนเมตร (Comparative functional studies on two- and three-dimensional DNA origami nanostructures as nanocarriers in a drug delivery system) รหัสโครงการ MRG6080033 ได้รับงบประมาณรวมทั้งสิ้น 600,000 บาท (หก แสนบาทถ้วน)

ระยะเวลาดำเนินงาน 2 ปี 8 เดือน (ระหว่างวันที่ 3 เมษายน 2560 - 31 ธันวาคม 2562)

#### ข้อเสนอแนะ

นอกเหนือจากคุณสมบัติของตัวนำส่งยาที่ได้ทำการทดสอบไปแล้วนั้น ยังควรมีการทดสอบ เพิ่มเติมเกี่ยวกับ ความสามารถในการย่อยสลายทางชีวภาพ (biodegradability) และชีวปริมาณออกฤทธิ์ (bioavailability) ของโครงสร้างดีเอ็นเอโอริกามิในสิ่งมีชีวิต (*in vivo*)

#### Research problem and its significances

Deoxyribonucleic acid (DNA) is one of important biomolecules in biological systems. It has been known as a genetic material in most organisms. The double helical structure of DNA was elucidated by James D. Watson and Francis Crick in 1974 (Watson and Crick, 1974). The double helices are made of two single-stranded DNA molecules specifically bind to each other via complementary base pairing, also known as Watson-Crick base pairing. The physical and chemical properties of DNA make it a promising candidate as a structural building block for nano-scale construction. Nadrian C. Seeman is the first person who proposed to use this fascinating biomolecule as a building block to construct nano-scale structures (Seeman, 1982). This specific research field is called "Structural DNA nanotechnology". Various shapes of DNA nanostructures have been reported such as a cube (Chen and Seeman, 1991), a truncated octahedron (Zhang and Seeman, 1994), and a tetrahedron (Goodman, Berry and Turberfield, 2004). However, size and complexity of DNA nanostructures made by a conventional method is quite limited. To construct large DNA nanostructures, in 2006, scaffolded DNA origami technique was demonstrated by Paul Rothemund (Rothemund, 2006). This technique, a breakthrough in DNA nanotechnology, is based on the folding of a long single-stranded DNA (scaffold) with help from hundreds of short single-stranded DNA (staples) to hold the scaffold in place as shown in Figure 1. Since then, DNA origami nanostructures in different sizes and shapes have been published, for example, a nanobox (Andersen et al., 2009), a nanotube (Douglas, Chou, and Shih, 2007), an ellipsoid and a nanoflask (Han et al., 2011). Also, many applications have been proposed for these DNA origami nanostructures, such as a platform for single-molecule study (Voigt et al., 2010), a nanoassembly line (Gu et al., 2010), a platform for enzymatic study (Fu et al., 2012), and a transcription regulation system (Endo et al., 2012).

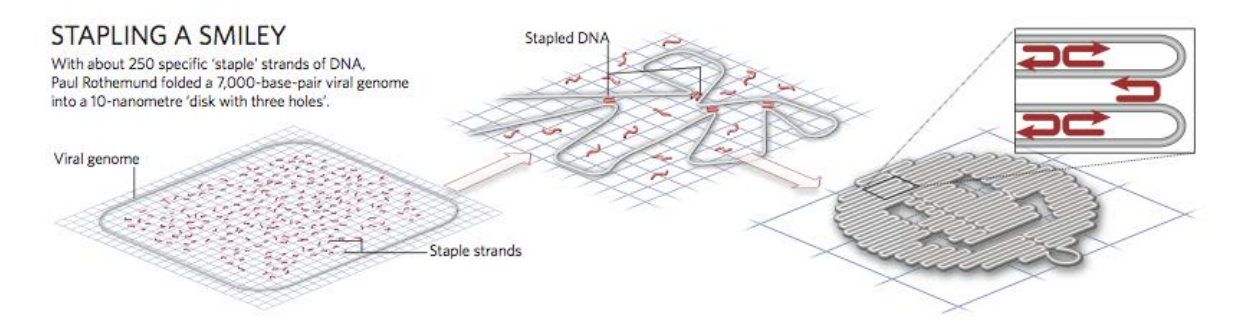


Figure 1 Scaffolded DNA origami technique.

(Reproduced from <a href="http://www.nature.com/news/2010/100310/pdf/464158a.pdf">http://www.nature.com/news/2010/100310/pdf/464158a.pdf</a>)

It is believed that nanomedicine, a research field that nanotechnology is applied for medical applications, would be a future medicine as this technology could enhance efficacy of diagnosis, treatment, and even monitoring. The advancement of nanomedicine would be benefit for cancer therapy since conventional chemotherapeutic agents for cancer treatment have some drawbacks such as low solubility, low stability, and cytotoxicity, leading to low efficiency of chemotherapy. These obstacles could be overcome by using a drug delivery system which a drug-loaded nanocarrier will directly deliver drugs to specific target cells. A great deal of research has been focused on targeted drug delivery since the magic bullet concept was introduced by Paul Ehrlich (Sanna, Pala, and Sechi, 2014). Various materials have been explored to be utilized for nanocarrier construction such as liposome (Zamboni, 2005), poly(lactic-co-glycolic acid) (PLGA) (Chen, Ushida and Tateishi, 2000), and magnetic nanoparticles (Chomoucka et al., 2010). However, these materials still have some disadvantages such as rapid clearance, long-term toxicity, and no specificity. Alternatively, DNA is another promising nanomaterial which could be used for nanocarrier construction. Based on structural DNA nanotechnology, DNA nanocarriers could be designed in a controllable manner with nanoscale precision. Not only they are biocompatible and biodegradable, but also, they could be modified with a wide range of functional entities making DNA nanostructures more attractive as a platform for drug delivery system.

In 2006, Erben and coworkers demonstrated that they could encapsulate a single protein, cytochrome c, in a central cavity of a tetrahedral-shaped DNA nanostructure as shown

in Figure 2 (Erben, Goodman and Turberfield, 2006). This work has inspired the idea of using DNA nanostructures as a nanocarrier in drug delivery system. Since then, different sizes and shapes of DNA nanostructures have been developed for being used as drug delivery vehicles. For example, nanotubes (Ko et al., 2008), icosahedrons (Bhatia et al., 2011; Chang, Yang and Huang, 2011), tetrahedrons (Li et al., 2011; Walsh et al., 2011; Lee et al., 2012; Kim et al., 2013; Liang et al., 2014), as well as some DNA origami nanostructures.

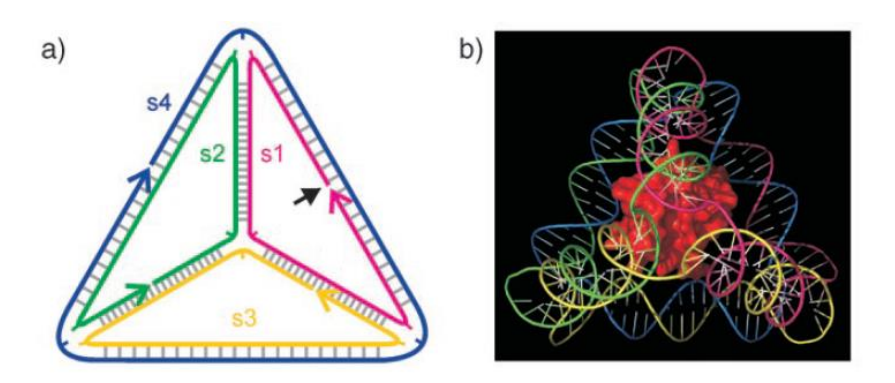


Figure 2 DNA tetrahedron (a) and a single-molecule protein inside DNA tetrahedron (b) (Reproduced from Erben, Goodman and Turberfield, 2006)

Although DNA origami nanostructures in various shapes were examined as drug carriers in a biological system, essential criteria for a structural design as drug nano-carriers have not been elucidated yet. Therefore, this proposal proposes to investigate the effects of dimensional difference of DNA origami nanostructures on the purpose of nanocarriers in biological conditions. Disc-like shaped and donut-like shaped DNA origami nanostructures will be used as representatives for two-dimensional (2D) and three-dimensional (3D) nanostructures, respectively. These two structures are similar in term of shape (circular) but they are different in term of dimension (2D and 3D). Modified versions of disc-shape and donut-shape DNA origami nanostructures reported by Han et al. (Figure 3) will be used in these experiments. The effects on certain aspects, namely, stability, drug loading and releasing capabilities, cytotoxicity, cellular internalization and also anti-cancer efficiency (with encapsulated drug), will be investigated. Their properties as nanocarriers will be compared.

Knowledge gained from these experiments could be useful information for designing efficient DNA nanocarriers in drug delivery system.

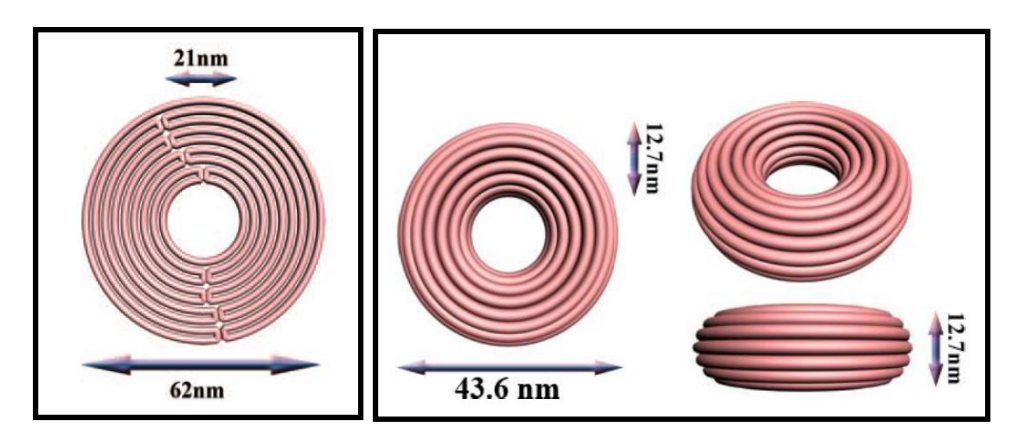


Figure 3 DNA origami nanostructures; 2D disc (left) and 3D donut (right).

(Reproduced from Han et al., 2011)

#### Literature reviews

As promising nanocarriers, several studies showed that DNA origami nanostructures could enhance anti-cancer activity and circumvent drug resistance (Jiang et al., 2012). Jiang et al. demonstrated that gold-nanorod modified DNA origami nanocarriers could enhance cellular uptake leading to higher antitumor efficacy compared with bare gold nanorod when treated in tumor-bearing mice (Jiang et al., 2015). Recently, Halley et al. found that daunorubicin delivered by rod-like DNA nanostructures could reduce more HL-60/ADR cells relative to free daunorubicin (Halley et al., 2016). Also, DNA nanostructure improves retention of daunorubicin in cancer cells leading to increased ability to disrupt cell proliferation.

To use as a nanocarrier in a biological system, these DNA origami nanostructures have to pass some requirements. The stability of these DNA nanostructures in physiological environment is a primary consideration. Many results showed that DNA origami nanostructures could survive in biological conditions. For example, 2D rectangular, 2D equilateral triangular and 3D multilayer rectangular DNA origami nanostructures (Figure 4) could stay intact after incubated in cell lysate at room temperature for 12 hours as verified by atomic force microscope (AFM) or transmission electron microscope (TEM). They concluded that the stability of the nanostructure does not depend on size and shape (Mei et al., 2011). Consistent

with most evidences that different-shaped DNA origami nanostructures such as DNA nanotubes (Shen et al., 2012; Zhao et al., 2012), DNA triangle (Zhang et al, 2014), and a rod-like DNA nanostructure (Halley et al, 2016) were stable under investigated biological conditions.



**Figure 4** Three different DNA origami nanostructures tested for stability in cell lysate; a rectangle (left), an equilateral triangle (middle), and a multilayer rectangle (right). (Reproduced from Mei et al., 2011)

Interestingly, Hahn and co-workers studied the stability of three different-shaped DNA origami nanostructures (Figure 5), namely, octahedron, 6-helix bundle, and 24-helix nanorod, in low Mg<sup>2+</sup> conditions. Since Mg<sup>2+</sup> concentrations in mammalian tissue culture medium is relatively low compared to Mg<sup>2+</sup> concentration in solutions used for nanostructure assembly. They found that 6-helix bundle exhibits the highest stability when incubated in RPMI with different Mg<sup>2+</sup> concentrations ranging from 0.4 - 10 mM at 37 °C for 24 hours while the other two structures showed some degree of degradation. They claimed that the stability of DNA nanostructures in very low Mg<sup>2+</sup> might be dependent on the design and also the length of time (Hahn et al., 2014). Therefore, DNA origami nanostructures should be designed to have optimal stability in cellular conditions.

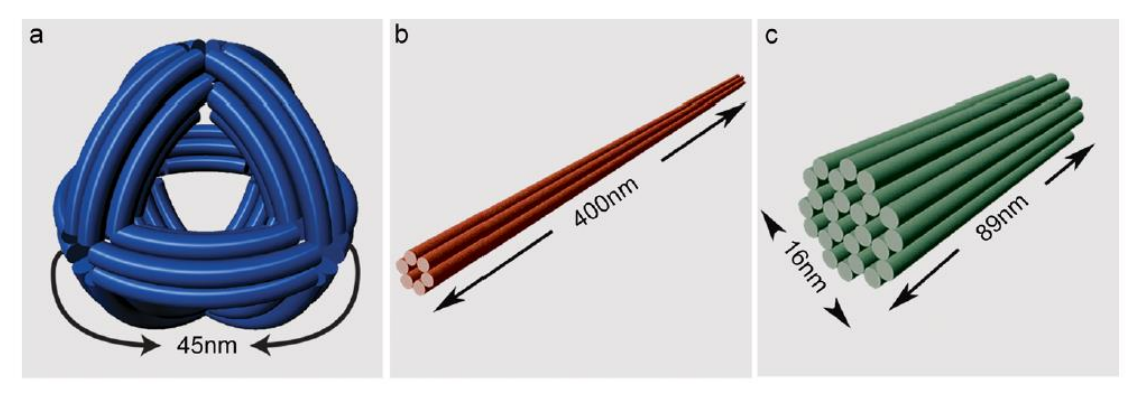


Figure 5 Three different DNA origami nanostructures tested for stability in tissue culture.

(Reproduced from Hahn et al., 2014)

Next, these DNA nanocarriers should be tested for their cytotoxicity since they should not be toxic to normal cells. Several studies reported that DNA origami nanostructures, such as a triangle (Jiang et al., 2012), a tube (Zhao et al., 2012), a rectangle (Mikkila et al., 2014), and an octahedron (Hahn et al., 2014), showed no significant cytotoxicity as analyzed by cell viability assay after incubated with cancer cells. Moreover, Zhang et al. demonstrated that no systemic toxicity and no immune response were observed in nude mice after injected with doxorubicin-containing DNA origami nanostructures for 6 hours (Zhang et a., 2014). From these results, DNA nanostructures could be bio-friendly nanomaterials for being used as drug delivery vehicles.

Drug loading and releasing capabilities should also be considered. To test drug loading capacity of the nanocarriers, doxorubicin, a well-known chemotherapeutic drug, is usually used as a model drug since it can intercalate into double helical molecules. Jiang et al. showed that doxorubicin could be loaded into 2D triangular DNA origami nanostructures slightly lower than 3D tubular DNA origami nanostructures. They concluded that this might be the case that 3D structures have more space available than 2D structures (Jiang et al., 2012). They also investigated the release profile in different conditions and found that in cell lysate 2D triangular nanocarriers have a higher release rate than 3D tubular nanocarriers. The 3D tubular nanocarriers showed a similar release profile as normal double-stranded DNA. In addition, Zhao et al. constructed tubular DNA origami nanostructures in two different shapes; a straight tube and a twisted tube. They found that the twisted tube has higher loading

capacity about 33% compared with the straight tube (Zhao et al., 2012). Also, the individual twisted tube could encapsulate more doxorubicin than the straight tube. They explained that the twisted tube contains 14% more base pairs per structure and its structure also has a higher relaxation. Both tubular structures exhibited different drug release profiles as the twisted tube has a slower release rate. It seems like drugs could be loaded into 3D DNA origami nanostructures more than 2D DNA origami nanostructures. However, 2D DNA origami nanostructures exhibit a faster release profile.

It has been known that negatively-charged nucleic acid could not easily pass through biological lipid membrane. Surprisingly, huge DNA origami nanostructures, compared to normal DNA molecules, could be uptake by different cell lines. Schuller et al. demonstrated that a hollow 30-helix DNA origami nanotube with 20-nm diameter and 80-nm in length could internalized into mouse splenocytes as verified by flow cytometry. They claimed that the larger size and higher compactness of DNA origami nanostructures make it more efficiently internalized than individual single-stranded DNA (Schuller et al., 2011). There is a hypothesis that mammalian cells would uptake any DNA nanostructures with the size larger than 7 kb by endocytosis (Zhao et al., 2012). Ouyang et al. used rolling circle amplification (RCA)-based origami technique to construct DNA nanoribbons in various sizes. They found that the nanostructures with high length-to-width ratio would be preferentially internalized by cells (Ouyang et al., 2013). In contrast, Zhang et al. investigated the in vivo biodistribution of DNA origami nanostructures in three different shapes (Figure 6); triangle, rectangle, and tube, using quantum dot (QD) as a label (Zhang et al., 2014). Even though, the tubular nanostructures have higher length-to-width ratio than the triangular nanostructures. They found that after 24 hours of intravenous tail injection into mice, the triangular nanostructures could accumulate at the tumor site more than the tubular nanostructures.

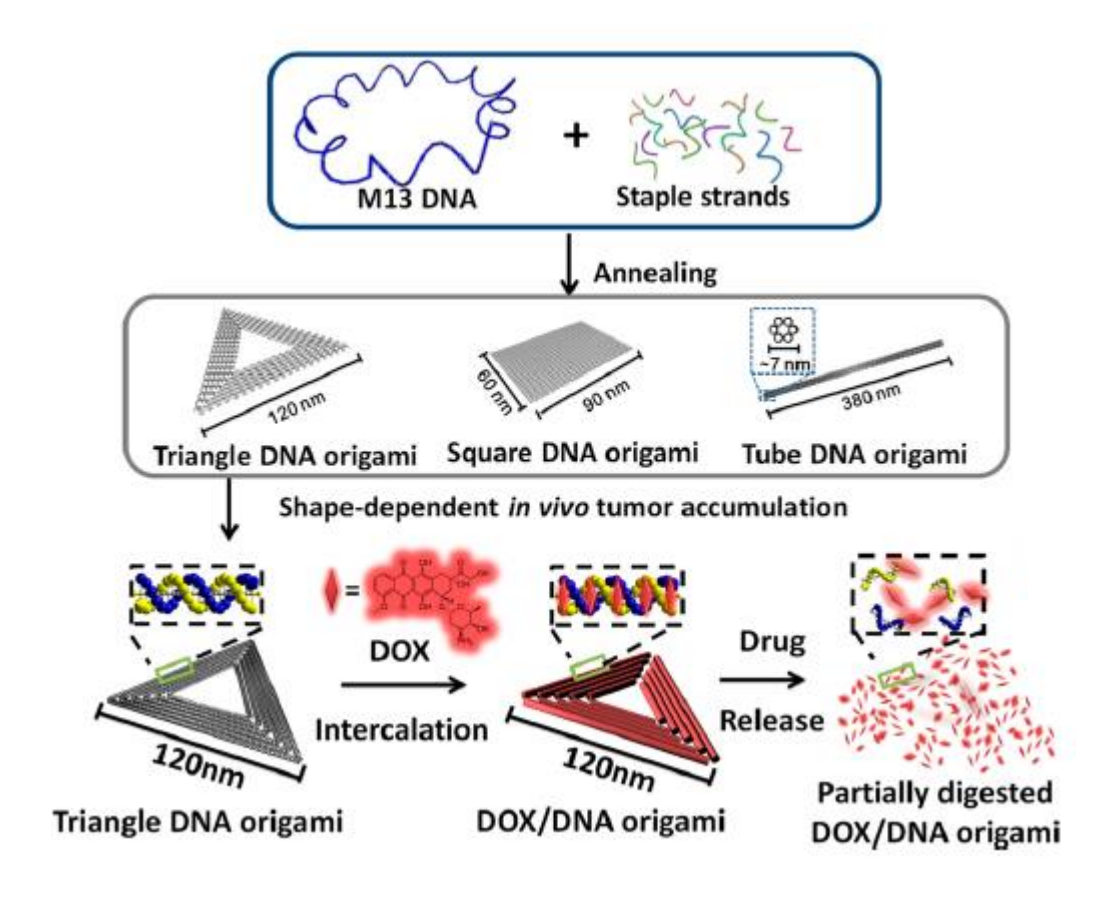


Figure 6 Three different shapes of DNA origami nanostructures tested as nanocarriers.

(Reproduced from Zhang et al., 2014)

In consistent, Jiang et al. investigated the internalization of gold nanorod modified tubular and triangular DNA origami nanostructures (Figure 7) into MCF-7 cells using two-photon luminescence (TPL) imaging (Jiang et al., 2015). They found that the triangular structures exhibited better internalization, which might be because of size and shape differences. These consistent results might confirm that the cellular uptake effect is dependent on size and shape of the nanostructures (Jiang et al., 2012). Anyway, it is still unclear that which structural design of DNA origami nanostructures would be preferable for cellular internalization.

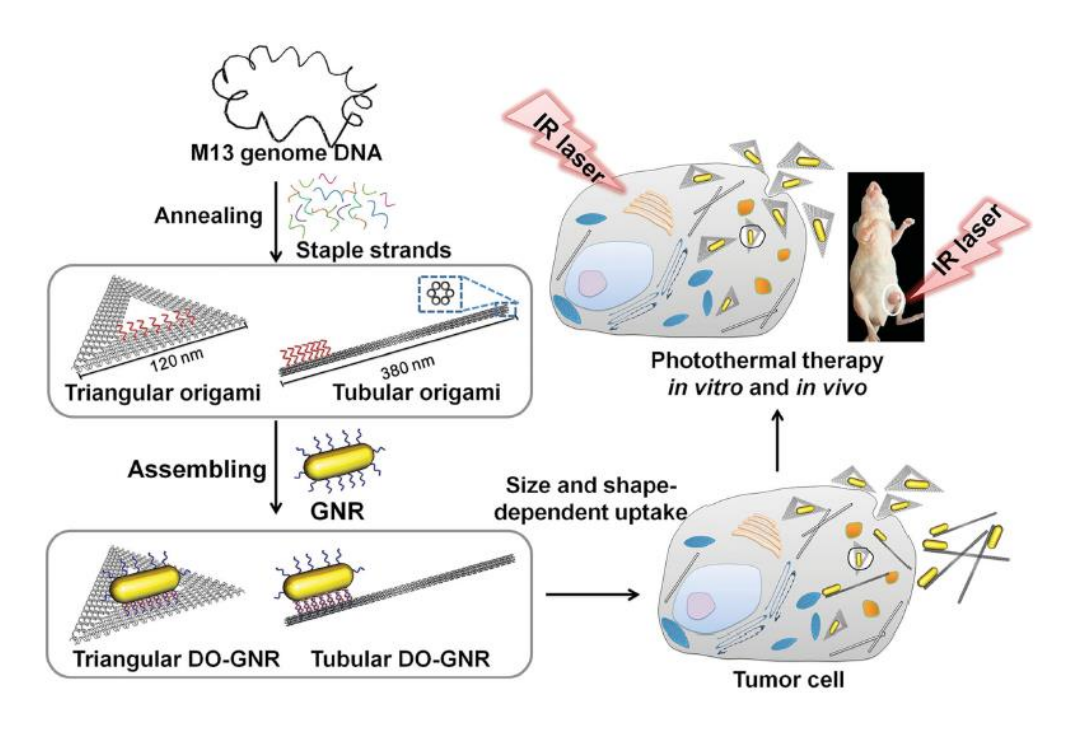


Figure 7 Gold nanorod modified DNA origami nanostructures as a theranostic system.

(Reproduced from Jiang et al., 2015)

Appropriate properties of nanocarriers such as optimal stability, low cytotoxicity, high drug loading and releasing capability along with enhanced cellular internalization could lead to high efficiency in cancer therapy. Schuller et al. reported that the efficiency of immune-activating does not depend on the structural 3D shape but the efficiency mainly depends on the compactness, size and stability of the nanocarriers (Schuller et al., 2011). In 2012, Jiang et al. demonstrated that 2D triangular and 3D tubular DNA origami nanostructures could enhance anti-cancer activity of doxorubicin in doxorubicin-resistant MCF-7 cells (Jiang et al., 2012). They also found that the anti-cancer efficiency depends on the length of incubation time and drug concentration.

As mentioned above, the structural design of DNA nanostructures could have some impacts on the properties of nanocarriers used for drug delivery system. Therefore, this proposal proposes to investigate the effects of 2D and 3D DNA origami nanostructures on being used as a nanocarrier in biological conditions. Knowledge gained from these experiments could be useful for designing efficient DNA nanocarriers as drug delivery system.

#### Objectives

To gain more knowledge about the effects of 2D and 3D DNA origami nanostructures on functional properties (stability, cytotoxicity, cellular uptake, drug loading and release capability, growth inhibitory efficiency) as nanocarriers in a drug delivery system.

#### Methods

#### 1. Preparation and characterization of DNA origami nanostructures

To construct 2D and 3D DNA origami nanostructures, each nanostructure was separately annealed according to previous report (Chaithongyot et al., 2018). For preparing 10 nM DNA origami nanostructures (using 1:10 ratio), 10 nM M13mp18 scaffold was mixed with 100 nM staple strands in TAE/Mg²+ buffer containing 40 mM Tris-HCl (pH 8.0), 20 mM acetic acid, 2 mM EDTA, and 12.5 mM magnesium acetate. For preparing 10 nM DNA origami nanostructures (using 1:2 ratio), 10 nM M13mp18 scaffold was mixed with 20 nM staple strands in TAE/Mg²+ buffer containing 40 mM Tris-HCl (pH 8.0), 20 mM acetic acid, 2 mM EDTA, and 12.5 mM magnesium acetate. The mixture was heated at 68 °C, then gradually cooled from 68 °C to 25 °C at 0.6 °C/minute and finally from 25 °C to 4 °C at 1 °C/minute. After assembly step, the excess staple strands were removed by using a PEG purification method (Stahl et al., 2014). The samples were combined with PEG8000 purification buffer and then centrifuged at 13,000 rpm at 16 °C for one hour. The supernatant was discarded and the pellet was resuspended in desired buffer.

To characterize the annealed DNA origami nanostructures, several techniques were utilized including agarose gel electrophoresis, NanoSight, atomic force microscopy (AFM), and transmission electron microscopy (TEM). First, the annealed structures were analyzed in 1.5% agarose gel under non-denaturing condition. Electrophoresis was carried out at 75 V for 2 hours in 0.5X TBE (44.5 mM Tris-HCl pH 8, 44.5 mM boric acid, and 1 mM EDTA) containing 11 mM MgCl<sub>2</sub>. The agarose gel was stained with ethidium bromide and imaged by a gel imaging system. Next, the hydrodynamic size of each DNA origami nanostructure was investigated using NanoSight NS300 (Malvern). Then, AFM was utilized with a tapping-in-air mode. Briefly, a sample will be deposited onto freshly cleaved mica and leave at room temperature for 5 minutes. Then the mica will be washed with distilled water twice and air-dried with

compressed air. After being mounted onto the microscope, the imaging will be performed. Lastly, the origami nanostructures were visualized using TEM. The samples were deposited onto a negatively glow-discharged carbon-coated grid for 3 minutes and then the excess solution was removed using a filter paper. Next, the grid was negatively stained with 0.7% uranyl acetate solution for 45 seconds and blotted using a filter paper. After dried, the analysis was performed using a Tecnai F20 FEG transmission electron microscope operating at 120 kV in bright field mode. TEM images were taken digitally by the CCD camera with magnification between 15,000 and 150,000.

#### 2. Examination of stability of DNA origami nanostructures

As the DNA nanostructures will be incubated with human breast cancer cells, MCF-7 and MDA-MB231 cells, the stability of the annealed DNA origami nanostructures in cell culture media was examined and compared with the stability in the annealed buffer. The annealed DNA origami nanostructure samples were incubated in TAE/Mg<sup>2+</sup> buffer containing 40 mM Tris-HCl (pH 8.0), 20 mM acetic acid, 2 mM EDTA, and 12.5 mM magnesium acetate or incubated in DMEM supplemented with 10% FBS, 100 U/mL penicillin, and 100 µg/mL streptomycin at room temperature and 37 °C for 30 minutes, 1, 3, 6, 12, and 24 hours. Then the stability was verified by using 1.5% agarose gel electrophoresis under non-denaturing condition. Electrophoresis was carried out at 75 V for 2 hours in 0.5X TBE (44.5 mM Tris-HCl pH 8, 44.5 mM boric acid, and 1 mM EDTA) containing 11 mM MgCl<sub>2</sub>. The agarose gel was stained with ethidium bromide and imaged by a gel imaging system.

#### 3. Analysis of drug loading capability of DNA origami nanostructures

#### 3.1 Agarose gel electrophoresis

The annealed DNA origami nanostructures (5 nM) were incubated in 250  $\mu$ M doxorubicin solution at 37 °C for 24 hours. After that the mixtures were analyzed using 1.5% agarose gel electrophoresis under non-denaturing condition. Electrophoresis was carried out at 75 V for 2 hours in 0.5X TBE (44.5 mM Tris-HCl pH 8, 44.5 mM boric acid, and 1 mM EDTA) containing 11 mM MgCl<sub>2</sub>. The agarose gel was stained with ethidium bromide and imaged by a gel imaging system.

#### 3.2 Fluorescence spectrophotoscopy

The annealed DNA origami nanostructures at various concentrations (3, 5, 7, and 9 nM) were incubated in 10  $\mu$ M doxorubicin solution at two different temperatures, room temperature and 37 °C, for 3 hours. Then the mixtures were measured the fluorescent intensity by fluorescence spectrophotometry (Agilent) using the excitation wavelength at 470 nm and the emission wavelength ranging from 500-750 nm.

#### 3.3 Absorption spectrophotoscopy

The annealed DNA origami nanostructures (5 nM) were incubated with 250  $\mu$ M doxorubicin in either PBS or TAE/Mg<sup>2+</sup> buffer at 37 °C, for 24 hours. After centrifuged at 15,000 rpm at 4 °C for 30 minutes, supernatant was separated for free doxorubicin measurement using the absorption at 480 nm by a microplate reader. Then the loading capability of each DNA origami nanostructure was calculated using a method as previously reported (Jiang et al., 2012). The loading capacity of the origami nanostructures was calculated using equations below.

% loading capacity = 
$$(D_{in} / D_{total}) \times 100$$

when  $D_{in}$  is the final content of doxorubicin in DNA origami nanostructures  $D_{total}$  is the initial content of doxorubicin in the solution

#### 4. Analysis of drug release rate of DNA origami nanostructures

The annealed DNA origami nanostructures (5 nM) were incubated with 250  $\mu$ M doxorubicin in TAE/Mg<sup>2+</sup> buffer at 37 °C, for 24 hours. After centrifuged at 15,000 rpm at 4 °C for 30 minutes, supernatant was removed. Then the pellet was re-suspended in TAE/Mg<sup>2+</sup> buffer and the mixture was incubated at 37 °C for 15 and 60 minutes. After incubated, the mixture was centrifuged at 15,000 rpm at 4 °C for 30 minutes and supernatant was removed. The pellet was re-suspended in TAE/Mg<sup>2+</sup> buffer and the absorbance at 480 nm was measured using a microplate reader before and after incubation. Then the release capability of each DNA origami nanostructure was calculated using an equation below.

% Release = 
$$[(A_0 - A_i) / A_0] \times 100$$

when  $A_0$  is the initial content of doxorubicin in DNA origami nanostructures  $A_i$  is the content of doxorubicin in DNA origami nanostructures after incubation

#### 5. Determination of cytotoxicity of DNA origami nanostructures

Cytotoxicity of each DNA origami nanostructure was tested on MCF-7 and MDA-MB-231 cells. Cell viability was analyzed by the MTT assay. Cells were be seeded in 96-well plates at a density of 3,500 cells/well for MCF-7 cells and 3,000 cells/well for MDA-MB-231 cells and cultured overnight in DMEM supplemented with 10% FBS, 100 U/mL penicillin, and 100 ug/mL streptomycin at 37 °C in a 5% CO<sub>2</sub> atmosphere. Then cells were incubated with 1 nM of empty DNA origami nanostructures for 48 hours. After that, the MTT assay was performed by adding MTT to get a final concentration of 0.5 mg/mL for each well and incubated at 37 °C for three hours. Then the crystal formazan product was dissolved in DMSO and the absorbance at 540 nm was measured using a microplate reader. The percentage of cell viability can be calculated using an equation below. The absorbance of DMSO treatment was subtracted from all data.

% cell viability =  $100 - \{ [ (A_{540} \text{ of control} - A_{540} \text{ of treated} ) / A_{540} \text{ of treated} ] \times 100 \}$ 

when  $A_{540}$  of control is the absorbance of the cells incubated in culture media only  $A_{540}$  of treated is the absorbance of the cell treated with DNA nanostructures

#### 6. Investigation of cellular internalization of DNA origami nanostructures

#### 6.1 Cy5 modified DNA origami nanostructures

The cellular internalization of Cy5-modified DNA origami nanostructures into MCF-7 and MDA-MB-231 cells was examined by fluorescence microscope. MCF-7 and MDA-MB-231 cells were seeded at a density of 100,000 cells/well and cultured overnight in DMEM supplemented with 10% FBS, 100 U/mL penicillin, and 100 ug/mL streptomycin at 37 °C in a 5% CO<sub>2</sub> atmosphere. After 24 hours, cells will be incubated with 1 nM Cy5-modified DNA origami nanostructures for three hours. Cells were washed 3 times with PBS buffer. The imaging will be done using fluorescence microscope.

#### 6.2 doxorubicin-loaded DNA origami nanostructures

The cellular internalization of dox-loaded DNA origami nanostructures into MCF-7 and MDA-MB-231 cells was examined by fluorescence microscope. MCF-7 and MDA-MB-231 cells were seeded at a density of 100,000 cells/well and cultured overnight in DMEM supplemented with 10% FBS, 100 U/mL penicillin, and 100 ug/mL streptomycin at 37 °C in a 5% CO<sub>2</sub> atmosphere. After 24 hours, cells will be incubated with 1 nM dox-loaded DNA origami nanostructures for three hours. Cells were washed 3 times with PBS buffer. The imaging will be done using fluorescence microscope.

# 7. Investigation of selectivity of aptamer-modified DNA origami nanostructures 7.1 MUC1 expression: Western blot analysis

For Western blot analysis, cells were seeded at a density of 1 x 10 $^6$  cells in a 6-cm petri dish and cultured at 37  $^\circ$ C with 5% CO $_2$  for 48 hours. Total proteins of each cell were extracted from sub-confluent cells using the lysis buffer supplemented with protease inhibitors (pH 7.4). Cell pellets were lysed in the TENT lysis buffer (50 mM Tris pH 8.0, 150 mM NaCl, 2 mM EDTA, 1 mM NaF, 1% (v/v) TritonX-100, 1 mM Na $_3$ VO $_4$ , 1 mM PMSF). Lysates were centrifuged at 12,000g for 15 minutes at 4  $^\circ$ C. The concentration of protein was quantified by using Bradford assay. The proteins (40 mg) were subjected into 8% SDS-PAGE and then transferred to a nitrocellulose membrane by Semi-Dry Transfer Cell (Bio-Rad). The membranes were blocked in 5% BSA at room temperature for 2 hours to block the non-specific binding sites. Immunodetection was performed with the primary antibody; mouse anti-mucin1 (Cell Signaling Technology, Denver, MA) overnight at 4  $^\circ$ C. After washing, membranes were incubated with the secondary antibody; rabbit anti-mouse antibody labeled with horseradish peroxidase (HRP) for 1 hour at room temperature.  $\beta$ -actin was used as an internal control. The detection of ECL signals was verified by the G-box chemiluminescence.

#### 7.2 MUC1 expression: Immunofluorescence staining

The immunocytochemistry was performed to examine the biomarker protein, MUC1, localized on the plasma membrane of both MCF-7 and MDA-MB-231 cells. Cells were cultured in 12-well plates at a density of 20,000 and 10,000 cells/well for MCF-7 and MDA-MB-231 cells, respectively. After 24 hours, cells were washed twice with PBS and fixed with 4%

paraformaldehyde at room temperature for 15 minutes. Cells were blocked in 20% FBS in PBS for 30 minutes. Immunodetection of MUC1 was evaluated first with a primary antibody, mouse anti-mucin1 antibody, and then with a secondary antibody, FITC-conjugated anti-mouse antibody. Cells were counterstained with Hoechst 33342 (0.1 ug/mL), and phalloidin. The stained cells were visualized and imaged by Live Cell Fluorescence Imaging System (Olympus, Japan).

#### 7.3 Selectivity of aptamer-modified DNA origami nanostructures

The cellular internalization of dox-loaded, MUC1-aptamer-modified DNA origami nanostructures into MCF-7 and MDA-MB-231 cells was examined by fluorescence microscope. MCF-7 and MDA-MB-231 cells were seeded at a density of 100,000 cells/well. After 24 hours, cells will be incubated with 1 nM dox-loaded, MUC1-aptamer-modified DNA origami nanostructures in serum-free media (no FBS) for one hours. Cells were washed 3 times with PBS buffer. The imaging will be done using fluorescence microscope.

#### 8. Examination of anti-cancer activity of drug-containing DNA origami nanostructures

The anti-cancer activity of dox-loaded DNA origami nanostructures with and without MUC1-aptamer modification was investigated via cell viability assay. Both MCF-7 and MDA-MB-231 cells were cultured in DMEM supplemented with 10% FBS, 100 U/mL penicillin, and 100 ug/mL streptomycin at 37 °C in a 5% CO<sub>2</sub> atmosphere. Cells were seeded in 96-well plates at a density of 3,500 cells/well for MCF-7 cells and 3,000 cells/well for MDA-MB-231 cells and cultured overnight. Both cells were incubated with dox-loaded DNA origami nanostructures with and without MUC1-aptamer modification for 1 hour in serum-free media (no FBS). Then, cells were washed twice before cultured in normal media for 48 hours. After that, the MTT assay was performed. The MTT reagent was added to a final concentration of 0.5 mg/mL for each well and incubated at 37 °C for three hours. Then the crystal formazan product was dissolved in DMSO and the absorbance at 540 nm was measured using a microplate reader. The percentage of cell viability can be calculated using an equation below.

% cell viability = 100 – { [ (  $A_{540}$  of control –  $A_{540}$  of treated ) /  $A_{540}$  of treated ] x 100 }

when  $A_{540}$  of control is the absorbance of the cells incubated in culture media only  $A_{540}$  of treated is the absorbance of the cell treated with DNA nanostructures. The absorbance of DMSO treatment was subtracted from all data. Then the anti-cancer efficiency of dox-loaded DNA origami nanocarriers was calculated.

#### Results

#### 1. Preparation and characterization of DNA origami nanostructures

After annealing step, the samples were analyzed with agarose gel electrophoresis under non-denaturing condition. As shown in **Figure 8**, the result suggests that DISC, DONUT, and SPHERE formed as distinct bands. The DISC migrates slower in the gel than the DONUT as it is slightly bigger according to the design. Two distinct bands in lane 5 are closed and open SPHERES. The open SPHERE migrates slower than the closed ones.



Figure 8 Characterization of DISC, DONUT, and SPHERE shaped DNA origami nanostructures using 1.5% agarose gel. Lane 1 contains 1 Kb DNA ladder, Lane 2 contains M13 scaffold, Lane 3 contains DISC, Lane 4 contains DONUT, Lane 5 contains closed SPHERE, and Lane 6 contains open SPHERE.

Next, the hydrodynamic size of three DNA nanostructures was examined using NanoSight NS300 (Malvern). The theoretical size of DISC is 62 nm in diameter with a 21-nm diameter hole in the middle. The experimental results, as shown in **Figure 9**, exhibited that the major

nanoparticles in the solution are around 103 nm and 138 nm which are larger than the expected size.

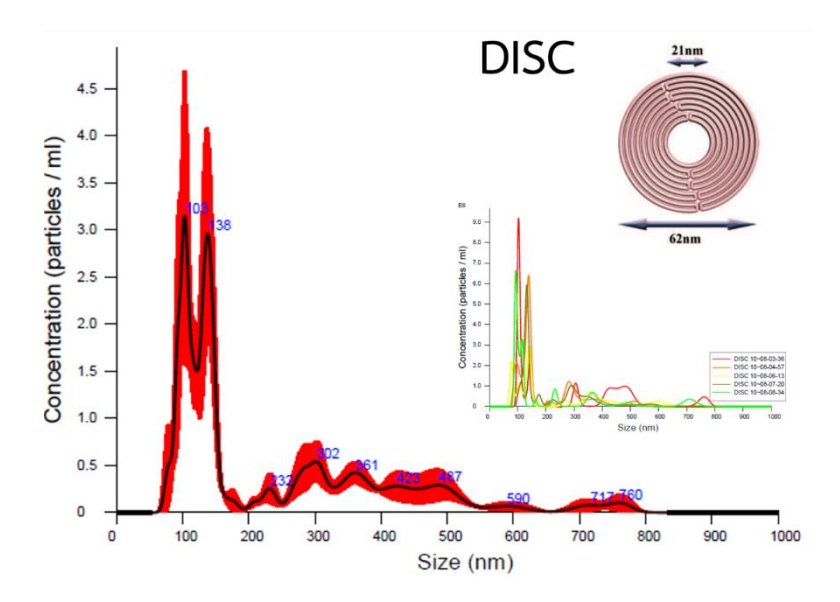


Figure 9 The hydrodynamic size analysis of DISC-like shaped DNA origami nanostructure.

The theoretical size of DONUT is 43.6 nm in diameter with a hole in the middle. The experimental results, as shown in **Figure 10**, exhibited that the major nanoparticles in the solution are around 100-148 nm which are larger than expected size.

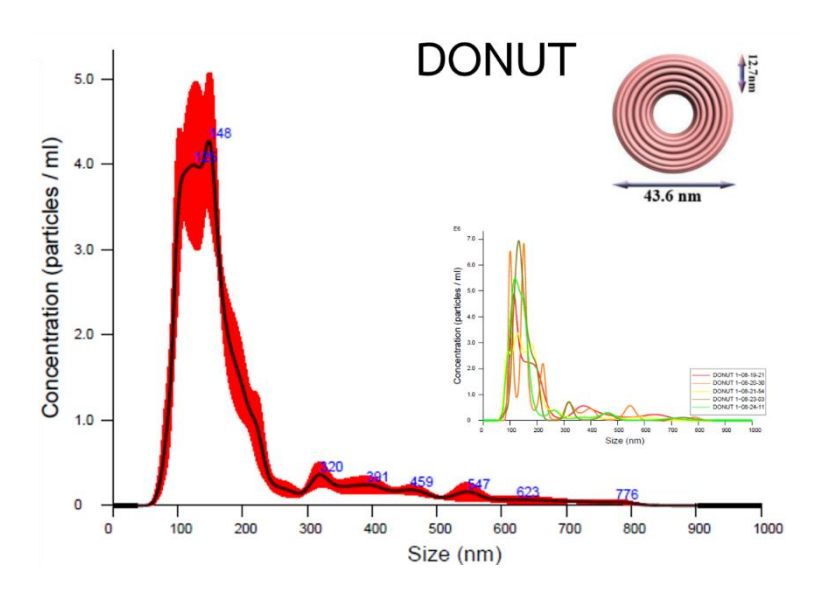


Figure 10 The hydrodynamic size analysis of DONUT-like shaped DNA origami nanostructure.

The theoretical size of SPHERE is 42 nm in diameter and the SPHERE could be in two conformations; open and closed ones. The experimental results, as shown in **Figure 11-12**, exhibited that the major nanoparticles in the solution are around 50-100 nm for open and closed SPHERE, which are larger than the expected size.

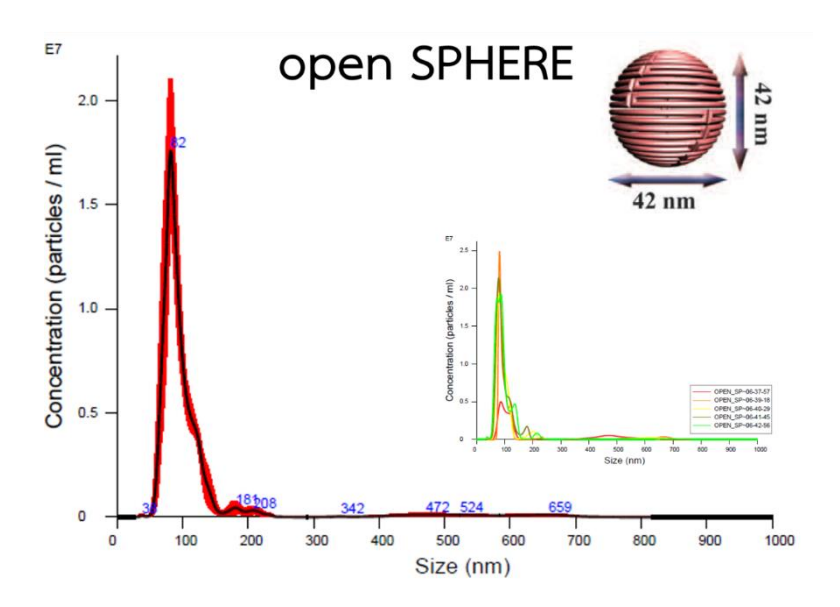


Figure 11 The hydrodynamic size analysis of open-SPHERE DNA origami nanostructure.

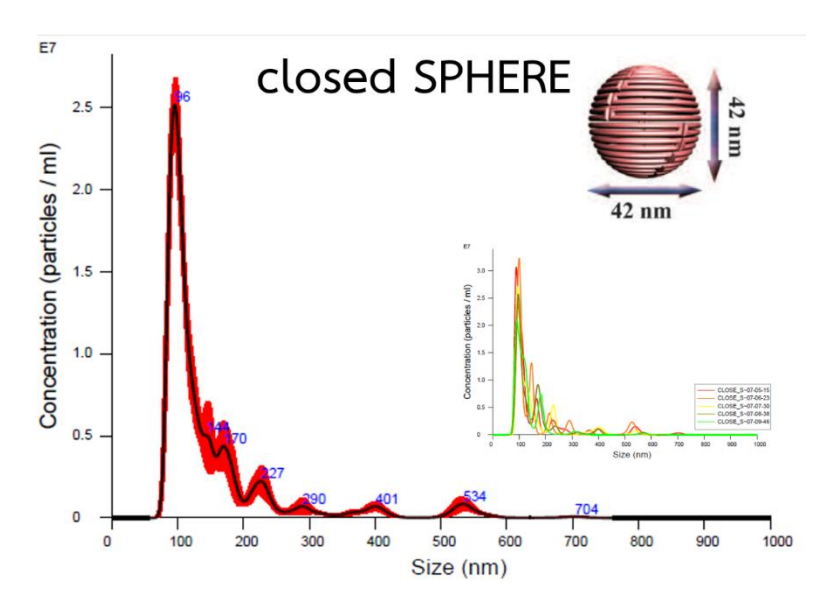


Figure 12 The hydrodynamic size analysis of closed-SPHERE DNA origami nanostructure.

The results from NanoSight showed that three shapes of DNA origami nanostructures exhibited the hydrodynamic sizes larger than the expected ones. This might be an effect of M13 tail which is ssDNA part hanging with the structures.

Moreover, the DNA origami nanostructures in DISC, DONUT, and SPHERE were analyzed via an atomic force microscopy (AFM) using a scan assyst mode. The AFM images demonstrated that they could form as designed with the expected size.

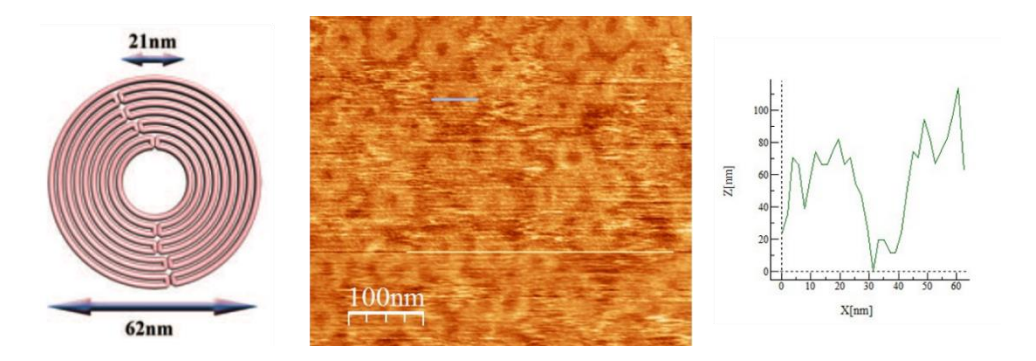


Figure 13 The AFM analysis of DISC-like shaped DNA nanostructure. The diagram of DISC structure (left), AFM image of DISC nanostructure (middle), and the graph showing the size of the DISC nanostructure (right).

As shown in **Figure 13**, under AFM conditions, the DISC nanostructure is a one-layered circular shape containing a hole in the middle. The diameter of the whole structure is about 60 nm and the diameter of the hole is about 20 nm which are very close to the theoretical ones.

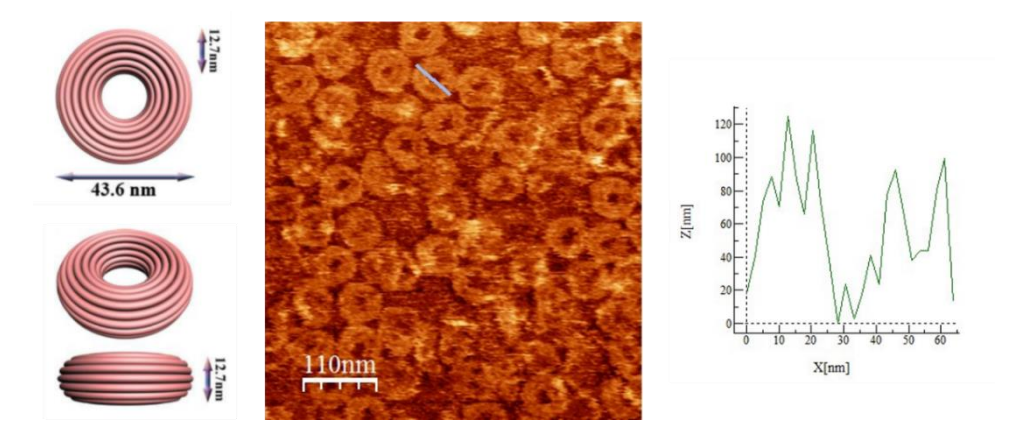
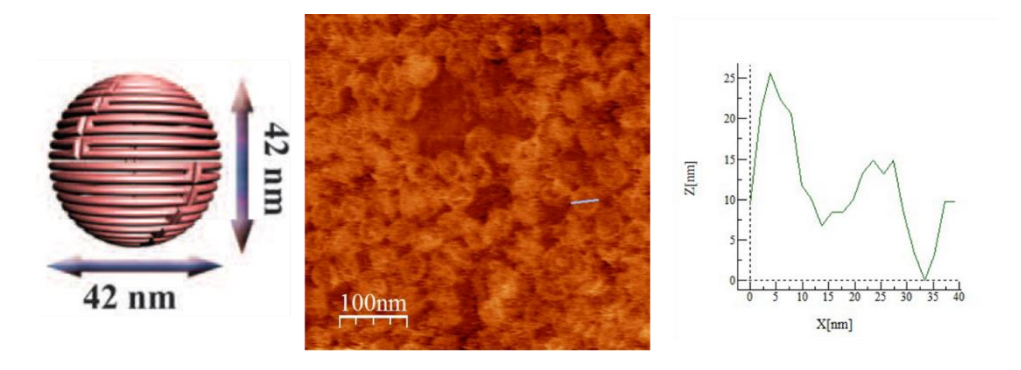


Figure 14 The AFM analysis of DONUT-like shaped DNA origami nanostructure. The diagram of DONUT structure (left), AFM image of DONUT nanostructure (middle), and the graph showing the size of the DONUT nanostructure (right).

As shown in **Figure 14**, under AFM conditions, the DONUT nanostructure is a two-layered circular shape containing a hole in the middle. The diameter of the whole structure is about 40 nm and the diameter of the hole is about 18 nm. The size of DONUT is a little bigger than a theoretical one since the AFM tip forces the structure onto the surface making the space inside the structure disappears. Compared with DISC nanostructure, the height of DONUT nanostructure is higher as it contains two layers of DNA.



**Figure 15** The AFM analysis of SPHERE-like shaped DNA origami nanostructure. The diagram of SPHERE structure (left), AFM image of SPHERE nanostructure (middle), and the graph showing the size of the SPHERE nanostructure (right).

As shown in **Figure 15**, under AFM conditions, the SPHERE nanostructure is a spherical shape with a hole inside and the closed SPHERE is formed with closed DNA strands which help hold the hemisphere together. The diameter of the whole structure is about 40 nm. Also, the AFM tip forces the structure onto the surface making the space inside the structure disappears and making the closed SPHERE open as the open conformation can be seen under AFM.

In addition, these DNA origami nanostructures were also analyzed via a transmission electron microscopy (TEM). Consistent with AFM results, the annealed DNA origami nanostructures could form into the desired shapes and sizes. Moreover, the M13 tail hanging on each DNA origami nanostructure could be clearly seen in TEM images for all DNA origami nanostructures; DISC, DONUT, and SPHERE, as shown in **Figure 16-18**, respectively.

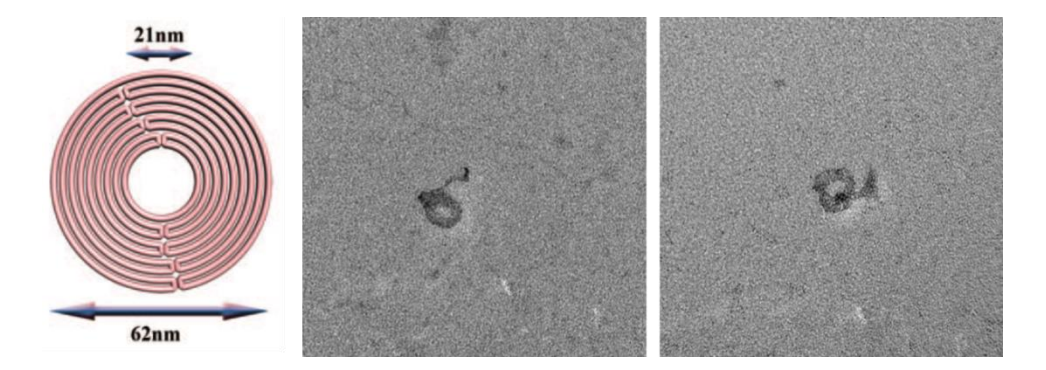


**Figure 16** The TEM analysis of DISC-like shaped DNA origami nanostructure. The diagram of DISC nanostructure (left) and the TEM images of DISC nanostructure (right).

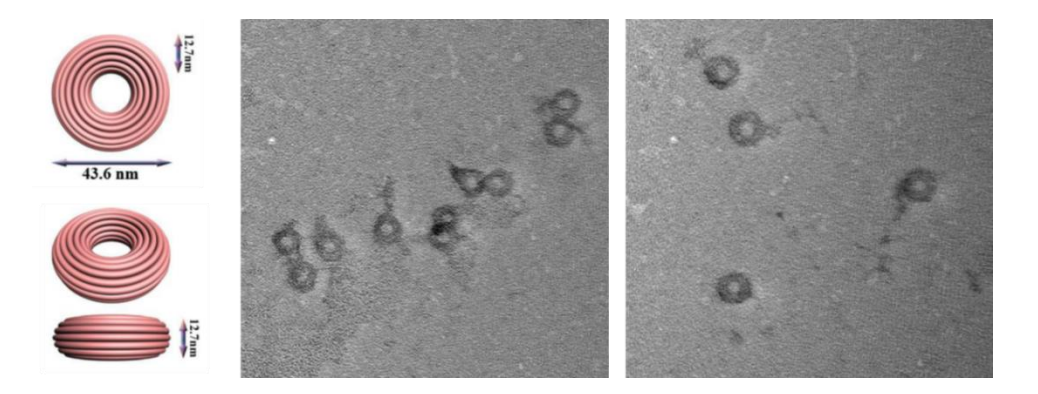


**Figure 17** The TEM analysis of DONUT-like shaped DNA origami nanostructure. The diagram of DONUT nanostructure (left) and the TEM images of DONUT nanostructure (right).

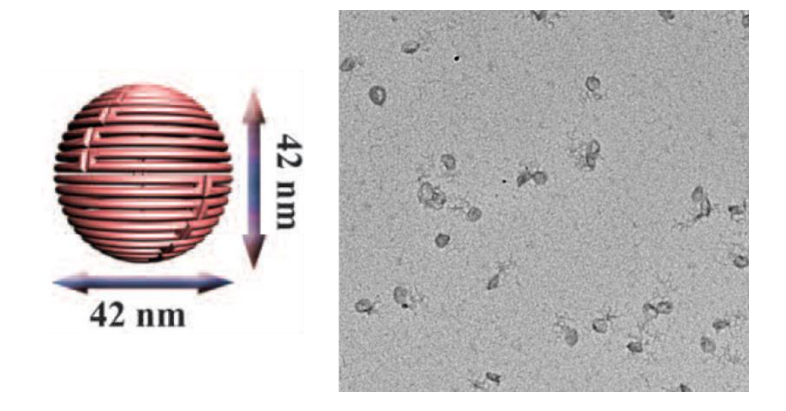


**Figure 18** The TEM analysis of SPHERE-like shaped DNA origami nanostructure. The diagram of SPHERE nanostructure (left) and the TEM images of SPHERE nanostructure (right).

#### 2. Examination of stability of DNA origami nanostructures

The stability of these DNA origami nanostructures in cell culture media (DMEM supplemented with 10% FBS, 100 U/mL penicillin, and 100 µg/mL streptomycin) was examined and compared with that in the annealing buffer at two different temperatures, room temperature and 37 °C for 0.5, 1, 3, 6, 12, and 24 hours as these structures have to be tested with breast cancer cells in further experiments. After incubated, the DNA nanostructures were loaded into 1.5% agarose gel running under non-denaturing conditions (75 V for 2 hours) for stability determination. The results showed that at room temperature condition, DISC structure in TAE/Mg<sup>2+</sup> buffer was stable up to 24 hours as shown in **Figure 19** whereas DISC structure in DMEM was stable up to only three hours as shown in **Figure 20**.

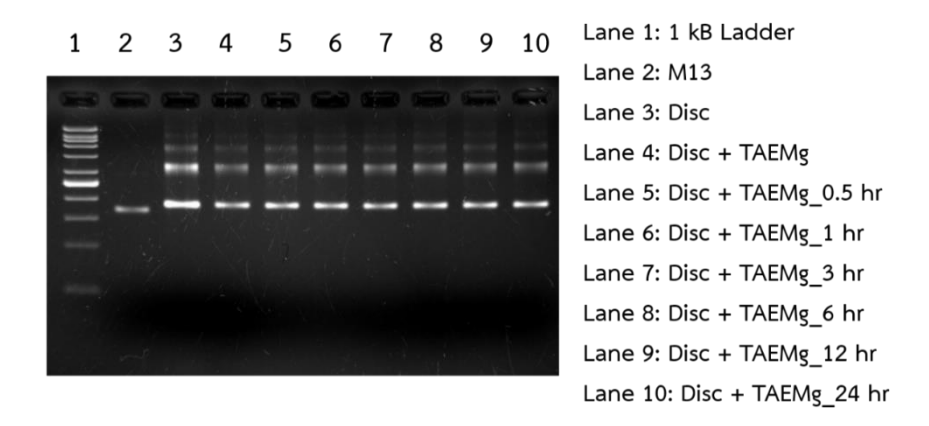


Figure 19 The stability of DISC nanostructure after incubated in TAE/Mg<sup>2+</sup> at RT.

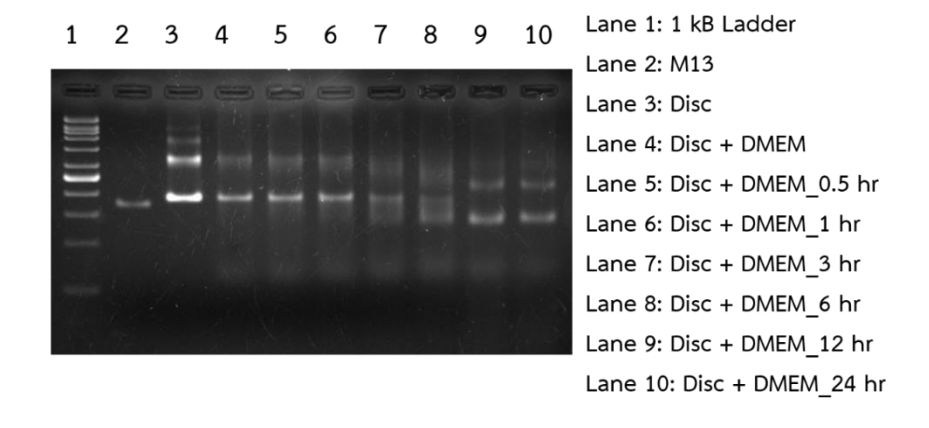


Figure 20 The stability of DISC nanostructure after incubated in DMEM at RT.

At 37 °C condition, DISC structure in TAE/Mg<sup>2+</sup> buffer was stable up to 24 hours as shown in **Figure 21** whereas DISC structure in DMEM was degraded within 30 minutes as shown in **Figure 22**.

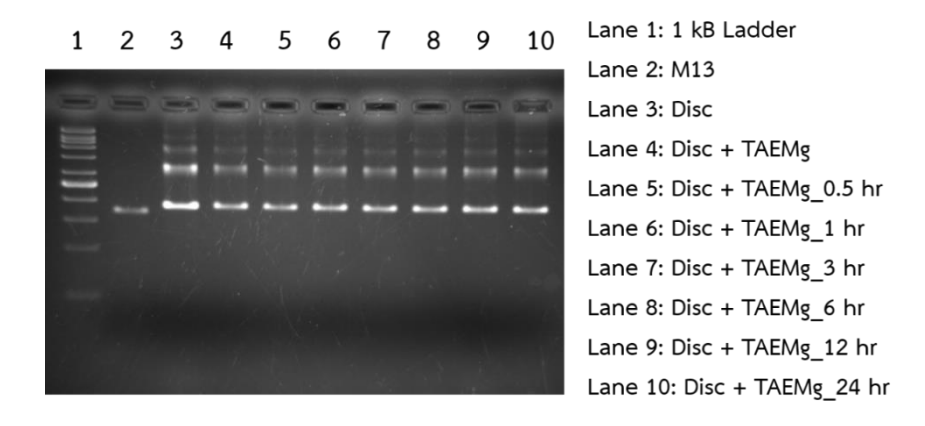


Figure 21 The stability of DISC nanostructure after incubated in TAE/Mg<sup>2+</sup> at 37 °C.

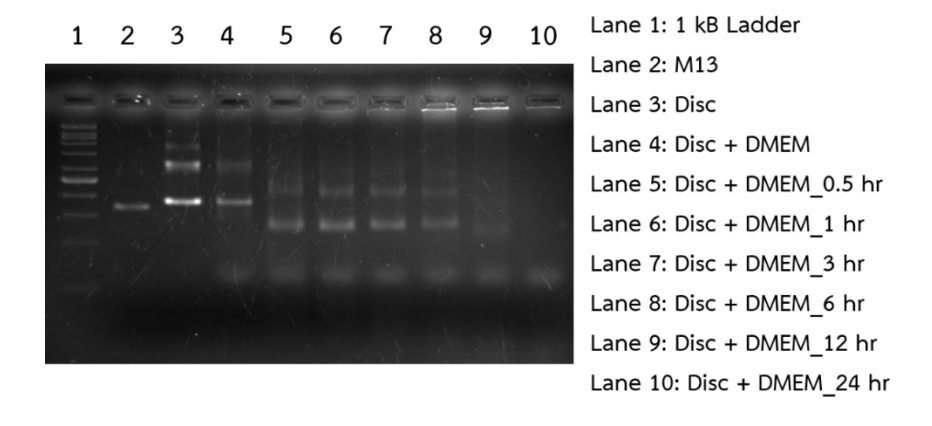


Figure 22 The stability of DISC nanostructure after incubated in DMEM at 37 °C.

At room temperature condition, DONUT structure in TAE/Mg<sup>2+</sup> buffer was stable up to 24 hours as shown in **Figure 23** whereas DONUT structure in DMEM was partially degraded after incubated for six hours as shown in **Figure 24**.

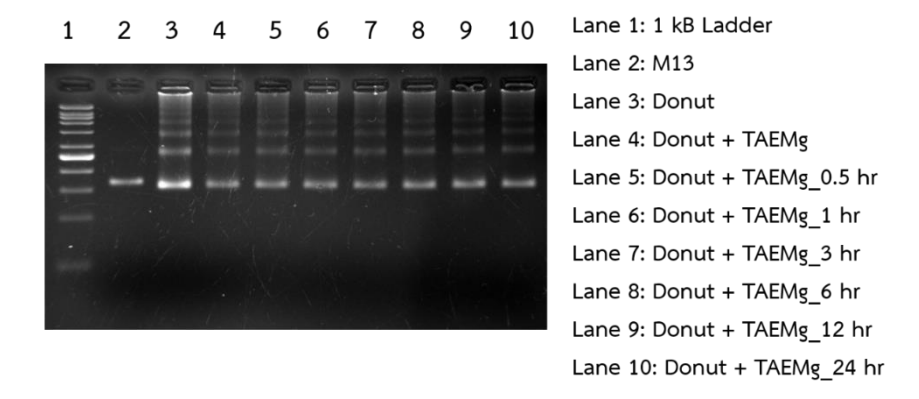


Figure 23 The stability of DONUT nanostructure after incubated in TAE/Mg<sup>2+</sup> at RT.

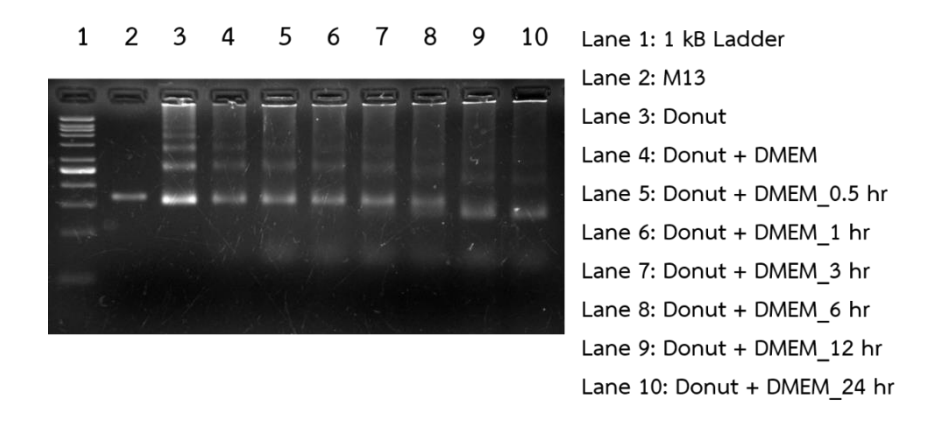


Figure 24 The stability of DONUT nanostructure after incubated in DMEM at RT.

At 37 °C condition, DONUT structure in TAE/Mg<sup>2+</sup> buffer was stable up to 24 hours as shown in **Figure 25** whereas DONUT structure in DMEM was degraded within 30 minutes as shown in **Figure 26**.

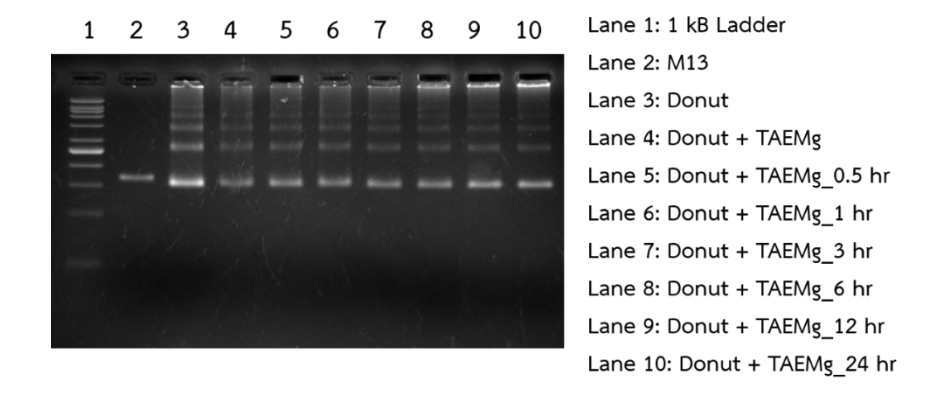


Figure 25 The stability of DONUT nanostructure after incubated in TAE/Mg<sup>2+</sup> at 37 °C.

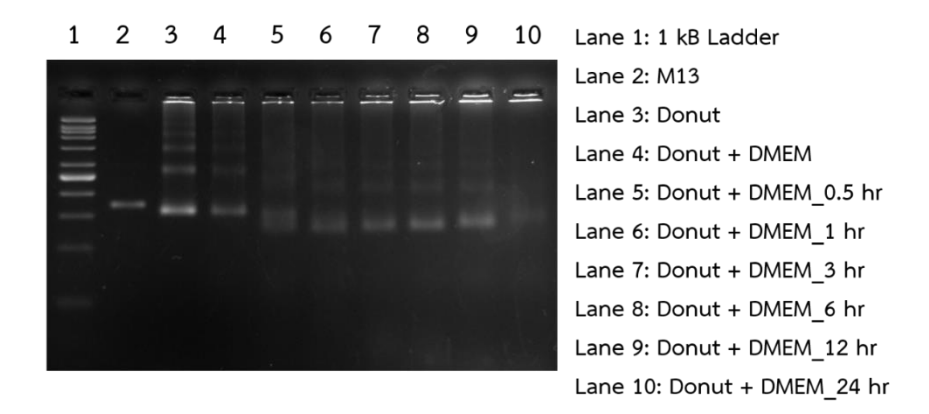


Figure 26 The stability of DONUT nanostructure after incubated in DMEM at 37 °C.

At room temperature condition, SPHERE structure in TAE/Mg<sup>2+</sup> buffer and DMEM was stable up to 24 hours as shown in **Figure 27-28**, respectively.

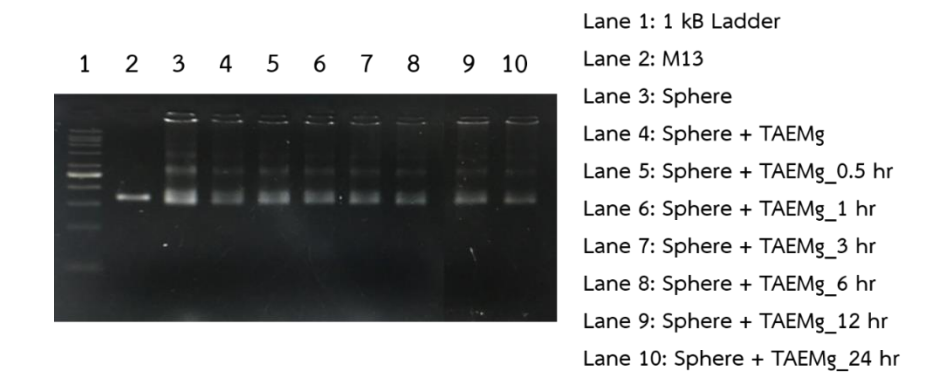


Figure 27 The stability of SPHERE nanostructure after incubated in TAE/Mg<sup>2+</sup> at RT.

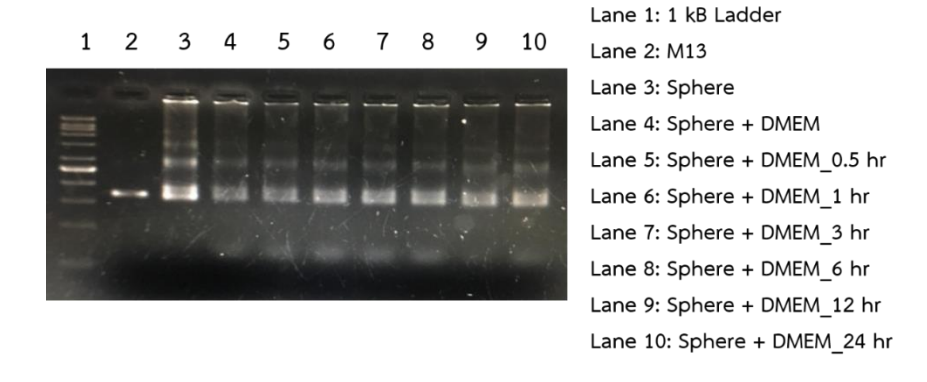


Figure 28 The stability of SPHERE nanostructure after incubated in DMEM at RT.

At 37 °C condition, SPHERE structure in TAE/Mg<sup>2+</sup> buffer was stable up to 24 hours as shown in **Figure 29** whereas SPHERE structure in DMEM was degraded within 30 minutes as shown in **Figure 30**.

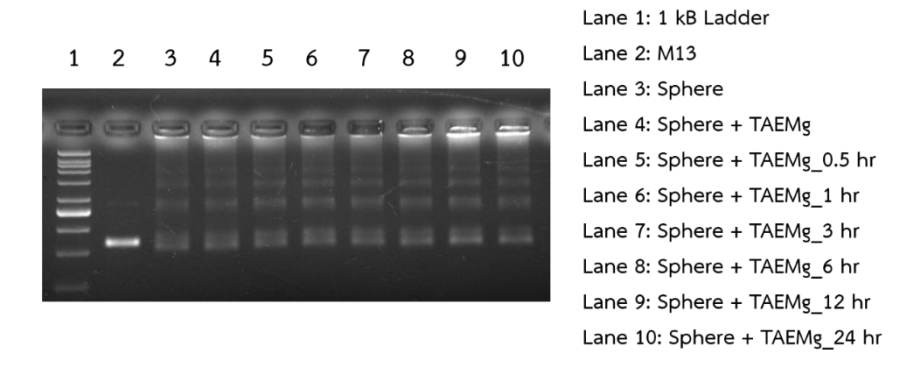


Figure 29 The stability of SPHERE nanostructure after incubated in TAE/Mg<sup>2+</sup> at 37 °C.

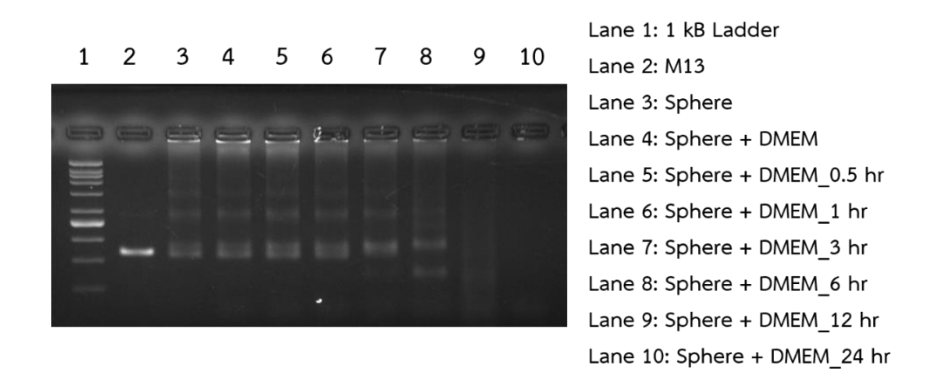


Figure 30 The stability of SPHERE nanostructure after incubated in DMEM at 37 °C.

As mentioned above, all DNA origami nanostructures exhibited relatively the same stability as they were stable up to 24 hours when incubated in the annealing buffer either at room temperature or at 37 °C. However, when incubated in the complete media, these three DNA origami nanostructures exhibited different stability either at room temperature or at 37 °C. The results above showed that SPHERE exhibited the highest stability while DISC exhibited the lowest stability in DMEM at both temperatures investigated.

#### 3. Analysis of drug loading capability of DNA origami nanostructures

For analysis of drug loading capability of each DNA origami nanostructure, doxorubicin (dox) was used as a model drug since dox could intercalate into the double helical structure of DNA. After incubated with dox, the mixtures were centrifuged to remove the excess dox before loaded into an agarose gel. As shown in **Figure 31**, dox-loaded DNA origami nanostructures have lower mobility than original DNA origami nanostructures for all three different structures.

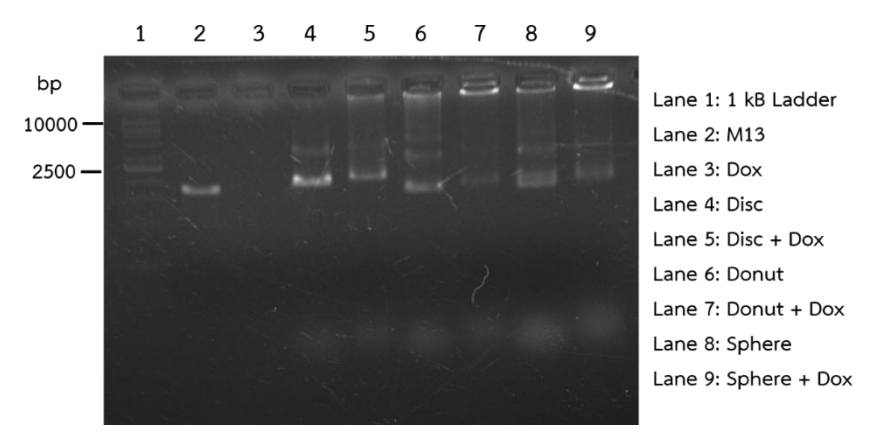


Figure 31 Agarose gel electrophoresis of dox-loaded DNA origami nanostructures.

It has been shown that dox is a fluorescent molecule with an excitation wavelength around 470 nm and an emission wavelength around 595 nm. Previous studies reported that the fluorescent signal of dox reduces after intercalation with DNA therefore the fluorescence spectrophotometry was utilized for dox-loading efficiency of each DNA origami nanostructure. The efficiency of drug loading was examined after incubation of DNA origami nanostructures at different concentrations (3 nM / 5 nM / 7 nM / 9 nM) with 10  $\mu$ M dox at room temperature and 37 °C for three hours. Then the fluorescent signals were measured. For DISC nanostructure, as shown in **Figure 32**, the dox signal was decrease when the concentration of DISC was increase. When compared loading efficiency at two temperatures, as shown in **Figure 33**, the efficiency at 37 °C is slightly better than room temperature except for 5 nM DISC nanostructure.

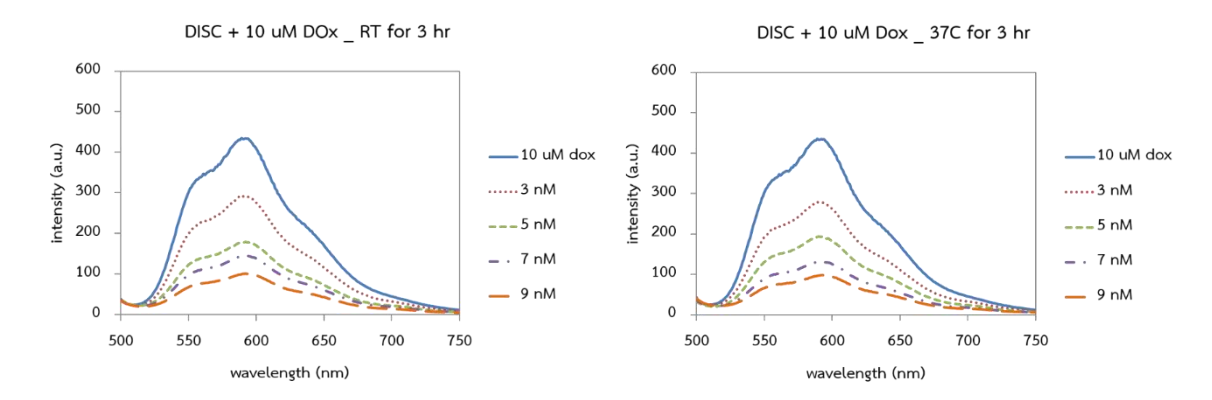
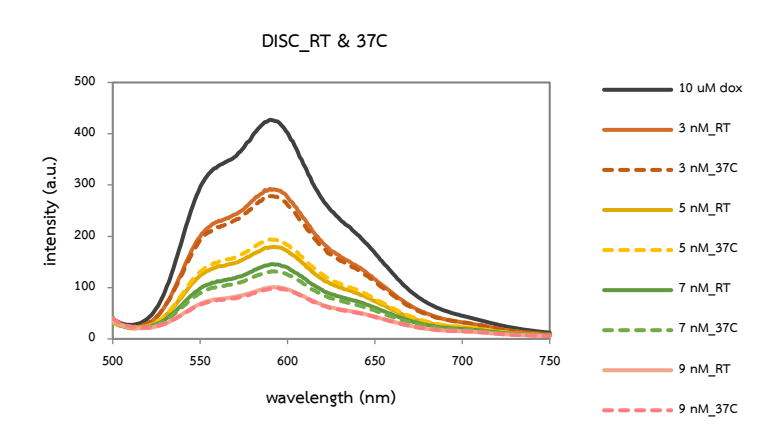


Figure 32 The fluorescence spectrum of dox-loaded DISC nanostructures after incubated at room temperature (left) and at 37 °C (right) for three hours.



**Figure 33** The comparison of fluorescence spectrum of dox-loaded DISC nanostructures incubated at room temperature and 37 °C.

For DONUT nanostructure, as shown in **Figure 33**, the dox signal was decrease when the concentration of DONUT was increase. When compared loading efficiency at two temperatures, as shown in **Figure 34**, the efficiency at 37 °C is slightly better than room temperature except for 5 nM DONUT nanostructure.

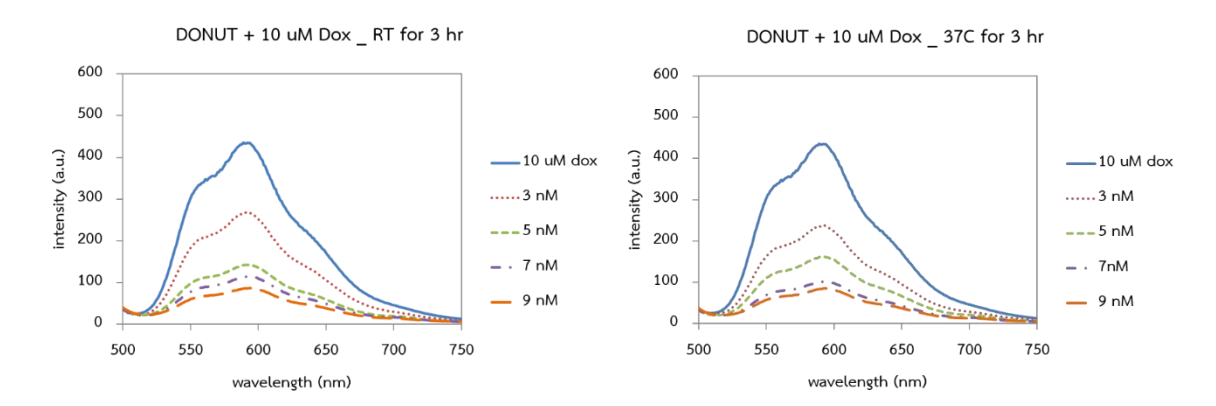


Figure 34 The fluorescence spectrum of dox-loaded DONUT nanostructures after incubated at room temperature (left) and at 37 °C (right) for three hours.

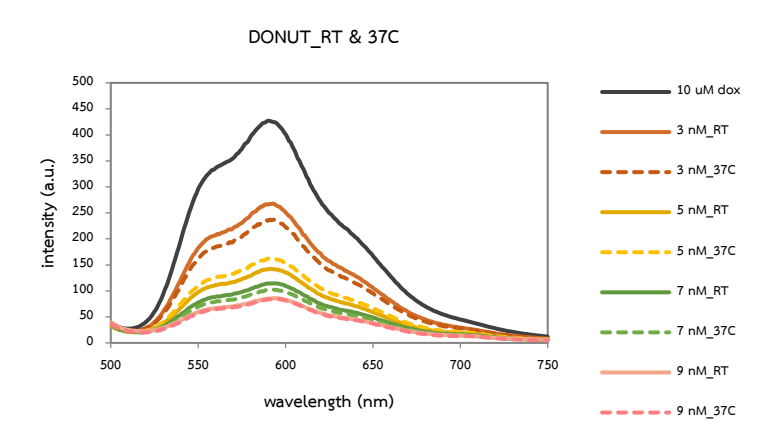


Figure 35 The comparison of fluorescence spectrum of dox-loaded DONUT nanostructures incubated at room temperature and 37 °C.

For SPHERE nanostructure, as shown in **Figure 36**, the dox signal was decrease when the concentration of SPHERE was increase. When compared loading efficiency at two temperatures, as shown in **Figure 37**, the efficiency at 37 °C is slightly better than room temperature for only 3 nM SPHERE nanostructure while the efficiency at room temperature is slightly better than 37 °C for 5 nM and 7 nM SPHERE nanostructure. Besides, the efficiency for 9 nM SPHERE nanostructure is not different for both temperatures.

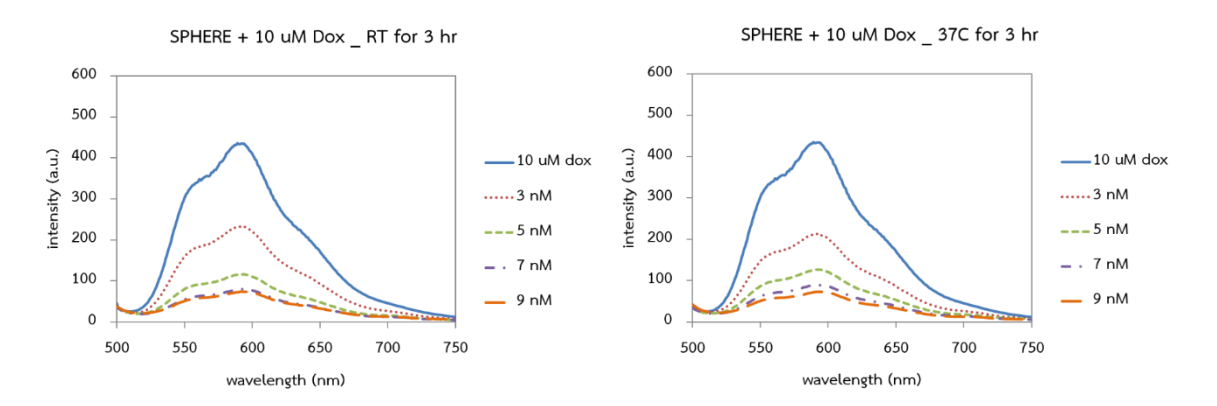
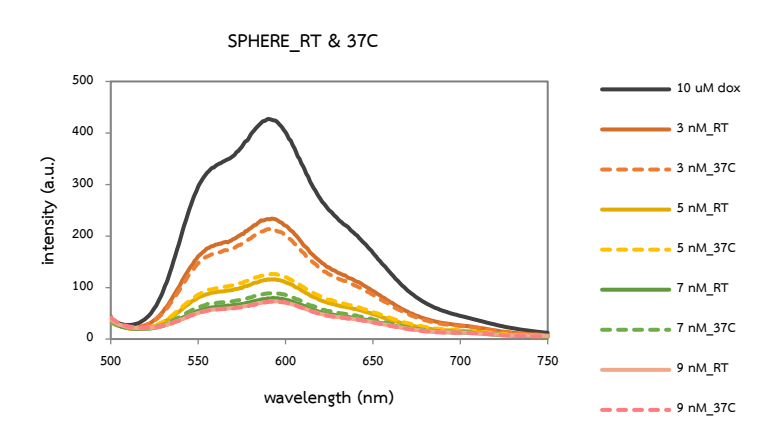


Figure 36 The fluorescence spectrum of dox-loaded SPHERE nanostructures after incubated at room temperature (left) and at 37 °C (right) for three hours.



**Figure 37** The comparison of fluorescence spectrum of dox-loaded SPHERE nanostructures incubated at room temperature and 37 °C.

The dox-loading capacities of DNA origami nanostructures in three different shapes were compared. As shown in **Figure 38-41**, these results demonstrated that SPHERE has the highest Dox-loading capacity while DISC has the lowest Dox-loading capacity. This might be the case that the more base pairings, the more Dox could be loaded in since SPHERE contains the highest amount of base pairings, which are 6,614 base pairs, whereas DONUT and DISC contain only 4,785 and 3,600 base pairs, respectively.

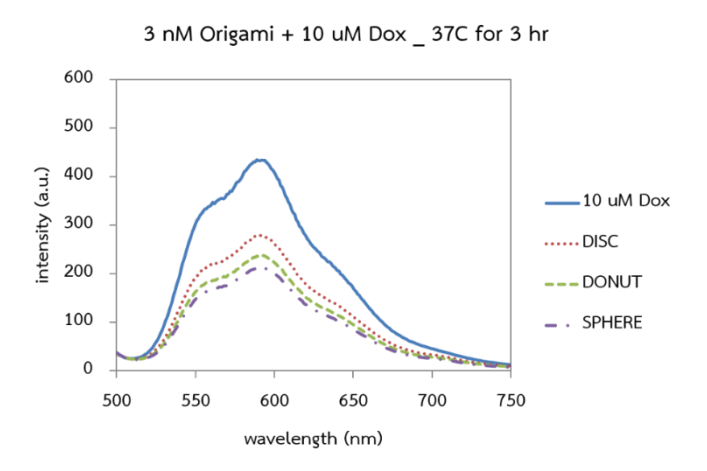


Figure 38 DNA origami nanostructures at 3 nM incubated with 10 μM dox at 37 °C.

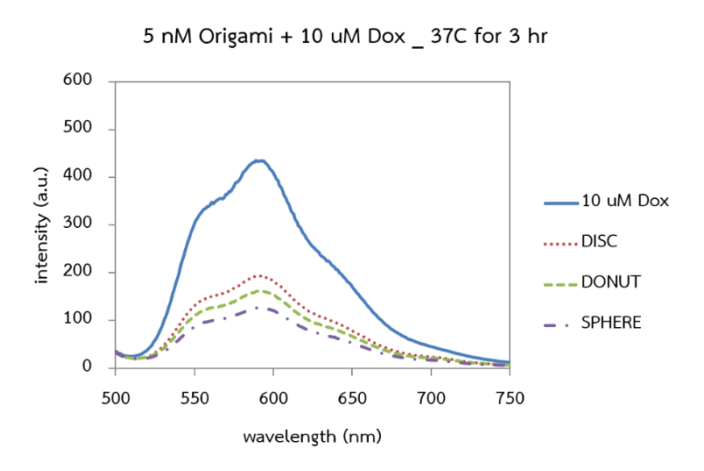


Figure 39 DNA origami nanostructures at 5 nM incubated with 10  $\mu$ M dox at 37 °C.

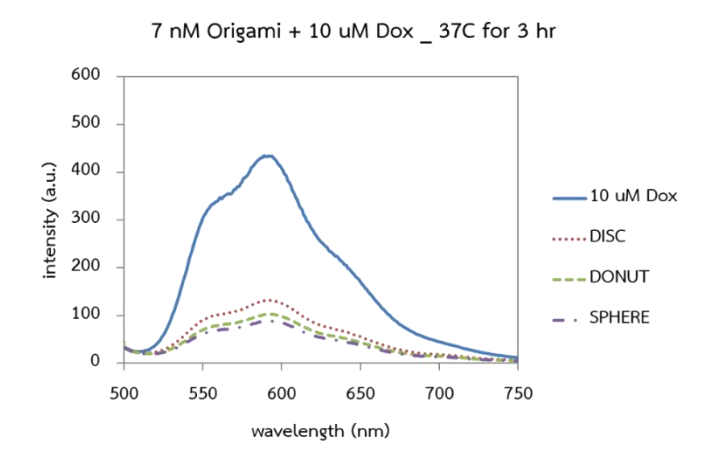


Figure 40 DNA origami nanostructures at 7 nM incubated with 10 µM dox at 37 °C.

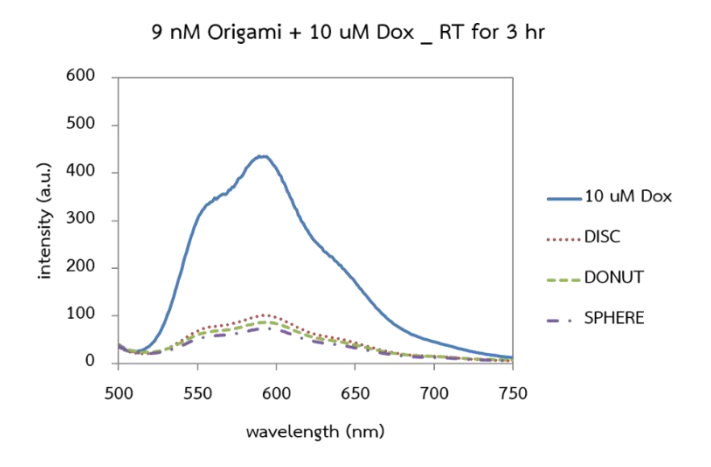


Figure 41 DNA origami nanostructures at 9 nM incubated with 10 μM dox at 37 °C.

In addition, the absorption spectrophotometry was also used for the drug-loading efficiency determination in PBS buffer and TAE/Mg<sup>2+</sup> buffer. For all DNA origami nanostructures, the loading efficiency in TAE/Mg<sup>2+</sup> buffer is higher than in PBS buffer as shown in **Figure 42-44**.

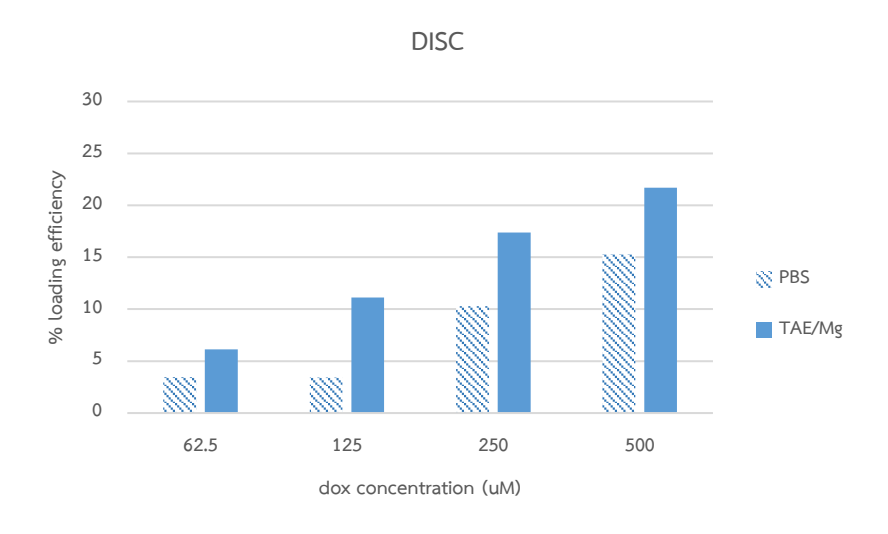


Figure 42 The dox-loading efficiency of DISC nanostructures.

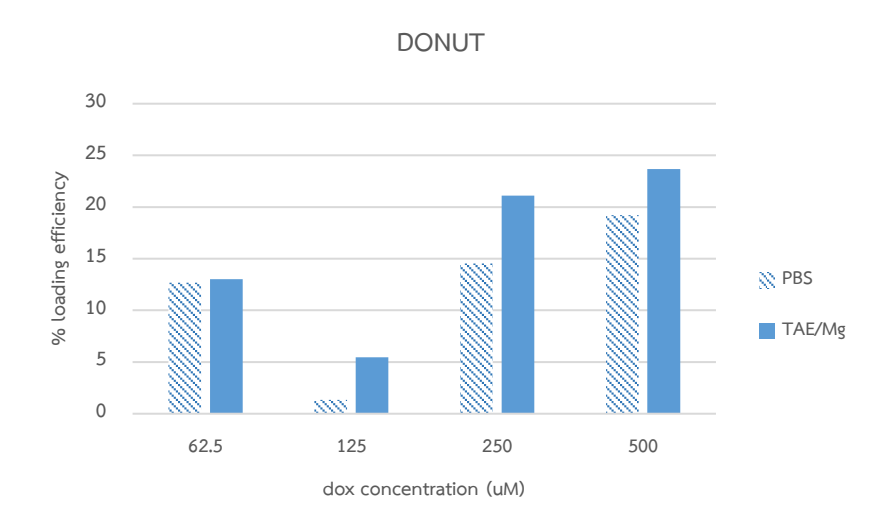


Figure 43 The dox-loading efficiency of DONUT nanostructures.

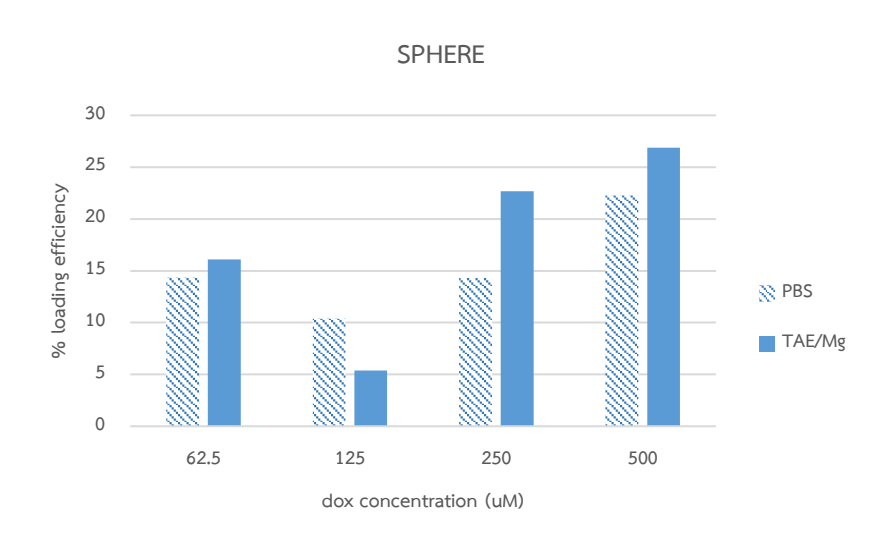


Figure 44 The dox-loading efficiency of SPHERE nanostructures.

The results showed that the loading efficiency of each DNA origami nanostructure increase with the increase of dox concentrations. DISC nanostructure has the loading efficiency around 7.48 $\pm$ 1.73%, 12 $\pm$ 1.89%, 16.69 $\pm$ 2.20%, and 19.83 $\pm$ 1.47% when incubated with 62.5  $\mu$ M, 125  $\mu$ M, 250  $\mu$ M, and 500  $\mu$ M of dox concentrations, respectively. DONUT nanostructure has the loading efficiency around 13.54 $\pm$ 1.28%, 9.23 $\pm$ 5.0%, 21.76 $\pm$ 0.69%, and 21.73 $\pm$ 2.42% when incubated with 62.5  $\mu$ M, 125  $\mu$ M, 250  $\mu$ M, and 500  $\mu$ M of dox concentrations, respectively. SPHERE nanostructure has the loading efficiency around 13.79 $\pm$ 1.57%, 9.57 $\pm$ 3.0%, 21.97 $\pm$ 2.75%, and 25.37 $\pm$ 1.98% when incubated with 62.5  $\mu$ M, 125  $\mu$ M, 250  $\mu$ M, and 500  $\mu$ M

of dox concentrations, respectively. Among these three DNA origami nanostructures, SPHERE exhibits the highest loading capacity and DISC exhibits the lowest loading capacity when compared at the same concentration of dox as shown in **Figure 45**.

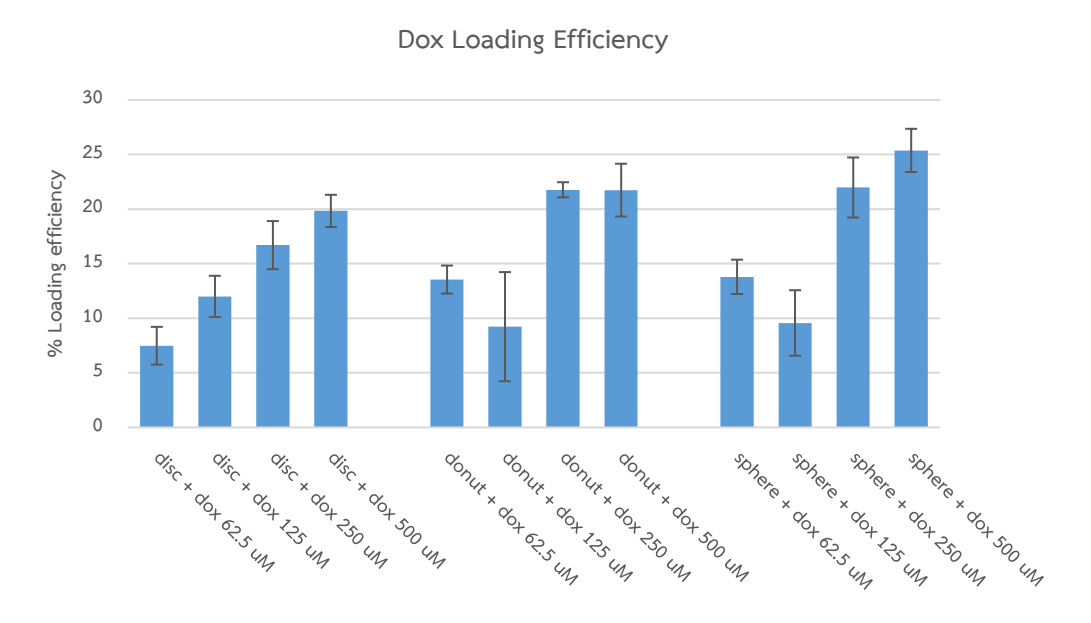


Figure 45 The dox loading efficiency of DNA origami nanostructures.

### 4. Analysis of drug release rate of DNA origami nanostructures

To determine the drug release rate of each DNA origami nanostructure, dox was loaded into DNA nanostructures and the excess dox was removed using centrifugation method. Then the pellets of dox-loaded DNA origami nanostructures were re-suspended in TAE/Mg<sup>2+</sup> buffer and absorbance at 480 nm was measured as the amount of dox in the DNA nanostructures at 0 min. After kept in dark at 37 °C for 15 and 60 minutes, the released dox was removed using centrifugation method. Then the pellet was re-suspended in TAE/Mg<sup>2+</sup> buffer and absorbance at 480 nm was measured as the amount of dox in the DNA nanostructures at 15 and 60 minutes. The rate of drug release was calculated. The results showed that dox was burst out from the origami nanostructures at the very beginning for all shapes as shown in **Figure 46-48**. At 15 minutes, dox was released around 30%, 27%, and 35% for DISC, DONUT, and SPHERE, respective.

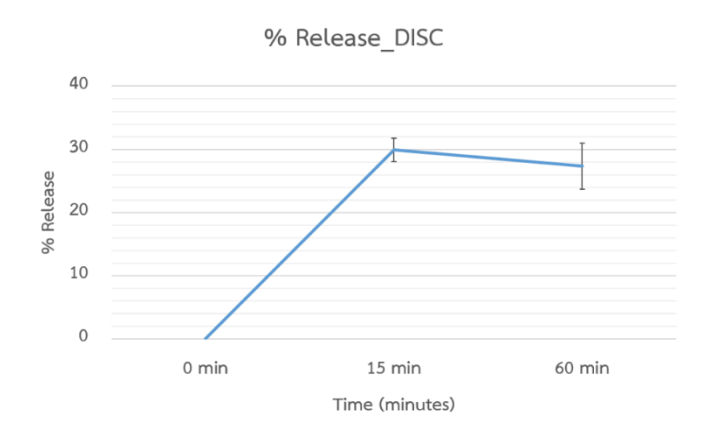


Figure 46 The release rate of dox from DISC nanostructures.

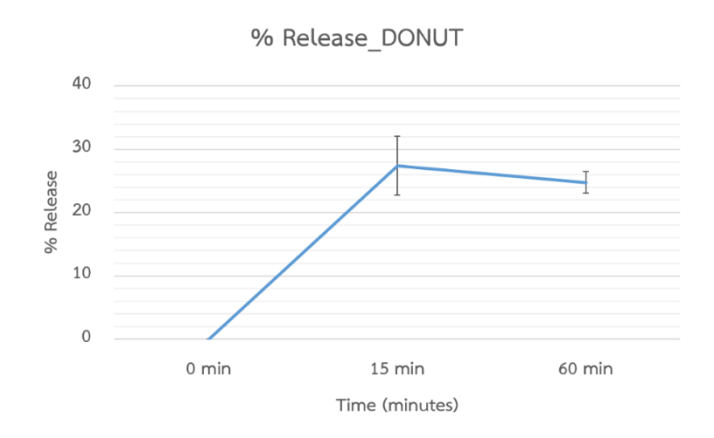


Figure 47 The release rate of dox from DONUT nanostructures.

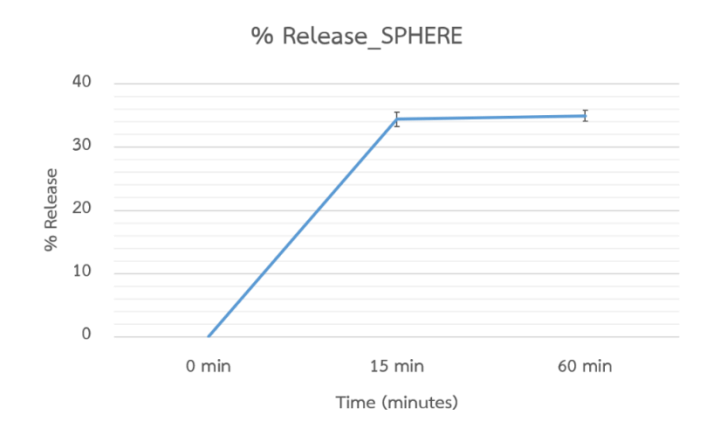


Figure 48 The release rate of dox from SPHERE nanostructures.

From the results above, dox could be released from SPHERE faster than DISC and DONUT while dox could be released from DISC faster than DONUT. Among these three DNA origami

nanostructures, SPHERE exhibits the fastest rate while DONUT exhibit the slowest rate as shown in Figure 49.

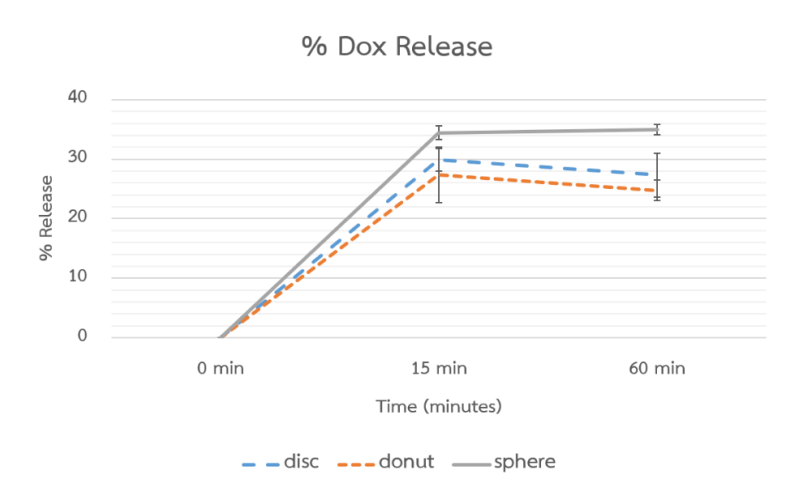


Figure 49 The comparison of the drug release rate of three DNA nanostructures.

## 5. Determination of cytotoxicity of DNA origami nanostructures

The cytotoxicity of DNA origami nanostructures was examined for all different shapes using MTT assay. Each DNA nanostructure was annealed separately and then incubated with MCF-7 and MDA-MB-231 cells. After cultured for 48 hours, the cell viability was determined using MTT assay. The results showed that empty DNA origami nanostructures in all shapes exhibited no toxicity to both cells as shown in **Figure 49**.

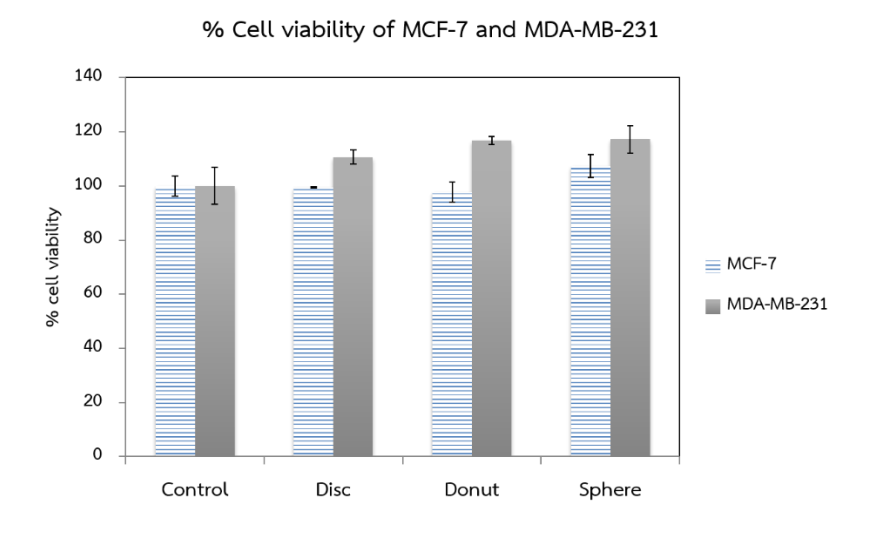


Figure 49 The cytotoxicity of DNA origami nanostructures against MCF-7 and MDA-MB-231 cells.

### 6. Investigation of cellular internalization of DNA origami nanostructures

The cellular internalization of each DNA origami nanostructure was examined by using Dox-loaded DNA origami nanostructures at 1 nM concentration. After an annealing step, each DNA nanostructure was loaded with Dox before incubated with both cells for an hour. The cells were washed with PBS buffer before measurement of Dox signal inside cells. The fluorescent images of MCF-7 cells after incubated with Dox-loaded DNA nanostructures were shown in **Figure 50**. The results indicated that DONUT exhibited the highest cellular internalization while DISC exhibited the lowest cellular internalization against MCF-7 cells.

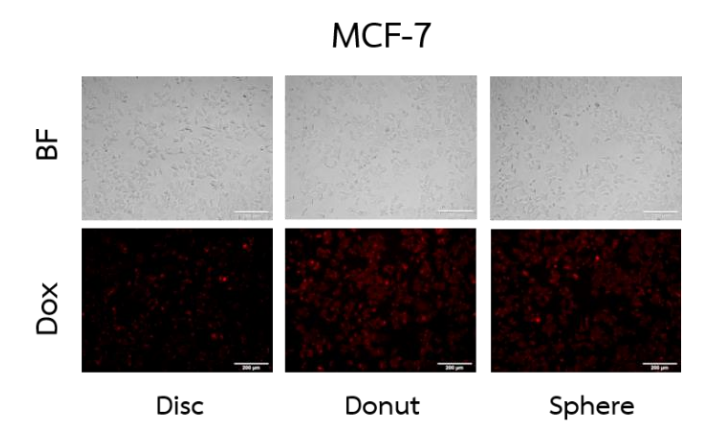


Figure 50 The cellular internalization of Dox-loaded DNA nanostructures into MCF-7 cells.

The fluorescent images of MDA-MB-231 cells after incubated with Dox-loaded DNA nanostructures were shown in **Figure 51**. The results indicated that all shapes of DNA origami nanostructures exhibited similar cellular internalization against MDA-MB-231 cells.

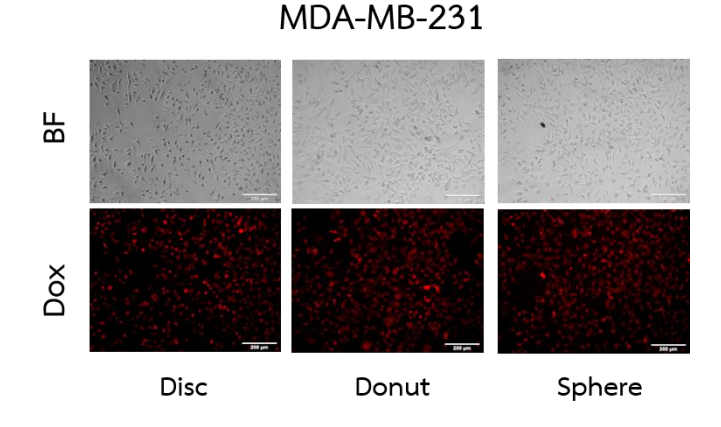


Figure 51 The cellular internalization of Dox-loaded DNA nanostructures into MDA-MB-231 cells.

In addition, free dox at 10  $\mu$ M concentration was incubated with both cells for cellular internalization determination. As shown in **Figure 52**, without DNA origami nanostructures as nanocarriers, only a small amount Dox could be internalized into both cells.

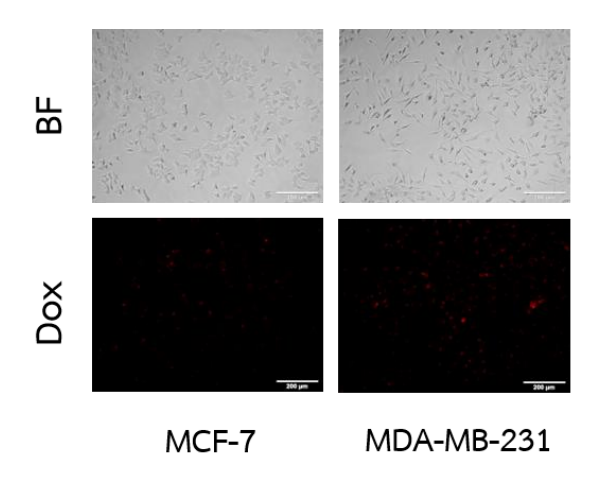


Figure 52 The cellular internalization of free Dox into MCF-7 and MDA-MB-231 cells.

## 7. Investigation of selectivity of aptamer-modified DNA origami nanostructures

To enhance the specificity of the DNA nanocarriers, MUC1 aptamer was chosen for DNA origami nanostructure modification. MUC1 aptamer can specifically bind to Mucin-1 proteins which overexpressed in MCF-7 cells but not in MDA-MB-231 cells. The expression of Mucin-1 proteins in both cells was confirmed using Western blot analysis and immunofluorescence staining. As shown in **Figure 53**, the result from Western blot indicated that Mucin-1 proteins were overexpressed only in MCF-7 cells.



Figure 53 The Mucin-1 protein expression using Western blot analysis.

The immunofluorescence staining experiment also showed that Mucin-1 proteins were obviously overexpressed only in MCF-7 cells not MDA-MB-231 cells as shown in **Figure 54**.

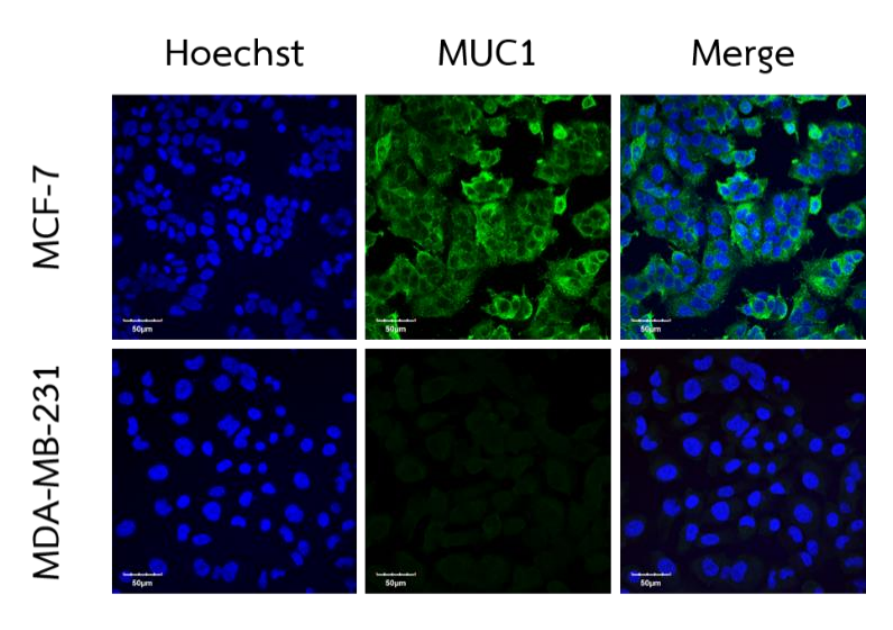
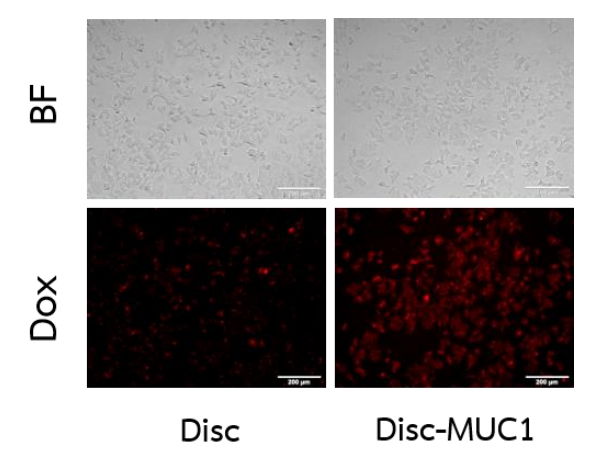


Figure 54 The Mucin-1 protein expression using Immunofluorescence staining.

In addition, the cellular internalization of Dox-loaded DNA origami nanostructures with and without MUC1 aptamer modification against MCF-7 and MDA-MB-231 cells was examined. As shown in **Figure 55**, Dox-loaded, MUC1 aptamer-modified DISC nanostructures can internalized into MCF-7 cells significantly higher than Dox-loaded DISC nanostructures.



**Figure 55** The internalization of Dox-loaded DISC and Dox-loaded, MUC1-modified DISC into MCF-7 cells.

However, as shown in **Figure 56**, Dox-loaded, MUC1 aptamer-modified DONUT nanostructures can internalized into MCF-7 cells slightly higher than Dox-loaded DONUT nanostructures.

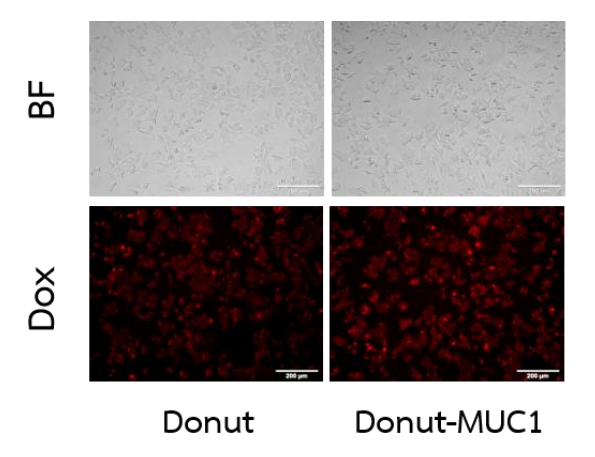
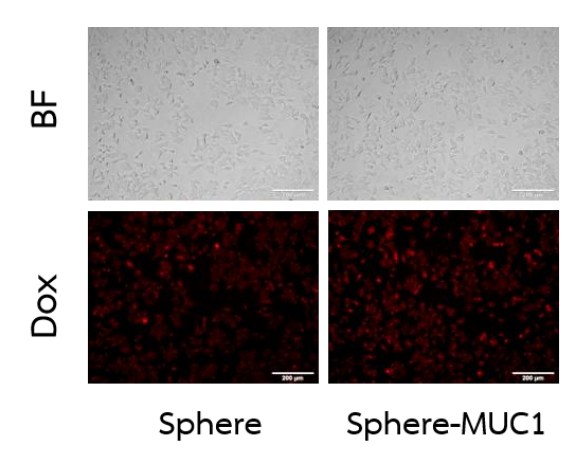


Figure 56 The internalization of Dox-loaded DONUT and Dox-loaded, MUC1-modified DONUT into MCF-7 cells.

Also, as shown in **Figure 57**, Dox-loaded, MUC1 aptamer-modified SPHERE nanostructures can internalized into MCF-7 cells slightly higher than Dox-loaded SPHERE nanostructures.



**Figure 57** The internalization of Dox-loaded SPHERE and Dox-loaded, MUC1-modified SPHERE into MCF-7 cells.

In contrast to MCF-7, Dox-loaded DISC nanostructures can be internalized into MDA-MB-231 cells similar to Dox-loaded, MUC1 aptamer-modified DISC nanostructures as shown in **Figure 58**.

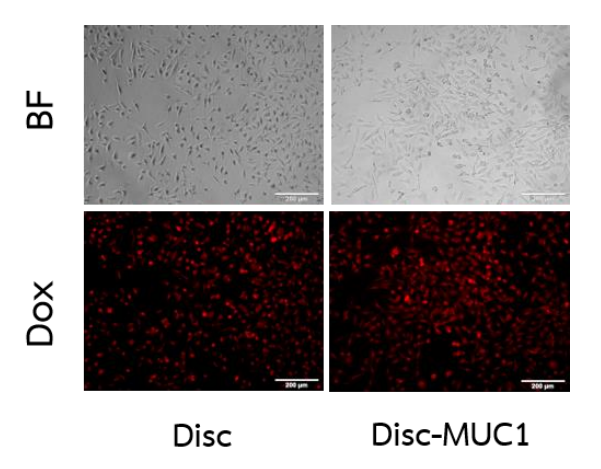


Figure 58 The internalization of Dox-loaded DISC and Dox-loaded, MUC1-modified DISC into MDA-MB-231 cells.

Similar to DISC nanostructures, **Figure 59** showed that Dox-loaded DONUT nanostructures with and without MUC1 aptamer modification can be internalized into MDA-MB-231 cells with no differences.

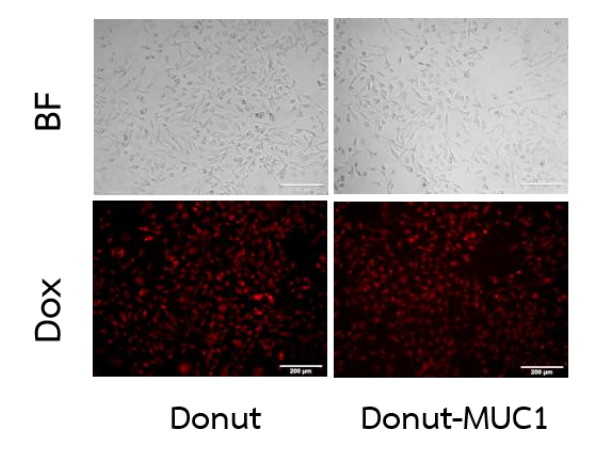
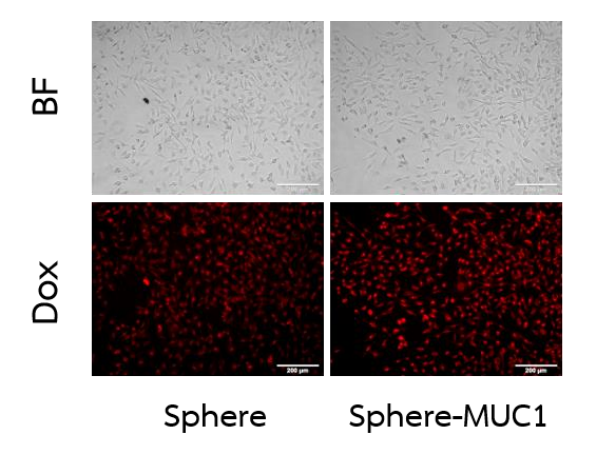


Figure 59 The internalization of Dox-loaded DONUT and Dox-loaded MUC1-modified DONUT into MDA-MB-231 cells.

Also, not much differences can be detected for the internalization of Dox-loaded SPHERE nanostructures with and without MUC1 aptamer modification into MDA-MB-231 cells as shown in **Figure 60**.



**Figure 60** The internalization of Dox-loaded SPHERE and Dox-loaded, MUC1-modified SPHERE into MDA-MB-231 cells.

### 8. Examination of anti-cancer activity of drug-containing DNA origami nanostructures

After cellular uptake of Dox-loaded DNA origami nanostructures was determined, the anti-cancer activity of each shape of Dox-loaded DNA nanostructures was evaluated against two cancer cells, MCF-7 and MDA-MB-231 cells. Each shape of DNA origami nanostructures with and without MUC1 aptamer was annealed and loaded with Dox. Each cancer cell was cultured in DMEM overnight before treated with Dox-loaded DNA nanostructure at various concentrations (0 – 2 nM) for one hour. After washed with PBS buffer, cells were cultured for 48 hours before cell viability was examined using MTT assay. For DISC nanostructures, the results showed that MDA-MB-231 cells have similar cell viability when treated with both Dox-loaded DISC nanostructures and Dox-loaded, MUC1 aptamer-modified DISC nanostructures as shown in Figure 61. However, MCF-7 cells treated with Dox-loaded, MUC1 aptamer-modified DISC nanostructures exhibit significantly lower cell viability compared to MCF-7 cells treated with Dox-loaded DISC nanostructures.

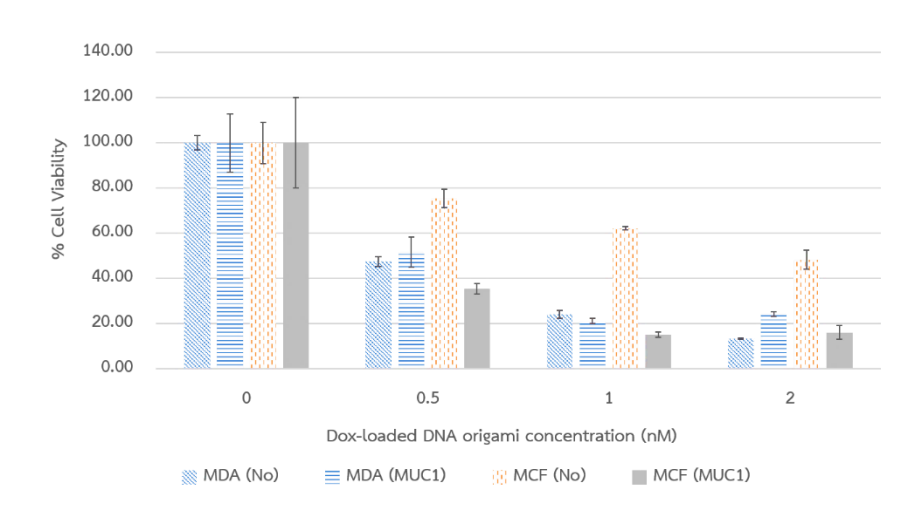


**Figure 61** The cell viability of MCF-7 and MDA-MB-231 cells after treated with Dox-loaded DISC nanostructures with and without MUC1 modification.

For DONUT nanostructures, the results showed that not much differences in cell viability among those MCF-7 and MDA-MB-231 cells treated with Dox-loaded DONUT nanostructures neither with nor without MUC-1 aptamer modification shown in **Figure 62**. However, higher concentrations of Dox-loaded DONUT nanostructures leading to lower cell viability of both MCF-7 and MDA-MB-231 cells.

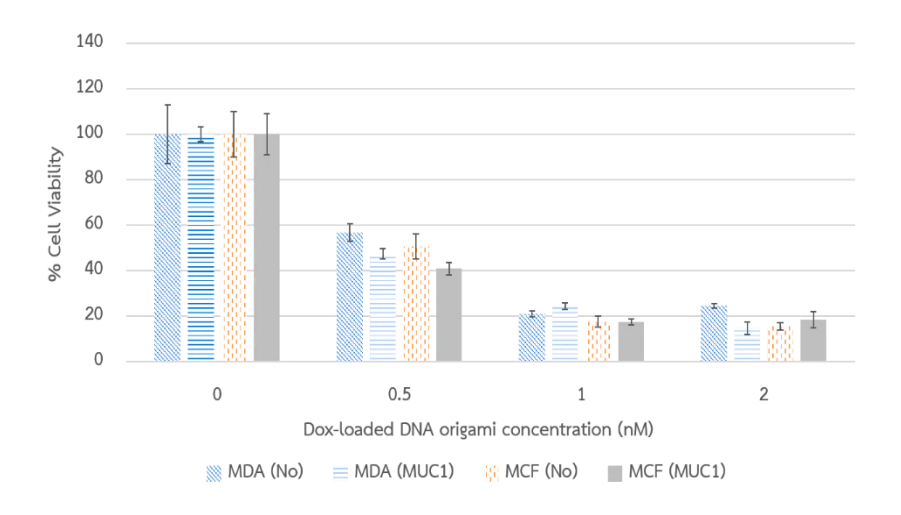


**Figure 62** The cell viability of MCF-7 and MDA-MB-231 cells after treated with Dox-loaded DONUT nanostructures with and without MUC1 modification.

For SPHERE nanostructures, the results showed that MDA-MB-231 cells have lower cell viability when treated with both Dox-loaded SPHERE nanostructures and Dox-loaded, MUC1 aptamer-

modified SPHERE nanostructures compared to MCF-7 cells as shown in **Figure 63**. However, for both MCF-7 and MDA-MB-231 cells, the ones treated with Dox-loaded, MUC1 aptamer-modified SPHERE nanostructures exhibit lower cell viability compared to the ones treated with Dox-loaded SPHERE nanostructures.

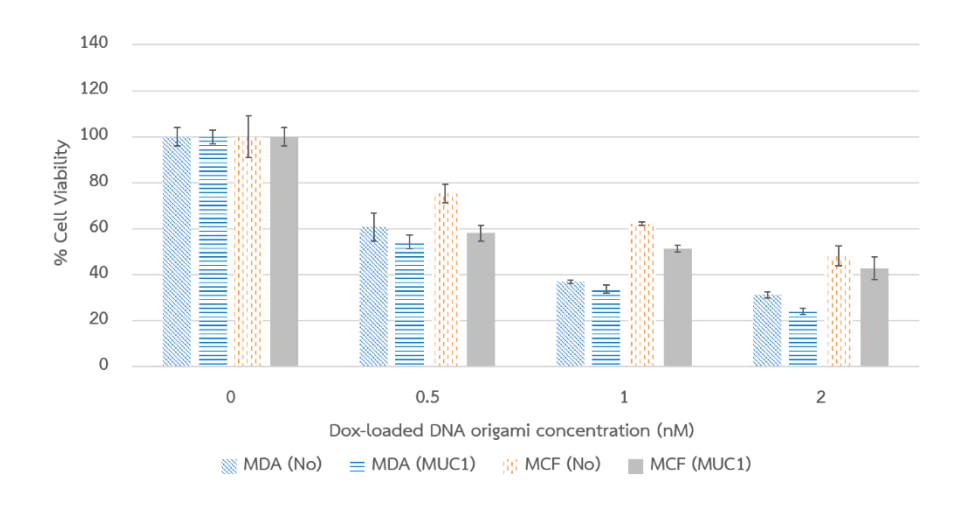
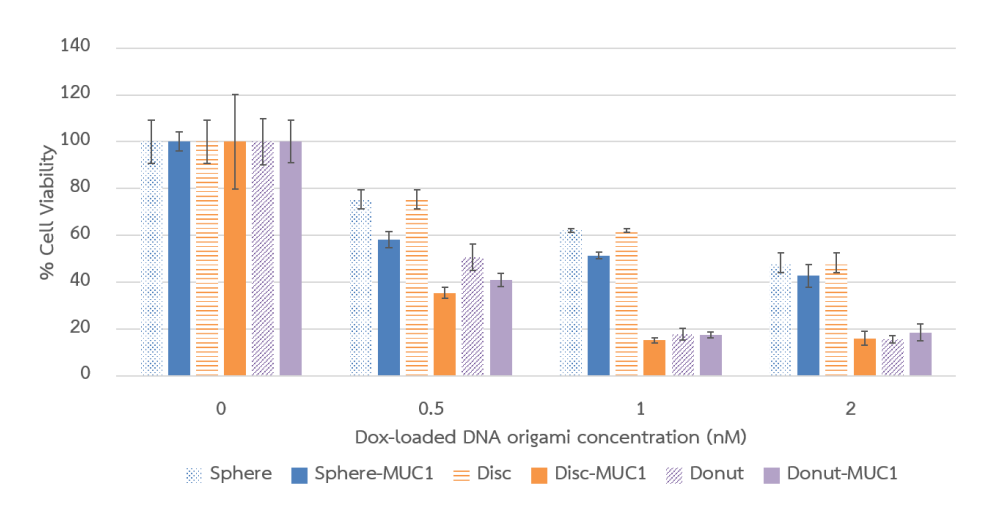


Figure 63 The cell viability of MCF-7 and MDA-MB-231 cells after treated with Dox-loaded SPHERE nanostructures with and without MUC1 modification.

To compare the anti-cancer efficiency of these three DNA nanostructures, the cell viability of MCF-7 cells, MUC-1 positive cells, after treated with each DNA nanostructure at 1 nM was compared as shown in **Figure 64**. The results obviously showed that the cell viability is subsequently lower when the concentration of Dox-loaded DNA nanostructures is higher. At 0.5 nM concentration, only DISC and DONUT nanostructures with MUC-1 aptamer modification can reduce the cell viability of MCF-7 cells to less than 50%. However, DONUT nanostructure without MUC-1 aptamer modification can reduce the cell viability similar to those DISC and DONUT nanostructures with MUC-1 aptamer modification at 1 nM and 2 nM concentrations. Also, these two concentrations exhibited similar anti-cancer efficiency. Anyway, for MCF-7 cells, MUC-1 aptamer modified DISC nanostructure showed the highest anti-cancer efficiency while SPHERE nanostructure without MUC-1 aptamer modification showed the lowest anti-cancer efficiency.



**Figure 64** The anti-cancer efficiency of Dox-loaded DNA origami nanostructures with and without MUC-1 aptamer modification on MCF-7 cells.

To compare the anti-cancer efficiency of these three DNA nanostructures, the cell viability of MDA-MB-231 cells, MUC-1 negative cells, after treated with each DNA nanostructure was compared as shown in **Figure 65**. The results obviously showed that the cell viability is subsequently lower when the concentration of Dox-loaded DNA nanostructures is higher. However, at each concentration of Dox-loaded DNA origami nanostructures even with or without MUC-1 aptamer modification, the cell viability of MDA-MB-231 cells is quite similar for all shapes of DNA origami nanostructures. The cell viability was reduced to less than 50% when treated with Dox-loaded DNA origami nanostructures at 1 nM or 2 nM. Anyway, for MDA-MB-231 cells, DISC nanostructure without MUC-1 aptamer modification showed the highest anti-cancer efficiency while SPHERE nanostructure without MUC-1 aptamer modification showed the lowest anti-cancer efficiency at 2 nM concentration.

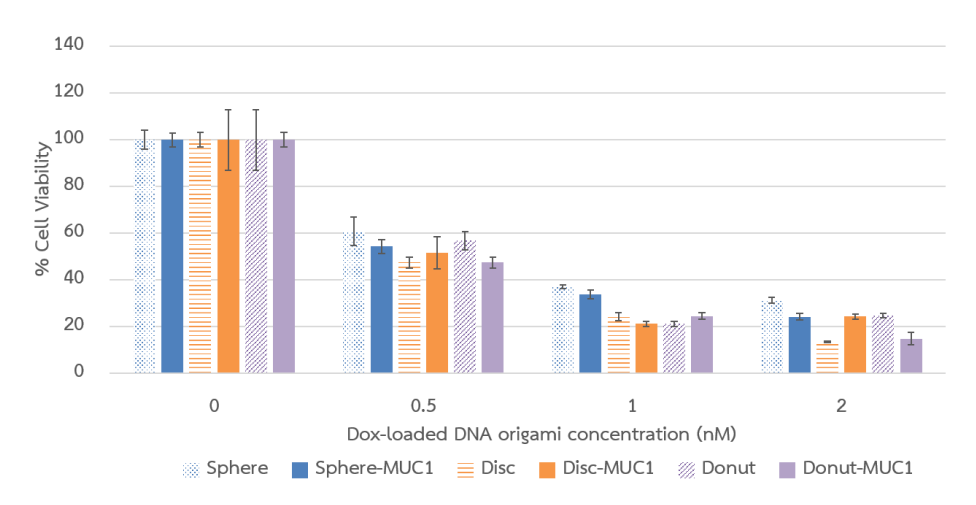


**Figure 65** The anti-cancer efficiency of Dox-loaded DNA origami nanostructures with and without MUC-1 aptamer modification on MDA-MB-231 cells.

#### Discussion and Conclusion

Nanomedicine could enhance the efficiency of conventional chemotherapeutic agents for cancer treatment by using a targeted drug delivery system which a nanocarrier will specifically deliver drugs to target cancer cells. Appropriate properties of nanocarriers such as optimal stability, low cytotoxicity, high drug loading and releasing capability along with enhanced cellular internalization could lead to high efficiency in cancer therapy. Due to its biological and physical advantages, DNA has been utilized as nanomaterials for nanostructure construction. Many DNA origami nanostructures in different sizes and shapes have been published, for example, a nanobox (Andersen et al., 2009), a nanotube (Douglas, Chou, and Shih, 2007), an ellipsoid and a nanoflask (Han et al., 2011). Several studies have investigated the possibilities of using DNA origami nanostructures as drug carriers both in vitro and in vivo and also demonstrated that some properties of nanocarriers are also depend on the structural design. Schuller et al. reported that the efficiency of immune-activating does not depend on the structural 3D shape but the efficiency mainly depends on the compactness, size and stability of the nanocarriers (Schuller et al., 2011). In 2012, Jiang et al. demonstrated that 2D triangular and 3D tubular DNA origami nanostructures could enhance anti-cancer activity of doxorubicin in doxorubicin-resistant MCF-7 cells (Jiang et al., 2012). They also found that the anti-cancer efficiency depends on the length of incubation time and drug concentration.

Although DNA origami nanostructures in various shapes were examined as drug carriers in a biological system, essential criteria for a structural design as drug nano-carriers have not been elucidated yet. Therefore, this study has been investigated the effects of 2D and 3D DNA origami nanostructures on being used as nanocarriers in biological conditions. The effects of 2D and 3D DNA origami nanostructures on functional properties as nanocarriers in a drug delivery system such as stability, cytotoxicity, cellular uptake, drug loading and release capability, cellular internalization, and anti-cancer efficiency have been examined. Disc-like shaped (DISC), donut-like shaped (DONUT), and sphere-like shaped (SPHERE) DNA origami nanostructures were used as representatives for two-dimensional (2D) and three-dimensional (3D) nanostructures. These three nanostructures are similar in term of shape (circular) but they are different in term of dimension. In addition, the specificity of the nanocarriers with and without aptamer modification was compared.

After the designing and annealing steps, these three DNA origami nanostructures, DISC, DONUT, and SPHERE, were characterized via agarose gel electrophoresis, NanoSight, AFM, and TEM. The results demonstrated that they could form as designed with the expected size. Then, the stability of DNA origami nanostructures was examined in various conditions. In the annealing buffer, all three DNA origami nanostructures exhibited relatively the same stability either at room temperature or 37 °C. However, when incubated in the complete media, these three DNA origami nanostructures exhibited different stability either at room temperature or at 37 °C. The results above showed that SPHERE exhibited the highest stability while DISC exhibited the lowest stability in DMEM at both temperatures investigated.

As the fluorescent intensity of Dox will be decrease after intercalating into DNA helices, the intensity of Dox was measured after incubating with each DNA origami nanostructure. The results showed that, with fluorescence experiment, SPHERE has the highest Dox-loading capacity while DISC has the lowest Dox-loading capacity. To calculate the loading capacity of each DNA origami nanostructure, the absorption spectrophotometry was utilized for Dox concentration measurement after excess Dox was removed by centrifugation after incubated DNA nanostructures with Dox at different concentrations. The results showed that the loading efficiency of each DNA origami nanostructure increase with the increase of dox concentrations. At 250  $\mu$ M Dox, DISC nanostructure has the loading efficiency around 16.69±2.20%, DONUT

nanostructure has the loading efficiency around 21.76±0.69%, and SPHERE nanostructure has the loading efficiency around 21.97±2.75%. Among these three DNA origami nanostructures, SPHERE exhibits the highest loading capacity and DISC exhibits the lowest loading capacity when compared at the same concentration of dox. For releasing capacity, the results showed that dox was burst out from the origami nanostructures at the very beginning for all shapes. At 15 minutes, dox was released around 30%, 27%, and 35% for DISC, DONUT, and SPHERE, respectively. Dox could be released from SPHERE faster than DISC and DONUT while dox could be released from DISC faster than DONUT. Among these three DNA origami nanostructures, SPHERE exhibits the fastest rate while DONUT exhibit the slowest rate.

The cytotoxicity of these DNA origami nanostructures without Dox was examined before treated with cancer cells. The cell viability of MCF-7 and MDA-MB-231 cells after incubated with empty DISC, DONUT, and SPHERE was evaluated by using MTT assay. The results showed that empty DNA origami nanostructures in all shapes exhibited no toxicity to both cells. For the internalization experiment, each DNA nanostructure was loaded with Dox before incubated with both cells for an hour. Then the cells were washed with PBS buffer before measurement of Dox signal inside cells. The results indicated that DONUT exhibited the highest cellular internalization while DISC exhibited the lowest cellular internalization against MCF-7 cells whereas all shapes of DNA origami nanostructures exhibited similar cellular internalization against MDA-MB-231 cells. In addition, the internalization of free dox at 10  $\mu$ M concentration was tested against both cells. The results showed that without DNA nanocarriers, only a small amount Dox could be internalized into both cells.

To enhance the specificity of the DNA nanocarriers, MUC1 aptamer was chosen for DNA origami nanostructure modification. MUC1 aptamer can specifically bind to Mucin-1 proteins which overexpressed in MCF-7 cells but not in MDA-MB-231 cells. The expression of Mucin-1 proteins in both cells was confirmed using Western blot analysis and immunofluorescence staining. The results showed that the expression of Mucin-1 proteins was obviously different in those two cancer cells. Then, the cellular internalization of Dox-loaded DNA origami nanostructures with and without MUC1 aptamer modification against MCF-7 and MDA-MB-231 cells was examined. For MCF-7 cells, the results showed that with MUC-1 aptamer modification, DISC nanostructures can be internalized into MCF-7 cells significantly

higher than the ones without aptamer modification while DONUT and SPHERE nanostructures showed slightly different internalization efficiency between the nano-carriers with and without aptamer modification. For MDA-MB-231 cells, not much differences in cellular internalization efficiency can be detected between the nano-carriers with and without MUC-1 aptamer modification of DNA nanostructures in three different shapes.

After cellular uptake of Dox-loaded DNA origami nanostructures was determined, the anti-cancer activity of each shape of Dox-loaded DNA nanostructures against two cancer cells, MCF-7 and MDA-MB-231 cells, was investigated. The cell viability was determined using MTT assay after treated with Dox-loaded DNA origami nanostructures with and without MUC-1 aptamer modification. For all tested groups, the higher concentrations of Dox-loaded DNA nanostructures, the lower cell viability of both MCF-7 and MDA-MB-231 cells. For DISC nanostructures, MCF-7 cells treated with Dox-loaded, MUC1 aptamer-modified DISC nanostructures exhibit significantly lower cell viability compared to MCF-7 cells treated with Dox-loaded DISC nanostructures while MDA-MB-231 cells have similar cell viability when treated with both Dox-loaded DISC nanostructures and Dox-loaded, MUC1 aptamer-modified DISC nanostructures. For DONUT nanostructures, the results showed that not much differences in cell viability among those MCF-7 and MDA-MB-231 cells treated with Dox-loaded DONUT nanostructures neither with nor without MUC-1 aptamer modification. For SPHERE nanostructures, MDA-MB-231 cells have lower cell viability than MCF-7 cells after treated with both Dox-loaded SPHERE nanostructures and Dox-loaded, MUC1 aptamer-modified SPHERE nanostructures. In addition, the results obviously showed that the cell viability is subsequently lower when the concentration of Dox-loaded DNA nanostructures is higher in both cancer cells. For MCF-7 cells, at 0.5 nM concentration, only DISC and DONUT nanostructures with MUC-1 aptamer modification can reduce the cell viability to less than 50%. However, DONUT nanostructure without MUC-1 aptamer modification can reduce the cell viability similar to those DISC and DONUT nanostructures with MUC-1 aptamer modification at 1 nM and 2 nM concentrations. Anyway, for MCF-7 cells, MUC-1 aptamer modified DISC nanostructure showed the highest anti-cancer efficiency while SPHERE nanostructure without MUC-1 aptamer modification showed the lowest anti-cancer efficiency. However, for MDA-MB-231 cells, at each concentration of Dox-loaded DNA origami nanostructures even with or without MUC-1

aptamer modification, the cell viability is quite similar for all shapes of DNA origami nanostructures. The cell viability was reduced to less than 50% when treated with Dox-loaded DNA origami nanostructures at 1 nM or 2 nM. Anyway, for MDA-MB-231 cells, DISC nanostructure without MUC-1 aptamer modification showed the highest anti-cancer efficiency while SPHERE nanostructure without MUC-1 aptamer modification showed the lowest anti-cancer efficiency at 2 nM concentration.

In conclusion, DISC, DONUT, and SPHERE nanostructures were used as representatives for DNA origami nanostructures with similar shape but different dimensions. Results above showed that different shapes and dimensions of DNA origami have some effects on functional properties as nanocarriers in drug delivery systems. Although SPHERE nanostructures exhibit the highest stability in cell culture media, SPHERE nanostructures showed the lowest anticancer efficiency. DONUT nanostructures have the highest Dox-loading capacity but DISC nanostructures exhibit the highest cellular internalization and anti-cancer efficiency. The knowledge gained from these experiments could be useful information for designing efficient DNA nanocarriers in drug delivery system.

#### Suggestions for further study

In this study, some functional properties as nanocarriers in the drug delivery systems of DNA origami nanostructures such as stability, drug-loading and release capacity, cellular internalization, anti-cancer efficiency and specificity after aptamer modification were investigated. However, the bioavailability and biodegradability *in vivo* should be examined.

#### References:

Andersen ES, Dong M, Nielsen MM, Jahn K, Subramani R, Mamdouh W, Golas MM, Sander B, Stark H, Oliveira CLP, Pederson JS, Birkedal V, Besenbacher F, Gothelf KV & Kjems J. (2009) Self-assembly of a nanoscale DNA box with a controllable lid. *Nature*. 459, 73–76.

Bhatia D, Surana S, Chakraborty S, Koushika SP & Krishnan Y. (2011) A synthetic icosahedral DNA-based host-cargo complex for functional in vivo imaging. *Nat. Commun.* 2, 339.

- Chaithongyot S, Chomanee N, Charngkaew K, Udomprasert A & Kangsamaksin T. (2016) DNA nanosphere as a drug delivery system for cancer cells. In *Proceedings of the 5<sup>th</sup> International Biochemistry and Molecular Biology Conference 2016.* (pp. 247-250). Songkhla: Prince of Songkla University.
- Chaithongyot, S, Chomanee, N, Charngkaew, K, Udomprasert, A & Kangsamaksin, T. (2018)

  Aptamer-functionalized DNA nanosphere as a stimuli-responsive nanocarrier. *Materials*Letters 214, 72-75.
- Chen J & Seeman NC. (1991) Synthesis from DNA of a molecule with the connectivity of a cube. *Nature*. 350, 631-633.
- Chen G, Ushida T & Tateishi T. (2000) Hybrid biomaterials for tissue engineering: a preparative method for PLA or PLGA-collagen hybrid sponges. *Adv. Mater.*, 12: 455-457.
- Chomoucka J, Drbohlavova J, Huska D, Adam V, Kizek R & Hubalek J. (2010) Magnetic nanoparticles and targeted drug delivery. *Pharmacol. Res.* 62, 144-149.
- Douglas SM, Chou JJ & Shih WM. (2007) DNA-nanotube-induced alignment of membrane proteins for NMR structure determination. *PNAS*. 104, 6644-6648.
- Endo M, Miyazaki R, Emura T, Hidaka K, & Sugiyama H. (2012) Transcription regulation system mediated by mechanical operation of a DNA nanostructure. *JACS* 134, 2852-2855.
- Erben CM, Goodman RP & Turberfield AJ. (2006) Single-molecule protein encapsulation in a rigid DNA cage. *Angew. Chem.* 118, 7574-7577.
- Fu J, Liu M, Liu Y, Woodbury NW & Yan H. (2012) Interenzyme substrate diffusion for an enzyme cascade organized on spatially addressable DNA nanostructures. *JACS*. 134, 5516-5519.
- Goodman RP, Berry RM, & Turberfield AJ. (2004) The single-step synthesis of a DNA tetrahedron. *Chem. Commun.* 21, 1372-1373.
- Gu H, Chao J, Xiao SJ & Seeman NC. (2010) A proximity-based programmable DNA nanoscale assembly line. *Nature*. 465, 202-205.
- Hahn J, Wickham SFJ, Shih WM & Perrault SD. (2014) Addressing the instability of DNA nanostructures in tissue culture. *ACS Nano*. 8, 8765-8775.

- Halley PD, Lucas CR, McWilliams EM, Webber MJ, Patton RA, Kural C, Lucas DM, Byrd JC & Castro CE. (2016) Daunorubicin-loaded DNA origami nanostructures circumvent drugresistance mechanisms in a Leukemia model. *Small*. 12, 308-320.
- Han D, Pal S, Nangreave J, Deng Z, Liu Y & Yan H. (2011) DNA Origami with Complex Curvatures in Three-Dimensional Space. *Science*. 332, 342-346.
- Jiang Q, Song C, Nangreave J, Liu X, Lin L, Qiu D, Wang ZG, Zou G, Liang X, Yan H & Ding B. (2012) DNA origami as a carrier for circumvention of drug resistance. *JACS*. 134, 13396-13403.
- Jiang Q, Shi Y, Zhang Q, Li N, Zhan P, Song L, Dai L, Tian J, Du Y, Cheng Z & Ding B. (2015) A self-assembled DNA origami-gold nanorod complex for cancer theranostics. *Small*. 11, 5134-5141.
- Kim KR, Kim DR, Lee T, Yhee JY, Kim BS, Kwon IC & Ahn DR. (2013) Drug delivery by a self-assembled DNA tetrahedron for overcoming drug resistance in breast cancer cells. *Chem. Commun.* 49, 2010-2012.
- Ko S, Liu H, Chen Y & Mao C. (2008) DNA nanotubes as combinatorial vehicles for cellular deliver. *Biomacromolecules*. 9, 3039-3043.
- Lee H, Lytton-Jean AKR, Chen Y, Love KT, Park AI, Karagiannis ED, Sehgal A, Querbes W, Zurenko CS, Jayaraman M, Peng CG, Charisse K, Borodovsky A, Manoharan M, Donahoe JS, Truelove J, Nahrendorf M, Langer R & Andersen DG. (2012) Molecularly self-assembled nucleic acid nanoparticles for targeted in vivo siRNA delivery. *Nat. Nanotechnol.*7, 389-393.
- Li J, Pei H, Zhu B, Liang L, Wei M, He Y, Chen N, Li D, Huang Q & Fan C. (2011) Self-assembled multivalent DNA nanostructures for noninvasive intracellular delivery of immunostimulatory CpG oligonucleotides. *ACS Nano.* 5, 8783-8789.
- Liang L, Li J, Li Q, Huang Q, Shi J, Yan H & Fan C. (2014) Single-particle tracking and modulation of cell entry pathways of a tetrahedral DNA nanostructure in live cells. *Angew. Chem.* 126, 7879-7884.

- Mei Q, Wei X, Su F, Liu Y, Youngbull C, Johnson R, Lindsay S, Yan H & Meldrum D. (2011) Stability of DNA origami nanoarrays in cell lysate. *Nano Lett*. 11, 1477-1482.
- Ouyang X, Li J, Liu H, Zhao B, Yan J, Ma Y, Xiao S, Song S, Huang Q, Chao J & Fan C. (2013)

  Rolling circle amplification-based DNA origami nanostructures for intracellular delivery of immunostimulatory drugs. *Small.* 9, 3082-3087.
- Rothemund PWK. (2006) Folding DNA to create nanoscale shapes and patterns. *Nature* 440, 279–302.
- Sanna V, Pala N & Sechi M. (2014) Targeted therapy using nanotechnology: focus on cancer. Int. J. Nanomedicine. 9, 467-483.
- Schuller VJ, Heidegger S, Sandholzer N, Nickels PC, Suhartha NA, Endres S, Bourquin C & Liedl T. (2011) Cellular immunostimulation by CpG-sequence-coated DNA origami structures. *ACS Nano*. 5, 9696-9702.
- Seeman NC. (1982) Nucleic acid junctions and lattices. J. Theor. Biol. 99, 237–247.
- Shen X, Jiang Q, Wang J, Dai L, Zou G, Wang ZG, Chen WQ, Jiang W & Ding B. (2012) Visualization of the intracellular location and stability of DNA origami with a label-free fluorescent probe. *Chem. Commun.* 48, 11301-11303.
- Stahl, E, Martin, TG, Praetorius, F & Dietz, H. (2014) Facile and scalable preparation of pure and dense DNA origami solutions. *Angew. Chem. Int. Ed.* 53, 12735-12740.
- Voigt NV, Torring T, Rotaru A, Jacobsen MF, Ravnsbaek JB, Subramani R, Mamdouh W, Kjems J, Mokhir A, Besenbacher F & Gothelf KV. (2010) Single-molecule chemical reactions on DNA origami. *Nature Nanotechnology* 5, 200–203.
- Walsh AS, Yin H, Erben CM, Wood MJA & Turberfield AJ. (2011) DNA cage delivery to mammalian cells. *ACS Nano.* 5, 5427-5432.
- Watson, J. D. & Crick, F. H. Molecular structure of nucleic acids: a structure for deoxyribose nucleic acid. *Nature* 248, 737-738 (1974).
- Zamboni WC. (2005) Liposomal, nanoparticle, and conjugated formulation of anticancer agents. *Clin. Cancer Res.*, 11: 8230-8234.

- Zhang Y & Seeman NC. (1994) Construction of a DNA-truncated octahedron. *J. Am. Chem. Soc.*, 116, 1661-1669.
- Zhang Q, Jiang Q, Li N, Dai L, Liu Q, Song L, Wang J, Li Y, Tian J, Ding B & Du Y. (2014) DNA origami as an in vivo drug delivery vehicle for cancer therapy. *ACS Nano*. 8, 6633-6643.
- Zhao YX, Shaw A, Zeng X, Benson E, Nystrom AM & Hogberg B. (2012) DNA origami delivery system for cancer therapy with tunable release properties. *ACS Nano*. 6, 8684-8691.

#### **Appendix**

### Sequence of Staple Strands

### DISC disc 1 (30) AATAGTAGCATTGCGCCTGTTTATCAA disc 2 (29) CAATAGATAAGTCCTAAAAACAGGGAAGC disc 3 (28) GCATTAGACGGGAGTAACCCTCGTTTAC disc 4 (29) CAGACGACGATAAAGGCATCAATTCTACT disc 5 (48) disc 6 (48) TAAATATTGACGTGTATCATCGCCTGATAAATTGTAGGCATAGTAAGA disc 7 (35) ACAACGGAGATTGAAATTATTCATTAAACCCTCAG disc 8 (39) AGCCACCACAAATCTCCAAAAAAAAGCGCGAAACAAGT disc 9 (44) ATTTTCATTTGGGGCGCGAGCTGAAAAGGTAACCAAAATAGCGA disc 10 (49) GAGGCTTTTGCAAATACATAACGCCAAAAGGAATTACGGTCGAAATCCG CGACCTGCTCCAGCGATTATACCAAGGCTCCAAAA disc 11 (35) disc 12 (24) GGAGCCTTTGAATTGCGAATAATA disc 13 (40) ATTTTTCACGTTGACCTCAGAGCCGCCACCGTATAAACA GTTAATGCCCCCTGCAGAACCGCCACCCTC disc 14 (30) disc 15 (34) AGAGCCACCAAAGGAACAACTAAAGAATTGTATC disc 16 (45) GGTTTATCAACTAAAACACTCATCTTTGACCCCCATGTTACTTAG disc 17 (49) CCGGAACGAGGGGAATACCACATTCAACTAATGCAGAAGAAGTTTTGCC AGAGGGGGTAATAGTCGCAAATGGTCAATAACCTGTTTAGCTAT disc 18 (44) AGTAGATTTAGTTTGACCATTAGATACATTTAAAATGTTTAGAC disc 19 (44) disc 20 (50) TGGATAGCGTCCAAAGAAAGATTCATCAGTTGAGATTTACGCAGACGGTC disc 21 (35) AATCATAAGGGAGAGGCGAAAGAATACGCTTGCTT disc 22 (36) TCGAGGTGACGGAGTGAGAATAGACCCTCATTTTCA GGGATAGCAAGCCCAGGAGGTTTAGTACCGCCA disc 23 (33) disc 24 (40) CCCTCAGAACCGCCACCCTCCTATTTCGGAACCTATTATT disc 26 (36) AGTAACAGTGCCCAGAACCACCACCAGGCCACCCTC disc 27 (45) AGAACCGCCAGGTGAATTATCACCGTCACCGACTAGGGCGACATT

disc 28 (49)	CAACCGATTGATCAGAGGGTAATTGAGCGCTAATATTAGCAGCCTTTAC
disc 29 (44)	AGAGAGAATAACATGAACAAGAAAAATAATATCCCATCCTAATT
disc 30 (44)	TACGAGCATGTAGAAACCAATCAATAATCGTTTTTTGTTTAACG
disc 31 (49)	TCAAAAATGAAAACAGAGAGATAACCCACAAGAATTGAGTTTACCAGCG
disc 32 (35)	CCAAAGACAAATGAGCCATTTGGGAAACCGCCTCC
disc 33 (48)	CTCAGAGCCAGCCGCCAGCATTGACAGGAGGTTGAGCCAGAGCCA
disc 34 (45)	CCACCGGATTAGAGCCAGCAAAATCACCAGTAGACAATCAAT
disc 35 (50)	AAATTCATATGGTTAAGCCCAATAATAAGAGCAAGATATTTATCCCAATC
disc 36 (44)	CAAATAAGAAACGAGCTGTCTTTCCTTATCATTCCAAGAACGGG
disc 37 (44)	TAAAGTACGGTGTCTGGAAGTTTCATTCCAGAATCCCCCTCAAA
disc 38 (49)	TGCTTTAAACAGTGAAAAATCTACGTTAATAAAACGAAAGGACAGTAGA
disc 39 (35)	ACGGTGTACAGATACGTAATGCCACTATACCGATA
disc 40 (48)	GTTGCGCCGATTTTGCTAAACAACTTTCAACAGTTTCAGATTTCTTAA
disc 41 (45)	ACAGCTTGACGAAGGCACCAACCTAAAACGAAAACCGAACTGACC
disc 42 (50)	AACTTTGAAAGCTAACGGAACAACATTATTACAGGTTACTGCGGAATCGT
disc 43 (44)	CATAAATATTCATTTGTAACAGTTGATTCCCAATTCTGCGAACG
disc 44 (44)	TATTAAACCAAGTACCGCACTCATCGAGAATTGCCAGTTACAAA
disc 45 (50)	ATAAACAGCCATATAACAATGAAATAGCAATAGCTATCTCCACGGAATAA
disc 46 (35)	GTTTATTTTGTCCACCATTACCATTAGAATCAAAA
disc 47 (36)	TCACCGGAAGCAGGTCAGACGATTGTGTACTGGTAA
disc 48 (33)	TAAGTTTTAACGGGAGGCTGAGACTCCTCAAGA
disc 49 (33)	GAAGGATTAGCGGGATACATGGCTTTT
disc 50 (36)	GATGATACAGGAGGCCTTGATATTCACCGTTTGCCA
disc 51 (45)	TCTTTTCATCAAGGCCGGAAACGTCACCAATGAAATATAAAAGAA
disc 52 (49)	ACGCAAAGACATACCGAAGCCCTTTTTAAGAAAAGTCTAACGAGCGTCT
disc 53 (44)	TTCCAGAGCCTAATCAAGCAAGCCGTTTTTATTTTCATCGTAGG
disc 54 (44)	TGGCTTAGAGCTTAATTGCTGAATCTGGTGAAAATCAGGTCTTT
disc 55 (50)	ACCCTGACTATTATCTTATGCGATTTTAAGAACTGGCTCCCTTCATCAAG
disc 56 (35)	AGTAATCTTCGAAAAGACTTTTTCATGGCCCACGC
disc 57 (36)	ATAACCGATAGACGTTAGTAAATGCTGAGTTTCGTC

disc 58 (33)	ACCAGTACAAACTTTGATATAAGTATAGCCCGG
disc 59-poly	A (53) AATAGGTGTATCACCGTACTCAATAGGAACCCATTTTTAAAAAAAA
disc 60 (36)	TGTACCGTAACAAATTTTCTGTATGGGACAATGACA
disc 61 (45)	ACAACCATCAGGAAGTTTCCATTAAACGGGTAAAACCAGGCGCAT
disc 62 (49)	AGGCTGGCTGAATTATACCAGTCAGGACGTTGGGAATCAGAAAACGAGA
disc 63 (44)	ATGACCATAAATCACTGTAGCTCAACATGTTTTAAATATGCAAC
disc 64 (44)	AATCATTACCGCGCCCAATAGCAAGCAAATACAATTTTATCCTG
disc 65 (49)	AATCTTACCAACGAAGCAGATAGCCGAACAAAGTTACCATACATA
disc 66 (35)	AAGGTGGCAACACCATCGATAGCAGCTCATAGCCC
disc 67 (48)	CCTTATTAGAAACGAATGGATCTTCATTAAAGCCAGAATTTCATCGGC
disc 68 (45)	ATTTTCGGACCGTAATCAGTAGCGACAGAATCACAGTATGTTAGC
disc 69 (50)	AAACGTAGAAAAGAAGGAAACCGAGGAAACGCAATAAAGATTAGTTGCTA
disc 70 (49)	TTTTGCACCCAGCTCAGATATAGAAGGCTTATCCGGTATTCTAAGAACG
disc 71 (50)	CGAGGCGTTTTAGCGAACCTCCCGAAAAGCGAACCAGACCGGAAGCAAAC
disc 72 (49)	TCCAACAGGTCAGGATTAGAGAGTACCTTTAATTGAAGATTAAGAGGAA
disc 73 (49)	GCCCGAAAGACTTTAAATTGGGCTTGAGATGGTTTAATAAATCAACGTA
disc 74 (35)	ACAAAGCTGCTCGGAACGAGGGTAGCCTTGCAGGG
disc 75 (48)	AGTTAAAGGCGTAACGATCTAAAGTTTTGTCGTCTTTCCATATTCGGT
disc 76 (45)	CGCTGAGGAACGGCTACAGAGGCTTTGAGGACTCAAGAACCGGAT
disc 77 (50)	ATTCATTACCCTTCAACTTTAATCATTGTGAATTACAGTCAGAAGCAAAG
disc 78 (44)	CGGATTGCATCAAACTCCTTTTGATAAGAGGTCATTTTTGCGGA
disc 79 (28)	TTAATTCGAGCTTCCTTGCGGGAGGTTT
disc 80 (26)	TGAAGCCTTAAATCATAACGGAATAC
disc 81 (26)	CCAAAAGAACTGGCTGACGAGAACAC
disc 82 (25)	CAGAACGAGTAGCAAATATCGCGTT
disc 83 (40)	CTCCTTATTACGAGTTTGCCTTTAGCGCACCCTCAGCAGC
disc 84 (45)	GAAAGACAGCATCATTCAGTGAATAAGGCTTGCCCATGATTAAGA
disc 85 (33)	CGGGATCGTTCAGACTGTAGCGCGTTGGAAAGC
disc 86 (32)	GCAGTCTCAGCCCTCATAGTTAGCCGCTTTTG
disc 87 (26)	GCATTCCACAGACTGAATTTACCGTT

### disc 88 (32) CCAGTAAGCGTCGTTTTGCTCAGTACCAGGCG

# 

### **DONUT**

donut 1 (33)	CAAGAAAATCTTTGACCCCCAGCAACGGCTAC
donut 2 (38)	AGGCAGAGGCATAAAACGAAAGAGGAGGAAGTTTCCAT
donut 3 (41)	CAGTAATAAACAGTAGGGCTTAATTGAGAATCTAGAAAAAG
donut 4 (37)	AAAGTAATTGTTTTTATTTTCATCGTAAGTATAAAGC
donut 5 (36)	ACGCGCCTAAGTACAACGGAGATCGTCACCCTCAGC
donut 6 (41)	GAGCATGTAAATAAGGCGTTAAATATTTAACCTCCGGCTTA
donut 7 (35)	CAACGCTCAGAGAATATAAAGTACCGGGAACGAGG
donut 8 (49)	GCAAGCCCTGTCCAGACGACGACAGTGTCGAAATCCGCACGGTGTACAG
donut 9 (44)	CCGCACTCATCGTAGAAGGCTTATCCGGTATTCATATTTTAGTT
donut 10 (39)	TCCTTATCATTTCTGACCTAAATTTAACAAATCCAATCG
donut 11 (34)	ACCGTGTGATAGAAACCAATCAATAAGTCCTGAA
donut 12 (40)	AATCATAATTACGCCATATTTAACAACGCCACTAATTTAC
donut 13 (41)	CCTGTTTTCTTACCAACGCTAACGAGTATCAAAATCATAGG
donut 14 (38)	TACAAATTCTTACCGGAATCATTACCTAAATCAAGATT
donut 15 (33)	AATTTCATCTCCAAGAACGGGTATTAATGCAGA
donut 16 (32)	ATATGTAAATGCTGATGTGGTTTGAAATACCG
donut 17 (49)	GGTTGGGTCTTAGAATCCTTGAAATAGCAATAGCTATCTTATGGCAACA
donut 18 (30)	TCTGAGAGACTACCTTAGAATAAACACCGG
donut 19 (29)	ATTTTATCCTGAAAGTATCATATGCGTTA
donut 20 (37)	AGTTGCTATTTTCCAATCCAAATAAGAAATAAAAACA
donut 21 (46)	GGTTTTGAAGCCTGCGCCCAATAGCAAGCAAATCAGATAAGAACAA
donut 22 (35)	TAGCGAACCTCAAATTAATTACATTTAATTATTCA
donut 23 (29)	CTTTTCAAATTAAGAACGCGAGGCGTTT
donut 24 (38)	CAAGACAAAGAAATCAATATGTGAGTGAAACCGAGG

donut 25 (49)	AATAAACAGACTGAACACCCTGAACATGATGGCAATTCATCTTAGCGTC
donut 26 (44)	TAACGTCAAAAATACAAACATCAAGAAAACACCGACTTGCGGGA
donut 27 (24)	ATTACCTTTTTAATGTTTGAATA
donut 28 (40)	TGTAAATCGTCGCTAAAAGTAAGCAGATAGCCGCAGTATG
donut 29 (47)	ACAATGAAAACATAGCGATAGCTTAGATTAAGACGCTGAGTTAAGCC
donut 30 (47)	CAATAATTGAGTAACATTATCAACAATTCGACAACTGCATCAAT
donut 31 (47)	AAGAATTGAGAAGAGTCAATAGTGAATTCGTCTTTCCAGGCGCTAAT
donut 32 (31)	ATCAGAGAGAGGAGCGGAATTTAGATAA
donut 33 (35)	GAGAATTACCATATTATCGCACCCAGCTACA
donut 34 (46)	GGGAAGCGATACTTCTGAATTATTAGCAGCACCGTAATTCTTTTCA
donut 35 (31)	AAGATGATGAAGAAAATAGCAGCAAAATTAT
donut 36 (47)	TTTCAATTATAGATTTTCAGGTTTATTTGGGAATTAGAGGGCTTAGA
donut 37 (47)	CCAAGTTACAGTACCTTTTACATCTATTCATTAAAGGTGTGTTTTAA
donut 38 (49)	AAACGCAATAATTTCGCCTGATTGCGAAACAGTACATAACGCGAGAAAA
donut 39 (49)	CATAAAGGCCGAAGCCCTTTTTAAGATTAATTTAATTTTCCTATATAACT
donut 40 (40)	TATAAAAGAAACCGTTATTAATTTTAAAAGTGAGCAAGAA
donut 41 (49)	GATTATCAGAAAGTCAGAGGGTAATTGAAGCCTAATTTGCCAGTTACAA
donut 42 (44)	AACCAACCATATCCTTTACAGAGAGAATAACACGATTTTTTGTT
donut 43 (32)	TAGCACGACCATTAGCAAGGCCAACCGCCTCC
donut 44 (44)	ATATACAGTAACAAAATCGCGCAGAGGCGAACAATTTCATTTGA
donut 45 (49)	CAAAAGAACTTTCAACCGATTGAGGTTCCATGTAACAGTTGAAGAGGAA
donut 46 (45)	ACTCCTTATTACGAACAAAGTTACCAGAAGGAATAACCTTGCTTC
donut 47 (48)	TTAGCAAAATTCATATGGTTTATTAGTTTGACCATTAGCCTTGAGTAA
donut 48 (32)	GTCACAATCAATAGAAACGTAGAAAATACATA
donut 49 (38)	CTTTGCCCGAAGCAAAGACACCACGGAATATGTTTAGC
donut 50 (48)	GTATTAGACTTTACAATTTTGCGGAACAAAGAAACCACCATAACCCAC
donut 51 (47)	TACATTTGGGAAGGTTATCTAAAAAATGGATCTTCATTAAGGAATTA
donut 52 (47)	AGACTGTAGCGCCTAATAGATTAGAGCCGTCAAATCATCATATTCCT
donut 53 (49)	GAATCAAGTTTGCCTAATATAATCCTGATTGTTTGGATTCATTAGACGG

donut 54 (49)	CAGTAGCACCATTTAAAACAGAAATAAAGAAATTGCGCCTGAGCAAAAG
donut 55 (28)	GTCACCGACTTGAGCCAACGTCAGATGA
donut 56 (45)	AAATATTGACGGAAATGGGAGAAACAATAACGGAAACGGAATACC
donut 57 (46)	TATATTTTATACAGGAGTGTACTGAAACATGAAAGTATTGATATAA
donut 58 (32)	TCTACTAAGAATTTACCGTTCCAAAGGATTAG
donut 59 (25)	GTGCACTAACAAGTTTTCATCGGCA
donut 60 (47)	TTTTCGGTGTTGAGGCAGGTCAGCCTCGTTTACCAGACGAACAACAT
donut 61 (46)	TAATCAAAACCAGAACCACCACCAGGCTTTTGCAAAAGGGAAGAAA
donut 62 (49)	AGCCACCACCGGGGAAACGTCACCAATGAAACCATCGAGGAAGGA
donut 63 (45)	CTCAGAGCCGCTAAGAGGTCATTTTTGCGGATCCAGCAAAATCAC
donut 64 (31)	GCTTAATTTCAGGATTAGAGAGTCGTCATAA
donut 65 (47)	ATATGCAAGAGCTTCAAAGCGAAACAGTTCAGAAAACGCCTCATTTT
donut 66 (49)	AACGAGTAGATCCAGCGCCAAAGACAAAAGGGCGACAGGCATGATTAAG
donut 67 (49)	AACGGGGTCAGTGATACATTTCGCAAATGGTCAATAACCAGTTTATTTT
donut 68 (49)	TGGCTTTTGATGCATTTGGGGCGCGAGCTGAAAAGGTGCGTATTAAATC
donut 69 (49)	AGCGCAGTCTCTTAGTAGTAGCATTAGAAAGGAATTGAAGGATTTAGAA
donut 70 (48)	ATTGACAGGAGCATAGCCCCCTTATTAGCGTTTGCCACAGTAGCGACA
donut 71 (34)	CCGCCACCCTAAAATGTTTAGACTAACTACAACG
donut 72 (48)	AACTCCAACAGGGCTGAATCTGGTGCTGTAGCTCAACAAATTATCACC
donut 73 (49)	CGCGTTTTAATTCCTAAAGTACGGTGTCTGGAAGTTTCAGAGGGAAGGT
donut 74 (49)	GCCCGAAGGTCTTTACCCTGACGCCACCCTCAGAACCGCACTTTCAACA
donut 75 (46)	CAGTGCCCGTGCGGATTGCATCAAAAAGATTATTCCCAATTCTGCG
donut 76 (44)	GATTAGCGGGGCAGATACATAACGCCAAAAAGCCAGAATGGAA
donut 77 (40)	CGAGGCATGAGATTTAGGAATACCAGTAAATTGGGCTTGA
donut 78 (48)	ACACTATCATAACACGATTGGCCTTGATATTCACAAACGTATCTTTAG
donut 79 (49)	GGGTAATAGTCAGAGCCACCACCCTCAGAGCCGCCATCACCGGAACCAG
donut 80 (48)	TCCAATACTGCGGAATACCTTTAATTGCTCCTTTTTGACACCCTCAGAA
donut 81 (40)	ATATTCACATGTACCGTAACACTGAGTTTTGTCGTCTTTC
donut 82 (26)	CAAATGCTTTAACCAGACCGGAAGCA

donut 83 (39) CAGAAGCAAAATAAACAGTTAATGCCCCCTTACTCAGGA
donut 84 (46) GTATCACCGGCCTATTTCGGAACCTATTATTCTGGTAATAAGTTTT
donut 85 (48) GTATAGCCCTAATTTTTCACGTTGAAAATCTCCAAAAAAAGTGCCGT
donut 86 (47) CGAGAGGGTTAAGAGGCTGAGACTCCTCAAGAGGTAAGCGTCATACA
donut 87 (23) ACCAGGCGGATAAAGGCTCCAAA
donut 88 (36) TATTACAGAACTTTAATCATTGTGAAAGCTGCTCAT
donut 89 (48) GAACTAACGGACGATAAAAACCAAAATAGCGAGAGAGCCGCCGCCAGC
donut 90 (45) AATCTACGTATTTTAAGAACTGGCTCATTATACCCACAGACAG
donut 91 (40) CCTGTAGCATTCAGTCAGGACGTTGAAGTTTTGCCAGAGG
donut 92 (38) CAGGGATATGAATTTTCTGTATGGTATATTCGGTCGCT
donut 93 (46) AGCCACCACAGAATGACCATAAATCAAAAATCAAGACTTCAAATAT
donut 94 (36) GGTTTAGTGAAAGGAACAACTAAAACCGATAGTTGC
donut 95 (42) AGGAGCCTTAGAACGAGTACATTCAACTAATTTTTGCTCAGT
donut 96 (43) GATGGTTTAATTTCGTAGAAAGATTCATCAGTTAGTAAGAGCA
donut 97 (42) CTCATAGTTAAGAGTAATCTTCGACAAGAACCGGGAAAGAGG
donut 98 (44) CAGACGTTAGTAAAGCAAGCCCAATAGGAACCTTGAATCCCCCT
donut 99 (47) GTTTCAGCGGAGTGAGAATAACCGCCACCCTCAGAACCTATTATAGT
donut 100 (34) AACAGCTTGATGGAATTGCGAATAAGGAATAGGT
donut 101 (41) ATCAGCTTGCTTTCTAAAGACTTTTTCATGCGAAAGAATAC
donut 102 (38) TCAGTGAATAAGTACGTAATGCCCAATCATAAGGGAAC
donut 103 (37) CAAATCAACGTAACAATTACCTTATGCGTAATAAAAC
donut 104 (48) CTTCATCAGCGTAACGATCTAAAGTTTCGTCACCAGTACAGGATAGCG
donut 105-polyA (48) GAGGCTTGCAGGGAGTAGGCTGGCTGACTTTTTAAAAAAAA
donut 106 (34) CGCATAACCGAGATTTTGCTAAACACACCCTCAG
donut 107 (39) GCCGACAATGACCATCGGAACGAGGGTAGCGATTATACC
donut 108-polyA (50) AGAGGCTTTGAGGACGAGGTGAATTTCTTATTTTTAAAAAAAA
donut 109 (49) TAAACGGGTAAAAGCTTGCCCTGACGAGAACACCTAATTGTATCGGTTT
donut 110-polyA (48) CGAACTGACCAACTTTATATTCATTACCTTTTTAAAAAAAA
donut 111 (40) ACAGATGAGACCTGCTCCATGTTACTTAGCCACAAAAGGT

donut 112 (42)	ACCAGGCGCATTAAAGGCCGCTTTTGCGGGATTTGTATCATC
donut 113 (27)	AGCGAAAGACAGCCATCGCCCA
donut 114 (36)	ACTAAAACACTCATAATATCCCATCACATGTAATTT
donut 115 (37)	CGCAGACGGTACTACGAAGGCACCAACCTTTTCGAGC
donut 116 (41)	GCCTGATAAATTATAAACAACATGTTCAGCTAAACCAAGTA
donut 117 (42)	AAGCGCGAAACAGTTTATCAACAATAGATAATCGGCTGTCTT

# **SPHERE**

north-1 (40)	TTCCATTAAATTAAAGGGATTTTAGACAGGGAGATAGAAC
north-2 (39)	CCTTCTGACCCAGCCCTCATAGTTAGCGTAATGAGGAAGT
north-3 (39)	CAGGGCGATGGAGCTAAACAGGAGGCCGACGGGTAAAAT
north-4 (39)	ACGTAATGCCATGGTTTAATTTCAACTTTAACCGTCTAT
north-5 (31)	AATGAATCGGCCAACGTGGACTCCAACGTCA
north-6 (37)	AAGGGCGAAAAATCATTGTGATCGTGCCAGCTGCATT
north-7 (50)	CCAACCTAAAACGGCTTTGAGGACTAAAGACTTTTTCACGATCTAAAGTT
north-8 (48)	TAAGAACTGGCTAACGAGTAGTAAATTGGGCTTGAGACTACGAAGGCA
north-9 (37)	ATAAATATCGGGAAACCTGATTACCTTATGCGATTT
north-10 (41)	GCGAAAGAGACGAGAACACCAGCATTATCTGCGGAATCGTC
N5 (50)	TTGTCGTCTTTCCAGACGTTAGTAAATGAGCAACGGCTACAGAGAAAGAG
north-12 (29)	ACTGCCCGCTTTCCAGTTCATTGAATCCC
north-13 (46)	CCTCAAATGCTTTGCTCCTTTTGATAAGAGGGGATGTGCTGCAAGG
north-15 (33)	CGATTAAGTTGGGTAATTAATTGCGTTGCGCTC
north-16 (40)	TGCATCTGCCTACGCCAGCTGGCGAAAGGGTCATTTTTGC
north-17 (31)	GGATGGCTTATAGATACATTCATCGTAACCG
north-18 (32)	CAATTCTAGATGGGCGTCGCAAATGGTGGCAT
N4 (44)	TCATCTTTGACGCGAAAGACAGCATCGGAACGAGGGTAATTTTC
north-20 (50)	GGAAGAAAATCTATTCAGTGAATAAGGCTTGCCCTATACACTAAAACAC
north-21 (32)	TGGATAGCGTCCAATAACCAGTCAGGACGTTG
north-22 (44)	GATTATACTAACAAAGCTGCTCACGTTAAGTAAAATGTTTAGAC
N3 (48)	ATTTTGCTAAACAACTTTCAACAGTTTCGTCACCCTCAGCACCCCAGC

north-24 (50)	AATAGAAAGGAACTAAAGGAATTGCGCTGAGGCTTGCAGAGATTTGT
north-25 (43)	ATCATCGCTTCGACAAGAACCACAGGTTTTTGCAAAAGAAGTT
north-26 (50)	TTGCCAGAGGGTAAATCAAAAATCAGGTCTTTACCCTGACCAGACCGGAA
north-27 (48)	GCAAACTCCAACAGATCTGGTGCTGTAGCTCAACATGTTTTTCTGCGA
north-28 (48)	ACGAGTAGACCTGTTTAGCTATATGCTGAAAAGGTCAATAATTTAGTT
north-29 (35)	TGACCATGAGCTTAATTGCTGAGTCAGGATTAGAG
north-30 (26)	AGTACCTTTAATTAAACAGTTCAGAA
north-31 (36)	AACGAGAATGACCAGGTAATATAAAACGAACTAACG
north-32 (49)	GAACAACATTATTGGATATTCATTACCCAAATCAACGCAAGCGCGAAAC
north-33 (50)	AAAGTACAACGGGGAGTTAAAGGCCGCTTTTGCGGGATCAGCGGAGTGAG
N2 (22)	TGACAACAACCATCGCGACCTG
north-35 (44)	CTCCATGTCCAGGCGCATAGGCACCACAAGACGACGATAAAAAC
north-36 (34)	CAAAATAGCGAGAGAGAAGATTCATCAGTTG
north-37 (48)	AGATTTAGGAATTGGCTGACCTTCATCAAGAGTAATCCTGATAAATTG
north-38 (63)	TGTCGAAATCCGCCCACGCATAACCGATATATTCGGTCGAATAATAATTTTTTCACGTTGAAA
north-39 (50)	AGTAATAAAAGGGACATTCTGGCCAACAAACGGTACGCCAGAAGTTGGAA
north-40 (44)	TCAGAGCGGGCCCACTACGTGAAGAACGCGCGGGGAGAGGCGGT
north-41 (50)	TTGCGTATTGGGGGGTGCCTAATGAGTGAGCTAACTCACACGCCAGGGTT
north-42 (49)	TTCCCAGTCACGACGGCGATCGGTGCGGGCCTCTTCGCTATAGTTTGAG
north-43 (47)	GGGACGACATAGGTTACGTTGGTGTACTAATAGTATGGGGACCGTAT
north-44 (35)	CGGCCTCACAACTGTTGGGAAGGTTGTAAAACGAC
north-45 (28)	GGCCAGTGCCAAGACGAGCCGGAAGCAT
north-46 (37)	AAAGTGTAAAGCCTGCGCCATCCAGTTTGGAACAAGA
north-47 (48)	GTCCACTATTAAACCATCACCCAAATCAAGTTTTTGAGCACGTATAAC
north-48 (50)	GTGCTTTCCTCTTGAGAAGTGTTTTTATAATCAGTCAGTC
N6 (37)	CATTGGCAGATTCACGAGGCCACCGAGTAATATGGTT
north-50 (44)	GCTTTGACTGGGGTGCTGTTGTGGGTGGTTTTTCTTTT
north-51 (31)	CACCAGTGAGACGGGCTCAAAAGAATAGCCC
north-52 (49)	GAGATAGGGTTGAGCGTAAAGCACTAAATCGGAACCCAATGCGCCGCTA
N7 (55)	CAGGGCGCGTACAAGAGTCTGTCCATCACGCAAATTACTCAATCGTCTGAAATGG

N8 (38)	TACCTACATTTTGACGACCGTTGTAGCAATAACACCCG
north-55 (44)	CCGCGCTTTAAAGGGAGCCCCCTATAAAAACAGCTGATTGCCCT
north-56 (50)	TCACCGCCTGGTGTTATCCGCTCACAATTCCACACAACATCTTGCATGCC
north-57-poly	/A (47) TGCAGGTCGACTCTAAGCGCCATTCGCTTTTTAAAAAAAA
north-58 (36)	CATTCAGGCTGCGGAAGATCGCACTCCCGGCGGAT
north-59 (43)	TGACCGTAAGTAGCATTTCGGATTGCGCGATTTCAACAGTTGA
north-60 (35)	TTCCCAATAAATATGCAACTAATTTTAATTCGAGC
north-61-poly	/A (47) TTCAAAGCGAACTATTATAGTCAGAAGTTTTTAAAAAAAA
north-62 (36)	CAAAGCGGATTGCATTTACCTTCAACTAATGCAGAT
north-63 (50)	ACATAACGCCAAAAGGACAGATGAACGGTGTACAGATACTTAGCCGGAAC
F64 (37)	GAGGCGCAGACCTTGATACCGATAGTTGCGCCGACAA
north-65 (41)	CCTTTAATTGTATCGGTTTATCAGCTTGCTTTCTGGTAATA
N1 (22)	TGCCTGAGTAGAAGAGGCGCTG
north-67 (44)	GCAAGTGTCGGCGAACGTGGCGCTGTTTGAGAGTTGCAGCAAGC
north-68 (30)	GGTCCACGCTGGCATAGTAAGAGCAACACT
north-69-poly	/A (47) ATCATAACCCTCGTCAAAAAGATTAAGTTTTTAAAAAAAA
north-70 (29)	AGGAAGCCCGTAATCATGGTCATAGCTGT
north-71 (38)	TTCCTGTGAAATCCCTGAGATGGTTGCTTCCGAAATC
north-72 (50)	GGCAAAATCCCTGATTTAGAGCTTGACGGGGAAAGCAGCGGTCACGCTGC
north-73 (62)	GCGTAACCACCCTTCTTTGATTAGTAATAACATCACTGCAACAGGAAAAACGCTCATGGAAA
north-74 (40)	TCGGCCTTGCGAGGTGAATTTCTTAAACAGGGTCAATCAT
north-75 (39)	AAGGGAACCGCGAAAGGAGCGGGCGCTAGACTCAAACTA
north-76 (51)	GGGAAGAAGAACTGACCAACTTTGAAAGAGGAATTACGAGGTTTGCCCCA
north-77 (22)	GCAGGCGAAAATCAGAAAGGAA
north-78 (48)	GGTACCGAGCTCGAAATCGAAAGACTTCAAATATCGCGAGTACGGTGT
north-79 (43)	CTGGAAGTTTTCTGGTGCCGGAAACCAGGCAAGAGGATCCCCG
north-80 (34)	CGGCACCGCTCATTCCATGTATTTGGGCTCCGTG
north-81 (19)	GGAACAAAAGCCAGCTTTC
south-1 (40)	TTATCATTTTACAGTGCCCGTATAAACAGTAACGCCTGTA
south-2 (40)	GCATTCCACAAAAGCGTAAGAATACGTGGCTTGAGTAACA

south-3 (39)	CCATCTTTTCGGGGTCAGTGCCTTGAGTAGCGGAACAAA
south-4 (39)	GAAACCACCACAATATATGTGAGTGAATATTAGCGTTTG
south-5 (31)	AAATTCATATGGTTTAGGCATTTTCGGTCAT
south-6 (37)	AGCCCCCTTAACCTTGCTTCTTGTCACAATCAATAGA
south-7 (50)	TTATCATCATATCCCGAACGTTATTAATTTTAAAAGTACAGACAATATTT
south-8 (48)	ATTAATTTTCCCTTTTAATGGAAACAGTACATAAATGAAGGAGCGGAA
south-9 (36)	AAGCCTGTTAAGTTTATTTGTAAATCGTCGCTATTA
south-10 (41)	TATCAGATATTTGAATTACCTTTTAGAATAATTACTAGAAA
south-11 (50)	TTGAATGGCTATTAGTCTTTAATGCGCGGTATTAAATCCTTTGTCCTGAT
south-12 (29)	GCAAAGACACCACGGAATTAGTATCATAT
south-13 (46)	GCGTTATACAAAAACAATAGATAAGTCCTGATAATTGAGCGCTAAT
south-15 (33)	ATCAGAGATAACCCCAACATATAAAAGAAAC
south-16 (40)	TTTCCAGAGCCCCTGAACAAAGTCAGAGGGACAAGAAAAA
south-17 (31)	TAATATCCCATTACCGCGCCTAACGAGCGTC
south-18 (32)	AACCTCTTACCAACGCCAATAGCAAGCTAGCG
south-19 (49)	AATATAATCCTAGACTTTACAAACAATTCGACAACTCAACTGATAGCCCT
south-20 (50)	GATAGCTTAGATTAATTACATTTAACAATTTCGATGGCAATTCATC
south-21 (32)	ATAAACACCGGAATCATCCTTGAAAACATAGC
south-22 (44)	TGGATTATCATCAAGAAAACAAAAGACGAAGGCGTTAAATAAGT
S4 (22)	GGATTTAGAAGTATTGATTGTT
S3 (50)	AGATAAAACAGAGGTGAGGCGGTCAGTCAACTAATAGATTAGAACCAACC
south-25 (43)	ATATCAAATTTCAATTACCTGAATCATTTAATGGTTTGAAATA
south-26 (50)	CCGACCGTGTGCAGTAGGGCTTAATTGAGAATCGCCATATGACGACAATA
south-27 (48)	AACAACATGTTCAGATGTAGAAACCAATCAATAATCGGCTCAAGCCGT
south-28 (48)	TTTTATTTAGATATAGAAGGCTTAGCGAGGCGTTTAAATCTCATCGTA
south-29 (35)	GGAATCATCCTAATTTACGAGCCTAATGCAGAACG
south-30 (26)	CGCCTGTTTATCTTCCAGTATA
south-31 (35)	AAGCCAACGCTCAAATAAATCTGAGAAGAGTCAATA
south-32 (49)	GTGAATTTATCAAAGCAAAAGAAGATGATGAAACAAAACTTCTGAATTA
south-33 (50)	TGGAAGGAATTGAGCCGTCAATAGATAATACATTTGAAACCACCAGCAGA

S1 (37)	GCTGAGAGCCAGCAGAATTGAGGAAGGTTATAAAGAA
south-35 (44)	ATTGCGTAAATACCAAGTTACAGCTTAGTATTTTAGTTAATTTC
south-36 (34)	ATCTTCTGACCTAAATAGGTCTGAGAGACTACCT
south-37 (48)	TTTTAACCTCCGAAATCGCGCAGAGGCGAATTATTCAATTATTAGCAC
S2 (55)	GTAAAACAGAAATCTAAAATATCTTTAGGTGCACTAAATTAACACCGCCTGCAAC
S5 (50)	ACTGAGTTTCGTCACCAGTACAAACTACTAATGCCCCCTGCCTG
south-40 (44)	AGTTTTAACATAATCAAAATCATTCATCCCAGCGCCAAAGACAA
south-41 (50)	AAGGGCGACATAAACGTAGAAAATACATACATAAAGGTGGACAAGAATTG
south-42 (49)	AGTTAAGCCCAATAACATTAGACGGGAGAATTAACTGAACACTAATTTG
south-43 (47)	CCAGTTACAATTTTATCCTGAATCCCGACTTGCGGCTACAAAATAAA
south-44 (35)	CAGCCATAAAAAACAGGGAAGCGTAAGAGCAAGAA
south-45 (28)	ACAATGAAATAGCTAAGACTCCTTATTA
south-46 (37)	CGCAGTATGTTAGCTCAACCTTGCCTTTAGCGTCAGA
south-47 (48)	CTGTAGCGCGTTCCGGAACCAGAGCCACCACCGGACTTTTGATGATAC
south-48 (50)	AGGAGTGTACTATTTCGGAACCTATTATTCTGAAACACATGTACCGTAAC
S6 (22)	TGAAAGTATTAAGAGAAGCGTC
south-50 (44)	ATACATGGACCGCCTCCCTCAGTCAAGTGATTGAGGGAGG
south-51 (31)	GTAAATATTGACGGAATAGCAGCACCGTAAT
south-52 (49)	CAGTAGCGACAGAAAGCCGCCACCCTCAGAACCGCCAAGTCTCTGAATT
south-53 (50)	TACCGTTCCAGTGCTGAGACTCCTCAAGAGAAGGATTCACCACCCTCATT
S7 (13)	TTCAGGGATAGCA
south-54 (50)	CCACCCTCAGAACCGCCACCCTCAGAGCAGGATTAGCGGGGTTCAGAATG
south-55 (44)	GAAAGCGCCCCTCAGAGCCACCCATCGAATTATTCATTAAAGGT
south-56 (50)	GAATTATCACCAACGGAATACCCAAAAGAACTGGCATGATAATAGCTATC
south-57 (27)	TTACCGAAGCCCTTAGCAGCCTTTACA
south-58 (36)	GAGAGAATAACATTTATTTATCCCAATCTGCTATTT
south-59 (43)	TGCACCCAGGAGGTTTTGAAGCCTAAGAACTCCGGCTCATCGA
south-60 (35)	GAACAAGGTCTTTCCTTATCATAAAGGTAAAGTAA
south-61 (27)	TTCTGTCCAGACTTAACAACGCCAACA
south-62 (36)	TGTAATTTAGGCAGCAAATAGTTGGGTTATATAACT

south-63 (50)	ATATGTAAATGCTAACGGATTCGCCTGATTGCTTTGGATTTTCAGGTTTA
south-64 (50)	ACGTCAGATGACAGTTGGCAAATCAACAGTAGAAAAGGCAAATGAAAAATC
S8 (47)	CGTACTCAGGAGGTTTAGTACCGCCCGTCGAGAGGGTTGATGGCCTT
south-67 (44)	GATATTCAACCACCAGAGCCGCTACCATGACTTGAGCCATTTGG
south-68 (30)	GAATTAGAGCCATCGCAAGACAAGAACGC
south-69 (27)	GAGAAAACTTTTTAGGCATTTTCGAGC
south-70 (29)	CAGTAATAAAGTTACCAGAAGGAAACCGA
south-71 (38)	GGAAACGCAATAATGTCACCTAGCAAGGCCGGAAACGT
south-72 (51)	CACCAATGAAACACCCTCAGAGCCGCCACCAGAACCCAAACGAATGGATC
south-73 (51)	TTCATTAAAGCTTGCTCAGTACCAGGCGGATAAGTGCACCCTCAGAACCG
south-74 (40)	GCCCGGAATAACCCTCAATCAATATCTGGTATATACAGTA
south-75 (39)	ACAGTACCTTTTGAGGCAGGTCAGACGATTATAAGTATA
south-76 (51)	TGACAGGAGGTTACATCGGGAGAAACAATGATGCAAATCCAAGCAAAATCA
south-77 (22)	CCAGTAGCACCATCGCCAGCAT
south-78 (48)	AAGCAGATAGCCGAACAAGAGAATATAAAGTACCGACATCCAAGAACG
south-79 (43)	GGTATTAAACTTTAACGTCAAAAATGAAAATTTTAAGAAAAGT
south-80 (35)	CGATTTTTTGCAAGTACCGCATATTCTTAAATCA
south-81 (19)	AGATTAGTCAAATAAGAAA
Lock-1 (34)	AGTGCCAC T CAGAACAATATTACCGCCAGCCATT
Lock-2 (35)	ATTATTTA T AACATCGCCATTAAAAATACCGAACG
Lock-3 (24)	TGTATCAC T ATCTCCAAAAAAAAG
Lock-4 (24)	TGTATGGG T AGCCCAATAGGAACC
Lock-5 (35)	GCTCCAAAAGGAG T GCTGAACCTCAAATATCAAGG
	south-64 (50) S8 (47) south-67 (44) south-68 (30) south-69 (27) south-70 (29) south-71 (38) south-72 (51) south-73 (51) south-74 (40) south-75 (39) south-76 (51) south-77 (22) south-78 (48) south-79 (43) south-80 (35) south-81 (19) Lock-1 (34) Lock-2 (35) Lock-3 (24) Lock-4 (24)

## Output จากโครงการวิจัยที่ได้รับทุนจาก สกว.

## 1. ผลงานตีพิมพ์ในวารสารวิชาการนานาชาติ

ระบุชื่อผู้แต่ง : Chaithongyot S., Duangrat R., Wootthichairangsan C., Hanchaina

R., Udomprasert A. & Kangsamaksin T.

ชื่อเรื่อง : Selective delivery of doxorubicin using the biomarker-specific,

aptamer-functionalized DNA nanosphere.

ชื่อวารสาร : Materials Letters

**៊ី**: 2020

เล่มที่ เลขที่ : 260

หน้า : 126952

ระบุชื่อผู้แต่ง : Udomprasert A. & Kangsamaksin T.

ชื่อเรื่อง : DNA origami applications in cancer therapy.

ชื่อวารสาร : Cancer Science

ปี : 2017

เล่มที่ เลขที่ : 108 (8)

หน้า : 1535-1543

## 2. การนำผลงานวิจัยไปใช้ประโยชน์

- เชิงพาณิชย์ : ไม่มี

เชิงนโยบาย : ไม่มีเชิงสาธารณะ : ไม่มี

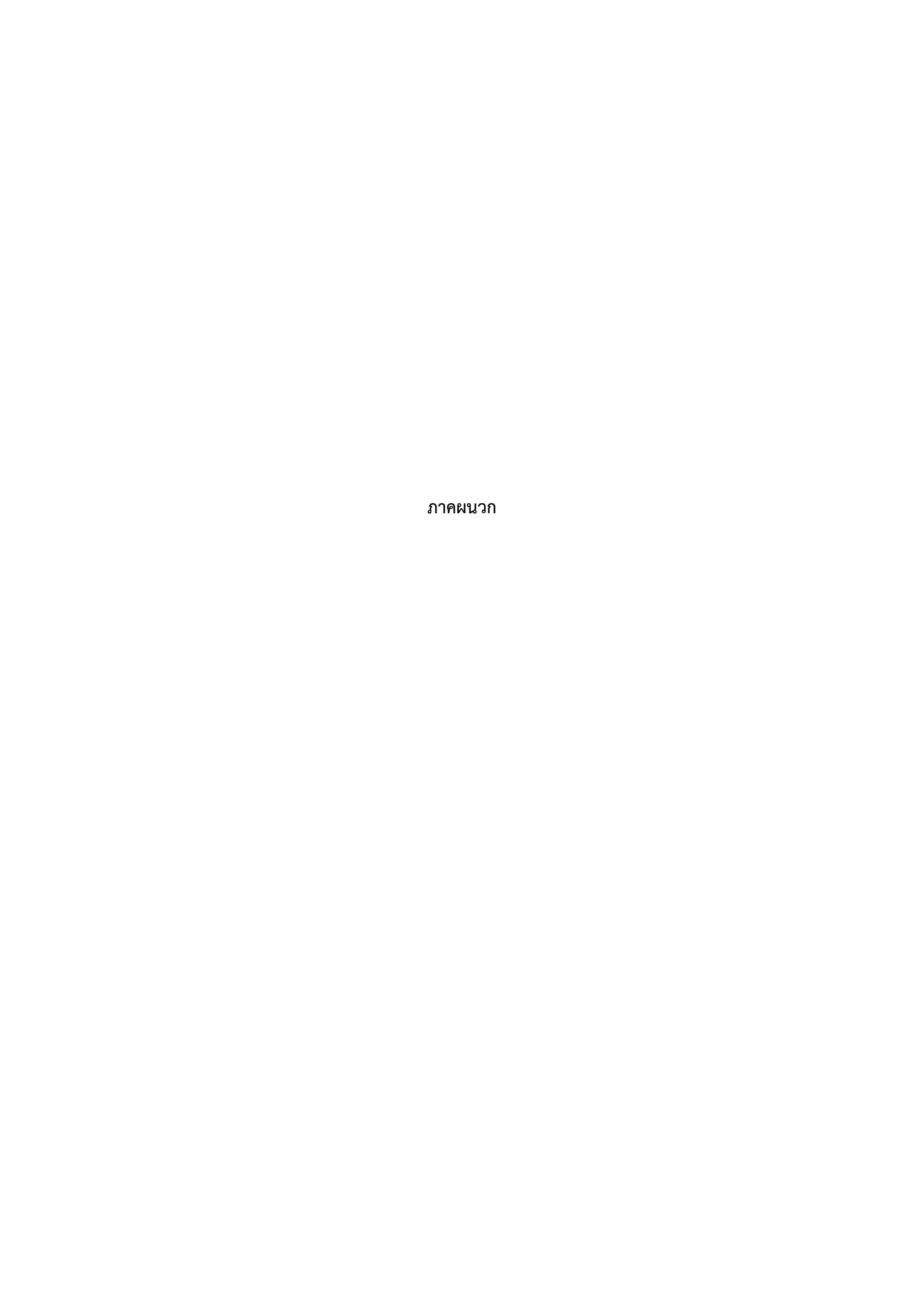
- **เชิงวิชาการ :** มีการนำความรู้ที่ได้ไปประยุกต์ใช้ในการเรียนการสอนและการทำวิจัย

3. อื่น ๆ (เช่น ผลงานตีพิมพ์ในวารสารวิชาการในประเทศ การเสนอผลงานในที่ประชุมวิชาการ หนังสือ การจดสิทธิบัตร)

Proceedings : ไม่มี

Poster presentation : ไม่มี

Oral presentation : ไม่มี



ELSEVIER

Contents lists available at ScienceDirect

### **Materials Letters**

journal homepage: www.elsevier.com/locate/mlblue



# Selective delivery of doxorubicin using the biomarker-specific, aptamer-functionalized DNA nanosphere



Supattra Chaithongyot <sup>a,1</sup>, Ratchanee Duangrat <sup>a,1</sup>, Chanida Wootthichairangsan <sup>a</sup>, Rattanavinan Hanchaina <sup>a</sup>, Anuttara Udomprasert <sup>b,\*</sup>, Thaned Kangsamaksin <sup>a,\*</sup>

#### ARTICLE INFO

Article history:
Received 11 September 2019
Received in revised form 15 October 2019
Accepted 4 November 2019
Available online 4 November 2019

Keywords: DNA origami Targeted drug delivery Nanostructure Doxorubicin Breast cancer MUC1

#### ABSTRACT

Targeted drug delivery systems have attracted much attention as they can enhance treatment efficiency and minimize cytotoxicity of chemotherapeutic drugs. Several nanomaterials with biological advantages have been explored for novel drug carrier invention. Here, a DNA origami nanosphere modified with a specific aptamer was developed for selective doxorubicin delivery. The specificity of the targeted nanocarrier was investigated against three cell lines with different levels of Mucin 1 (*MUC1*) expression. Our data showed that the doxorubicin-loaded, MUC1 aptamer-functionalized nanosphere (Dox-Apt-sphere) preferentially delivered drugs and exhibited cytotoxic effects at low Dox concentration in MUC1-high MCF-7 cells. These results also proved that the aptamer-modified DNA nanostructure may serve as a promising candidate for targeted drug delivery.

© 2019 Elsevier B.V. All rights reserved.

#### 1. Introduction

Chemotherapy suffers from adverse side effects as anti-cancer drugs non-selectively distribute throughout the body and harm normal cells. Previous evidence has shown that Dox exerts some toxic effects on cardiomyocytes [1-4]. To reduce cytotoxicity and increase treatment efficacy, a targeted drug delivery system has been developed. Many biomolecules have been utilized as targeting ligands, including peptides [5,6], transferrin [7], folate [8], antibodies [9], and aptamers [10,11]. DNA aptamers, single-stranded nucleic acids that specifically bind to target molecules [12], offer superior properties to antibodies due to their smaller size, lower production costs, and higher temperature stability. Specific aptamers with high affinity to a variety of cancer biomarkers have been investigated [11,13]. MUC1 is a cell-surface glycoprotein which is upregulated in several types of cancer and often used as a biomarker [14]. Various DNA nanostructures have been functionalized with a MUC1 aptamer [15] for targeted delivery purposes such as icosahedron [16], tetrahedron [17,18], and triangular DNA origami [19,20]. Here, we aimed to investigate the selective Dox delivery of the MUC1 aptamer-functionalized DNA origami nanosphere (Aptsphere) (Fig. 1(a)) against three cell lines with different levels of MUC1 expression to demonstrate the specificity of the nanostructure for future use in targeted drug delivery.

#### 2. Experimental section

Three cell lines MCF-7, HaCaT, and MDA-MB-231 cells were used in this study. MUC1 expression was determined by quantitative RT-PCR, Western blot, and immunocytochemistry. The sphere and Aptsphere were prepared in the TAE/Mg<sup>2+</sup> buffer as previously described [10], and the annealed nanostructures were purified using the PEG purification method [21] and verified by atomic force microscopy (AFM). For Dox loading and releasing efficiency, different concentrations of Dox were incubated with the nanosphere at 37 °C for 24 h and centrifuged at 15,000 rpm at 4 °C for 30 min. The pellet was resuspended and measured for 480-nm absorbance for loading and releasing efficiency. To evaluate selective delivery of Dox-loaded Apt-sphere, cellular internalization and cytotoxicity effects were examined. The sphere was fluorescently labeled with a quantum dot (QD). After incubation for six hours, cells were visualized by confocal fluorescence microscopy. For cytotoxicity effects, Apt-sphere containing different concentrations of Dox were incubated with each cell line. The MTT assay was performed after 48-hour incubation.

<sup>&</sup>lt;sup>a</sup> Department of Biochemistry, Faculty of Science, Mahidol University, Bangkok, Thailand

<sup>&</sup>lt;sup>b</sup> Department of Biochemistry, Faculty of Science, Burapha University, Chonburi, Thailand

<sup>\*</sup> Corresponding authors.

E-mail addresses: anuttara@go.buu.ac.th (A. Udomprasert), thaned.kan@mahi dol.edu (T. Kangsamaksin).

<sup>&</sup>lt;sup>1</sup> These authors contributed equally to this work.

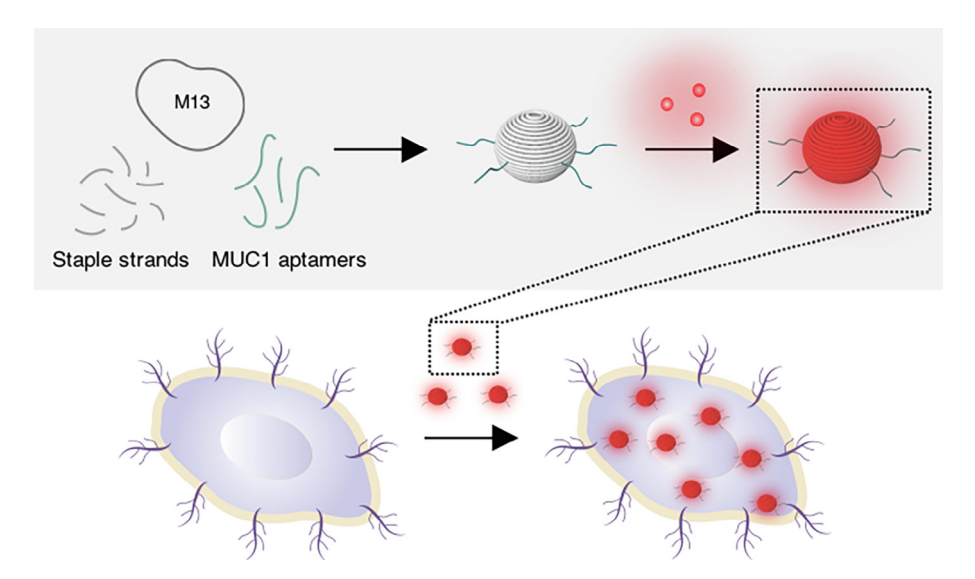


Fig. 1. The diagram illustrates the annealing process of Apt-sphere from M13, staple strands, and MUC1 aptamer strands and the loading process of Dox into Apt-sphere. Dox-Apt-sphere is more likely to bind cancer cells with MUC1 upregulation and be internalized.

#### 3. Result and discussion

As previous studies reported that *MUC1* is upregulated in certain breast cancer subtypes; therefore, we first determined *MUC1* expression levels in MDA-MB-231 and MCF-7 breast cancer cell lines, and immortalized keratinocytes, HaCaT, as control. We found that all cell lines differentially expressed *MUC1* at both mRNA and protein levels (Fig. S1 (a) and (b)). *MUC1* expression is highest in MCF-7 and lowest in MDA-MB-231. Immunocytochemical analysis demonstrated that MUC1 protein was localized on the plasma membrane (Fig. S1 (C)). So, we selected MUC1 as a target molecule to investigate the specificity of the DNA nanosphere. Next, Aptsphere was prepared as previously described, and verified by AFM (Fig. 2 (a)). Our data showed that the nanosphere was

successfully and homogeneously constructed with the diameter of approximately 50 nm, which is consistent with our previous report [10]. However, we noted that the closed spheres were not stable enough to resist the tip force in the AFM scanning process, resulting in connected hemispheres. Apt-sphere was relatively stable in various conditions (Fig. S2). Dox was added at various concentrations (62.5–500 μM) and centrifuged to remove remaining Dox in the supernatant. Dox-loaded Apt-sphere (Dox-Apt-sphere) pellets were subsequently resuspended for Dox measurement. Our results demonstrated that Dox loading efficiency increases when the concentration of Dox was increased up to 250 μM (Fig. 2(b)), implicating that the Dox/Apt-sphere ratio reached its saturation point. The calculated number of Dox molecules per structure was approximately 10<sup>4</sup>. We found that

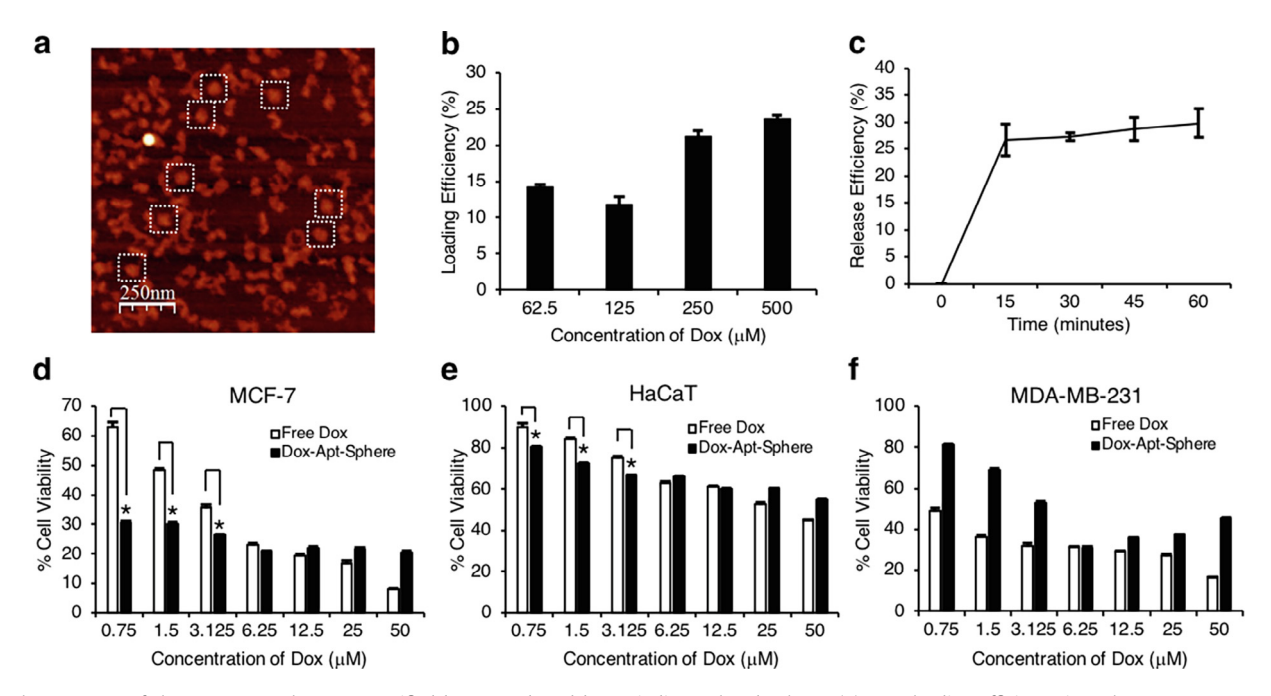


Fig. 2. The structure of the DNA nanosphere was verified by AFM; dotted boxes indicate closed spheres (a). Dox loading efficiency into the DNA nanostructure was determined at the concentration range between 62.5 and 500  $\mu$ M (b). Dox releasing efficiency of the DNA nanostructure was measured up to 60 min after resuspension (c). Cytotoxicity of free Dox and Dox-Apt-sphere was determined in MCF-7 (d), HaCaT (e), and MDA-MB-231 (f). \* P value < 0.05.

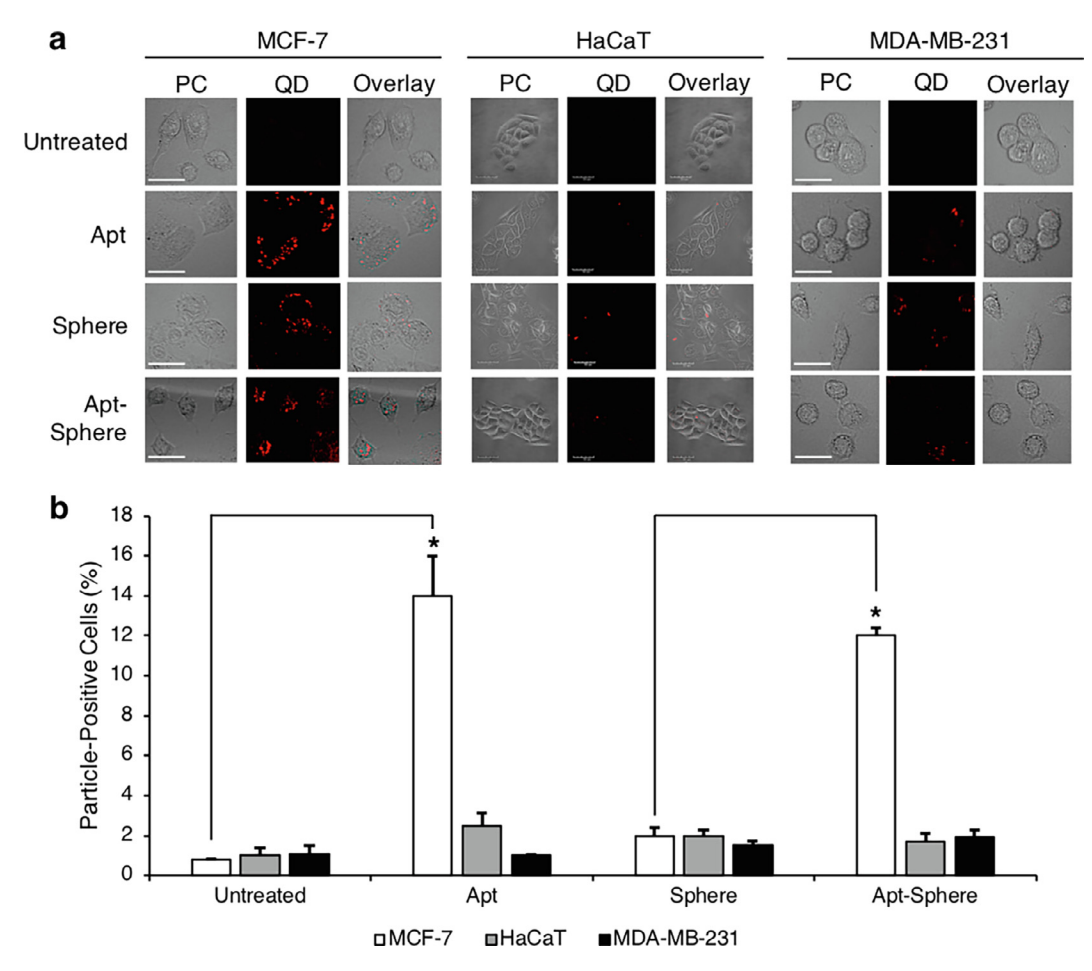


Fig. 3. The level of DNA nanostructure uptake was investigated via confocal microscopy of QD-labeled MUC1 aptamer, empty sphere, or Apt-sphere (a) and quantitated (b).

\* P value < 0.05.

the nanosphere loaded with high concentrations of Dox could not run into the gel (Fig. S3), likely due to its positive charge. In addition, it is also important that we understand the nature of the free Dox/Dox-Apt-sphere equilibrium; thus, we investigated Dox releasing efficiency by resuspending Dox-Apt-sphere pellets in the buffer for 0–60 min and then separating remaining Dox-Apt-sphere by centrifugation. The amount of released Dox was then determined by measuring 480-nm absorbance from the supernatant. Our results showed that our Dox-Apt-sphere had the maximum releasing efficiency of about 25% as early as 15 min after incubation (Fig. 2 (c)). After that, there is no significant change in Dox release. These data suggested that to calculate the actual amount of Dox in the structure we need to consider not only loading efficiency but also releasing efficiency in any given buffer used in the solution.

Next, we showed that the free nanosphere was not cytotoxic in all cell lines tested (Fig. S4). Then, we continued to determine the cytotoxic effects of the Dox-Apt-sphere when compared with those of free Dox in our cell line models with different levels of MUC1 expression. It has been shown that MUC1-modified DNA nanocarriers were internalized into cells via endocytosis and degraded in the lysosome, resulting in Dox release [16]. We found that in MCF-7 cells, free Dox showed a cytotoxic effect in a dose-dependent manner with the half maximal inhibitory concentration (IC50) of 1.5  $\mu$ M. Interestingly, Dox-Apt-sphere increased the cytotoxicity on MCF-7 cells by 50%, 40%, and 25% at 0.75, 1.5, and 3.125  $\mu$ M of Dox, respectively (Fig. 2 (d)). These results indicate that our DNA nanostructure may serve as promising nanocarrier helps to enhance therapeutic effects of Dox at very low concentrations

leading to less side effects. According to previous reports, the nanosphere enhanced the uptake of Dox or maintained its level inside the cell by interfering with efflux processes [22]. In HaCaT cells, Dox-Apt-sphere showed increased cytotoxicity by approximately 10% at the same range of Dox concentration (Fig. 2 (e)). This is likely due to the nature of HaCaT cells, which have a poor response to Dox treatment as the IC50 is about 50  $\mu$ M, more than 30-fold higher than that in MCF-7 cells. In contrast, MDA-MB-231 cells treated with Dox-Apt-sphere, had a significantly higher cell viability than those treated with free Dox (Fig. 2 (f)), implicating that MDA-MB-231 cells are less likely to uptake Dox-loaded Apt-sphere as efficiently as MCF-7, possibly due to lower levels of MUC1 on their surface.

In order to test our hypothesis, we determined the fate of QD-labeled Apt-sphere via confocal microscopy. Our data demonstrated that MUC1 aptamer, sphere, and Apt-sphere showed highest signals in MCF-7 cells (Fig. 3 (a) and (b)). These signals are localized intracellularly, indicating that Apt-sphere was internalized and that the internalization process is dependent on the presence of the MUC1 aptamer. Additionally, we observed the fate of Dox-Apt-sphere by visualizing Dox fluorescence signals (Fig. S5); however, there is no clear difference between Dox-Apt-sphere and Dox-sphere due to low intensity of the signals in culture media.

#### 4. Conclusion

In summary, the modification of the DNA origami nanosphere with the MUC1 aptamer offers a promising targeted drug delivery

vehicle. These results demonstrated that Apt-sphere could differentially deliver Dox into cells depending on levels of MUC1 expression. In addition, with Apt-sphere as the targeted carrier, low concentrations of Dox can only exhibit cytotoxic effects in MFC-7 cells. We have shown that not only do they enhance therapeutic efficiency, but DNA origami nanocarriers along with specific aptamers could also reduce side effects of drugs.

#### **Declaration of Competing Interest**

The authors declare that they have no known competing financial interests or personal relationships that could have appeared to influence the work reported in this paper.

#### Acknowledgements

This work was financially supported by Burapha University (A.U.), Mahidol University (T.K.), and the Thailand Research Fund, Grant No. MRG6080033 (A.U.) and MRG6180090 (T.K.). The authors thank the Central Instrument Facility and the Center of Nanoimaging, Faculty of Science, Mahidol University for technical assistance and Sarawut Cheunkar for AFM assistance and Jarinee Kongtrub for graphics.

#### Appendix A. Supplementary data

Supplementary data to this article can be found online at https://doi.org/10.1016/j.matlet.2019.126952.

#### References

- [1] C.F. Thorn, C. Oshiro, S. Marsh, T. Hernandez-Boussard, H. McLeod, T.E. Klein, et al., Pharmacogenet Genomics. 21 (2011) 440-446.
- [2] J.J. Bartlett, P.C. Trivedi, P. Yeung, P.C. Kienesberger, T. Pulinikunnil, Biochem. J. 473 (2016) 3769–3789.
- [3] D.L. Li, Z.V. Wang, G. Ding, W. Tan, X. Luo, A. Criollo, et al., Circulation 133 (2016) 1668-1687.
- [4] N. Koleini, E. Kardami, Oncotarget. 8 (2017) 46663-46680.
- [5] N. Zhao, Y. Qin, H. Liu, Z. Cheng, Anticancer. Agents Med. Chem. 18 (2018) 74-
- [6] Z. Jiang, J. Guan, J. Qian, C. Zhan, Biomater. Sci. 7 (2019) 461–471.
  [7] D.H. Schaffert, A.H. Okholm, R.S. Sorensen, J.S. Nielsen, T. Torring, C.B. Rosen, et al., Small, 12 (2016) 2634-2640.
- [8] G. Zhang, Z. Zhang, J. Yang, Nanoscale Res. Lett. 12 (2017) 495.
- [9] D.A. Richards, A. Maruani, V. Chudasama, Chem. Sci. 8 (2017) 63.
- [10] S. Chaithongyot, N. Chomanee, K. Charngkaew, A. Udomprasert, T. Kangsamaksin, Mater. Lett. 214 (2018) 72–75.
- [11] M. Kim, D.-M. Kim, K.-S. Kim, W. Jung, D.-E. Kim, Molecules 23 (2018) 830.
- [12] A.D. Ellington, J.W. Szostak, Nature 346 (1990) 818–822.
- [13] G. Zhou, O. Latchoumanin, L. Hebbard, W. Duan, C. Liddle, J. George, et al., Adv. Drug Deliv. Rev. 134 (2018) 107-121.
- [14] M.S. Nabavinia, A. Gholoobi, F. Charbgoo, M. Nabavinia, M. Ramezani, K. Abnous, Med. Res. Rev. 37 (2017) 1518-1539.
- [15] C.D. Pieve, E. Blackshaw, S. Missailidis, A.C. Perkins, Bioconjugate Chem. 23 (2012) 1377-1381.
- [16] M. Chang, C.-S. Yang, D.-M. Huang, ACS Nano 5 (2011) 6156-6163.
- [17] B. Dai, Y. Hu, J. Duan, X.-D. Yang, Oncotarget. 7 (2016) 38257-38269.
- [18] X. Han, Y. Jiang, S. Li, Y. Zhang, X. Ma, Z. Wu, et al., Nanoscale. 11 (2019) 339-
- [19] L. Song, Q. Jiang, J. Liu, N. Li, Q. Liu, L. Dai, et al., Nanoscale. 9 (2017) 7750-
- [20] J. Liu, L. Song, S. Liu, S. Zhao, Q. Jiang, B. Ding, Angew. Chem. Int. Ed. 57 (2018) 15486-15490.
- [21] E. Stahl, T.G. Martin, F. Praetorius, H. Dietz, Angew. Chem. Int. Ed. 53 (2014) 12735-12740
- [22] Q. Jiang, C. Song, J. Nangreave, X. Liu, L. Lin, D. Qiu, et al., J. Am. Chem. Soc. 134 (2012) 13396-13403.





## Unsolicited Review Article

## DNA origami applications in cancer therapy

Anuttara Udomprasert<sup>1</sup> and Thaned Kangsamaksin<sup>2</sup>



<sup>1</sup>Department of Biochemistry, Faculty of Science, Burapha University, Chonburi; <sup>2</sup>Department of Biochemistry, Faculty of Science, Mahidol University, Bangkok, Thailand

#### Key words

Cancer, DNA origami, drug delivery, nanotechnology, targeted therapy

#### Correspondence

Thaned Kangsamaksin, 272 Rama VI Road, Ratchathevi, Bangkok, 10400 Thailand.

Tel: +66-2201-5457; Fax: +66-2354-7174; E-mail: thaned.kan@mahidol.ac.th

#### **Funding Information**

Burapha University, Mahidol University.

Received April 25, 2017; Revised May 23, 2017; Accepted May 24, 2017

Cancer Sci 108 (2017) 1535-1543

doi: 10.1111/cas.13290

Due to the complexity and heterogeneity of cancer, the development of cancer diagnosis and therapy is still progressing, and a complete understanding of cancer biology remains elusive. Recently, cancer nanomedicine has gained much interest as a promising diagnostic and therapeutic strategy, as a wide range of nanomaterials possess unique physical properties that can render drug delivery systems safer and more effective. Also, targeted drug delivery and precision medicine have now become a new paradigm in cancer therapy. With nanocarriers, chemotherapeutic drugs could be directly delivered into target cancer cells, resulting in enhanced efficiency with fewer side-effects. DNA, a biomolecule with molecular self-assembly properties, has emerged as a versatile nanomaterial to construct multifunctional platforms; DNA nanostructures can be modified with functional groups to improve their utilities as biosensors or drug carriers. Such applications have become possible with the advent of the scaffolded DNA origami method. This breakthrough technique in structural DNA nanotechnology provides an easier and faster way to construct DNA nanostructures with various shapes. Several experiments proved that DNA origami nanostructures possess abilities to enhance efficacies of chemotherapy, reduce adverse side-effects, and even circumvent drug resistance. Here, we highlight the principles of the DNA origami technique and its applications in cancer therapeutics and discuss current challenges and opportunities to improve cancer detection and targeted drug delivery.

onventional chemotherapeutic agents have significant drawbacks, such as low solubility, low stability, and cytotoxicity, which have led to inadequate efficiency of cancer therapy. These obstacles can be minimized by a drug delivery system in which a carrier directly delivers the drug to specific target cells. Nanoparticles are now established and widely used as pharmaceutical delivery systems in the clinic for both diagnostic agents and therapeutic drugs. Various materials have been explored to be utilized for nanocarrier construction, including liposomes, (1) poly lactic-co-glycolic acid, (2) metals, such as gold and silver nanoparticles (AuNPs and AgNPs, respectively), (3) and magnetic nanoparticles. (4) However, these materials still have disadvantages. For instance, construction of liposomal nanoparticles with uniform size, shape, and charge is difficult, and multifunctional modification to some nanoparticles can be laborious and inefficient.

Self-assembly of DNA molecules could be programmed by complementary base pairing interactions. These properties make it a promising candidate as a structural building block for nanoscale construction. Nadrian C. Seeman pioneered the use of DNA to construct nanostructures, (5) that has culminated in the field of "structural DNA nanotechnology." Not only are DNA nanostructures biocompatible and biodegradable, but they can also be modified with a wide range of functional entities, such as aptamers, (6,7) lipids, (8,9) proteins, (10-12) and

inorganic nanomaterials, (13-15) making DNA nanostructures an attractive platform for the development of drug delivery systems.

#### **DNA Origami Technique**

Based on structural DNA nanotechnology, DNA nanocarriers could be designed and constructed in a controllable manner. However, the size and complexity of DNA nanostructures made by conventional methods are quite limited. In order to construct large DNA nanostructures, the scaffolded DNA origami technique was introduced in 2006 by Paul Rothemund. (16) This technique is based on the folding of a long single-stranded DNA (ssDNA) (scaffold) with the help of hundreds of short ssDNA (staples) to hold the scaffold in place (Fig. 1a,b). This technique has enhanced potential applications of DNA nanotechnology as the construction of larger DNA nanostructures has now become possible with less time and labor. Since then, DNA origami nanostructures in diverse sizes and shapes have been reported, including discrete objects like nanotubes, (21) a dolphin, (22) and a tetrahedron. (23) Later, researchers successfully generated 3D DNA origami nanostructures with multilayers, such as a monolith, a square nut, and a railed bridge (Fig. 1c), and DNA origami with complex curvatures, such as an ellipsoid, a sphere, and a nanoflask.

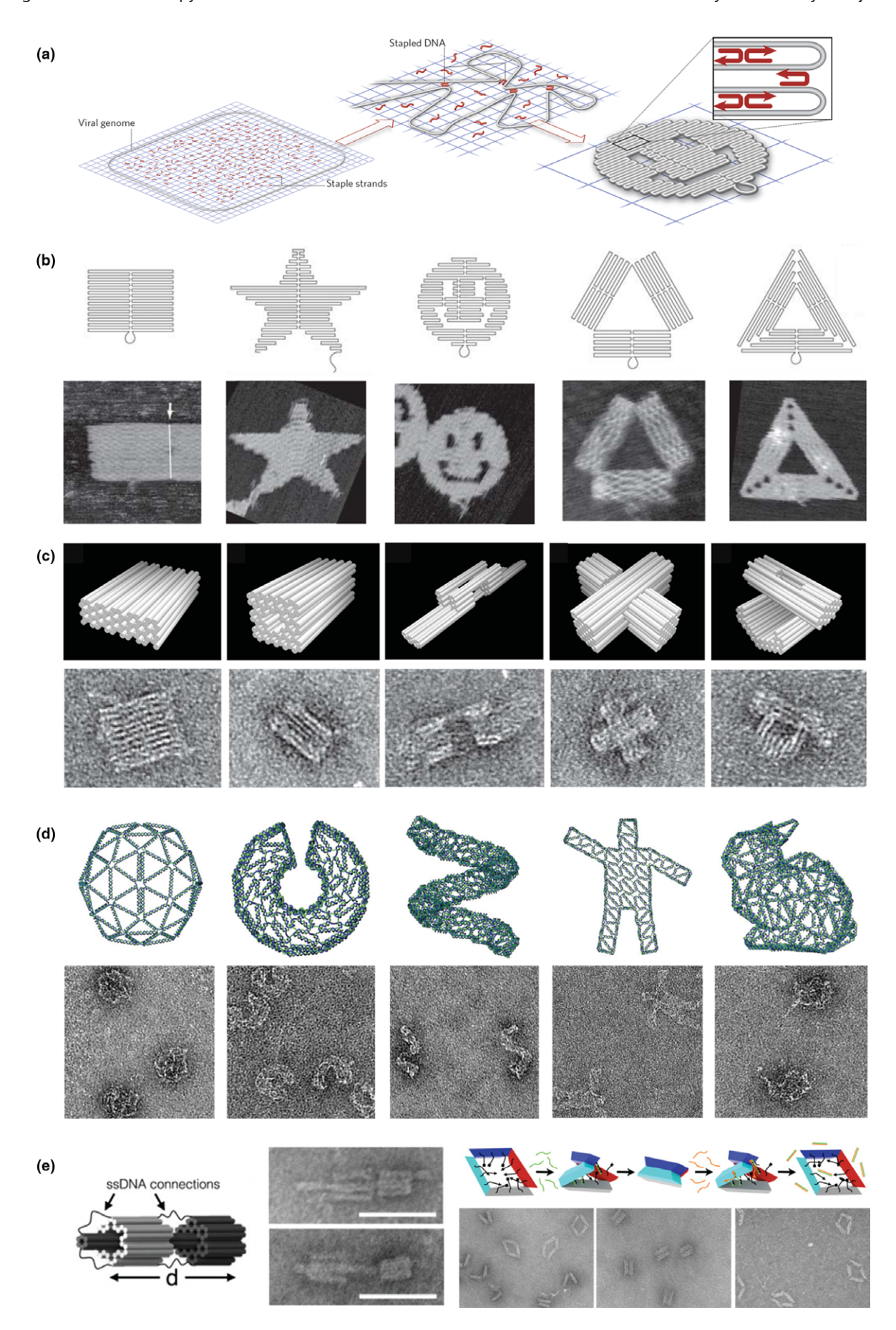


**Fig. 1.** DNA origami technique and nanostructures. (a) Principles of DNA origami technique. Hundreds of staples (red) fix the scaffold (gray) to create a desired shape. Reproduced from Sandersen (2010), with permission from [Nature Publishing Group].<sup>(17)</sup> (b) First examples of DNA origami nanostructures from Rothemund. Top panels are the designed shapes and bottom panels are atomic force microscope (AFM) images. Reproduced from Rothemund (2006), with permission from [Nature Publishing Group].<sup>(16)</sup> (c) Multilayered DNA origami nanostructures. Top panels, designed shapes; bottom panels, AFM images. Reproduced from Douglas *et al.* (2009), with permission from [Nature Publishing Group].<sup>(18)</sup> (d) Wireframe DNA origami nanostructures. Top panels, designed shapes; bottom panels, AFM images. Reproduced from Benson *et al.* (2015), with permission from [Nature Publishing Group].<sup>(19)</sup> (e) Movable DNA origami nanostructures. Reproduced from Marras *et al.* (2015), with permission from [US National Academy of Sciences].<sup>(20)</sup>

Recently, mesh-like, wireframe DNA origami structures have been developed and are reported to be more stable in low magnesium concentrations (Fig. 1d). (19) Moreover, the development of dynamic DNA origami, such as a nanobox, (25) a logic gated nanorobot, (6) a nanocapsule, (26) a movable slider, and an actuator (Fig. 1e), (20) have significantly advanced the scaffold DNA origami technique and hold great promise for highly complex DNA nanostructures.

Design software. Computer programs that could be used to assist researchers in visualizing designed DNA nanostructures in 3D perspectives, such as GIDEON<sup>(27)</sup> and Nanoengineer-1, (28) have been developed. However, they were not specifically designed for the scaffolded DNA origami technique. According to Rothemund's technique, this origami design process is much easier than the conventional process because the sequences of all DNA strands are already defined by that of the scaffold. However, there are certain steps that computer software could assist to complete complex configurations with less time and less human error. As a result, several computer programs have been developed to facilitate the origami design process and assure correct sequence identification and staple strand alignment.

In 2008, Andersen and colleagues demonstrated a software package for designing DNA origami nanostructures, which they used for the construction of a dolphin with a flexible tail. (22) After shape and folding path determination, the software fills in sequences of the M13mp18 DNA into a scaffold path, creates crossover patterns of staple strands, and then generates sequences of all staple strands. However, this program is semi-automated as the process of connecting the staple strands needs to be performed manually. The most popular software developed for DNA origami design called "caD-NAno" was launched in 2009. (29) It can be utilized for designing multilayer 3D DNA origami nanostructures where DNA helices can be aligned in two different patterns, a honeycomb lattice and a square lattice. This program also provides a list of scaffolds in different lengths besides M13mp18 that could be selected for origami constructions and then generates a set of staple strands including sequences ready to be synthesized. The simulation software developed for computing 3D DNA origami nanostructures designed by caDNAno is called "Cando." (30) It provides computational analysis for DNA nanostructures such as internal constraints. The latest origami design software, called DNA Origami Sequence Design Algorithm for User-defined Structures or "DAEDALUS," was released in 2016. (31) It can be used for designing arbitrary DNA nanostructures by top-down strategies. The research team claimed that this is a fully automated program that does not require any feedback from users. They also showed that 45 different DNA architectures can be designed and constructed using this program. Collectively, these automated programs effectively facilitate the DNA origami design process, allowing each step to be easier, faster, and more accurate.

**Functionalization.** In addition to self-assembly properties, DNA origami nanostructures also provide chemical sites for functionalization by a wide range of biomolecules and thus

represent a promising candidate to generate multifunctional nanomaterials. Addition of DNA aptamers onto DNA origami can be easily achieved as aptamer sequences can be extended from selected staple strands at predefined positions. With aptamer modification, conformational changes of DNA origami in response to target molecules could be achieved. (6) Moreover, aptamer-modified DNA origami nanostructures could be used as a malaria diagnostic tool (Fig. 2a).

DNA origami nanostructures can also be modified by hydrophobic moieties in order to interact with cell membranes. For instance, cholesterol motifs have been attached onto tube-like and monolith DNA origami nanostructures, which enable these DNA nanostructures to fuse with lipid bilayers, as shown in Figure 2(b). In addition, DNA origami nanostructures that are modified by protein moieties have been used in the regulation of many cellular processes. For example, an attachment of transforming growth factor- $\beta$  onto a rectangular DNA origami has led to protein translocation into the nucleus. As shown in Figure 2(c), transferrin proteins attached onto DNA origami nanostructures have been confirmed to enhance cellular internalization of these DNA nanostructures into KB cells.  $^{(12)}$ 

Organic fluorescent moieties, such as Cy3 and Cy5, have also been used to label DNA origami nanostructures by covalently conjugating to staple strands, and can be used in many applications, including cellular uptake experiments. (33-35) Several studies have also used quantum dot (QD)-conjugated DNA origami in bio-imaging and biodistribution studies in animal models. (13–15) Metal nanoparticles have also been incorporated into DNA origami, including AgNPs and AuNPs. With ssDNA-functionalized metal nanoparticles, the immobilization of both AgNP and AuNP onto a triangular DNA origami nanostructure at predefined positions has been demonstrated (Fig. 2d). (32) Interestingly, certain modifications result in stimuli-responsive DNA origami. For example, azo-benzene modification allows DNA origami structures to undergo conformational change following light activation (Fig. 2e). (26,36) Kohman and colleagues also utilized UV light to trigger the release of proteins that were encapsulated inside a DNA origami nanocage. (37)

As promising nanomaterials, many applications have been proposed for DNA origami nanostructures, such as platforms for single-molecule studies, (38) nano-assembly lines, (39) enzymatic studies, (40) and organization of amyloid fibrils. (41) In addition, the DNA origami technique also represents a promising strategy to generate DNA nanostructures for drug carriers and biosensors.

#### **DNA Origami as Drug Delivery Vehicles**

In 2006, Erben and coworkers demonstrated that they could encapsulate a single protein, cytochrome c, in a central cavity of a DNA tetrahedron. This work has inspired the idea of using DNA nanostructures as a nanocarrier in a drug delivery system. Several lines of evidence proved that DNA nanostructures possess abilities to enhance efficacies of chemotherapy,

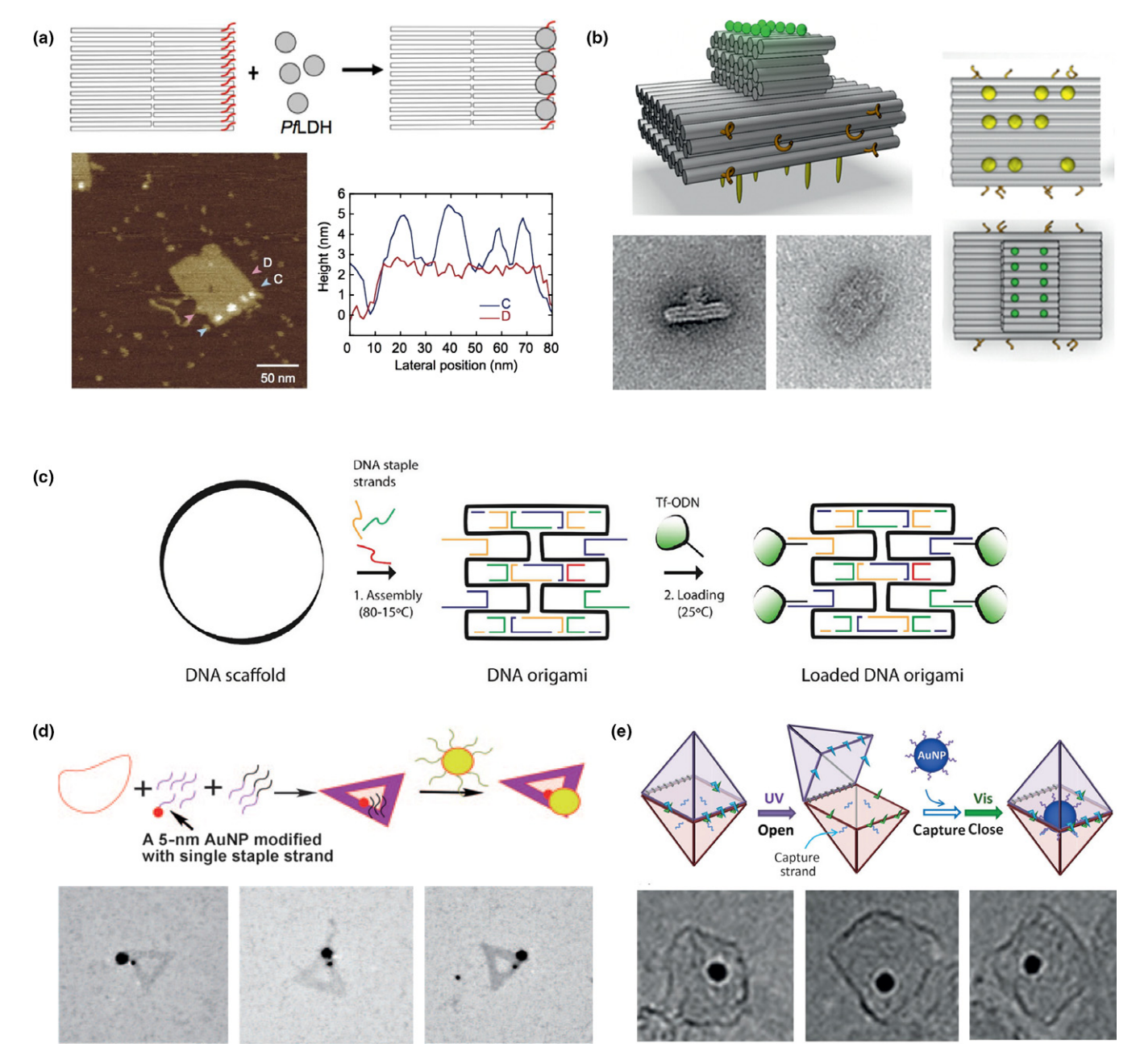


Fig. 2. Functionalized DNA origami nanostructures. (a) Anti-PfLDH aptamer-modified DNA origami rectangles as a diagnostic tool for malaria. Reproduced from Godonoga et al. (2012), with permission from [Nature Publishing Group]. (b) DNA origami monoliths modified with cholesterols (yellow) and fluorescent molecules (green). Reproduced from Czogalla et al., with permission from [John Wiley and Sons]. (c) Transferrinmodified DNA origami rectangles for enhanced cellular internalization. Reproduced from Schaffert et al. (2016), with permission from [John Wiley and Sons]. (d) Silver nanoparticles (AgNP) (yellow) and gold nanoparticles (AuNP) (red) precisely organized onto DNA origami ranocapsules which their conformational changes could be controlled by light. Reproduced from Takenaka et al. (2014), with permission from [John Wiley and Sons]. (26)

reduce adverse side-effects, and even circumvent drug resistance. Several studies have reported that DNA origami nanostructures of various sizes and shapes showed no significant cytotoxicity either *in vitro* or *in vivo*. (35,43–45) For use in a biological system, DNA origami nanostructures have to meet certain requirements.

**Stability.** The stability of DNA nanostructures in a physiological environment is an essential criterion. It has been shown that DNA nanostructures have higher stability than ssDNA and normal DNA duplexes in nuclease-containing conditions. (46)

This stability might be the case that unusual shapes and structures of the DNA nanostructures possess physical complexities and hinder the accessibility and functioning of nucleases. Different shapes of DNA origami nanostructures have been shown to remain intact in cell lysates at room temperature for 12 h. (46) Consistently, other reports showed that DNA nanotubes, (43,47) DNA triangles, (15) and rod-like DNA nanostructures (48) were stable under various biological conditions. In contrast, Hahn and co-workers found that the stability of different DNA nanostructures in very low Mg<sup>2+</sup> concentrations or

in the presence of nuclease might be dependent on structural design and incubation time length. (44) Later, Halley and colleagues also confirmed that structural design might be another key factor to the stability of DNA nanostructures in biological environments. (48) However, some DNA origami nanostructures have been utilized in *in vivo* experiments and the results have confirmed their adequate stability. By i.v. injection into mice, DNA origami could be transported to tumor sites through the bloodstream. (15, 49–51) DNA origami nanostructures have also been investigated inside living insects, *Blaberus discoidalis*, by hemocoel injection and the results showed that these DNA nanorobots could properly function inside living systems. (52,53)

To use as drug delivery vehicles, DNA origami nanostructures must be designed to have optimal stability in cellular conditions. Perrault and Shih showed that, after i.v. injection into mice, a lipid bilayer-encapsulated nanostructure remained in blood circulation significantly longer than the free form (Fig. 3a). Additionally, spermidine-stabilized DNA origami nanostructures have been recently reported to be more stable in cell lysates than plain structures. Therefore, it has been shown that extensive investigations into structural design and modifications have significantly improved the stability of DNA nanostructures and strengthened their potential for use in biological settings.

**Drug loading and release.** Drug loading and releasing capabilities of DNA origami nanostructures can vary between different shapes and, thus, can play an important role in structural design for nanocarriers. Unmethylated cytosine-phosphate-guanine

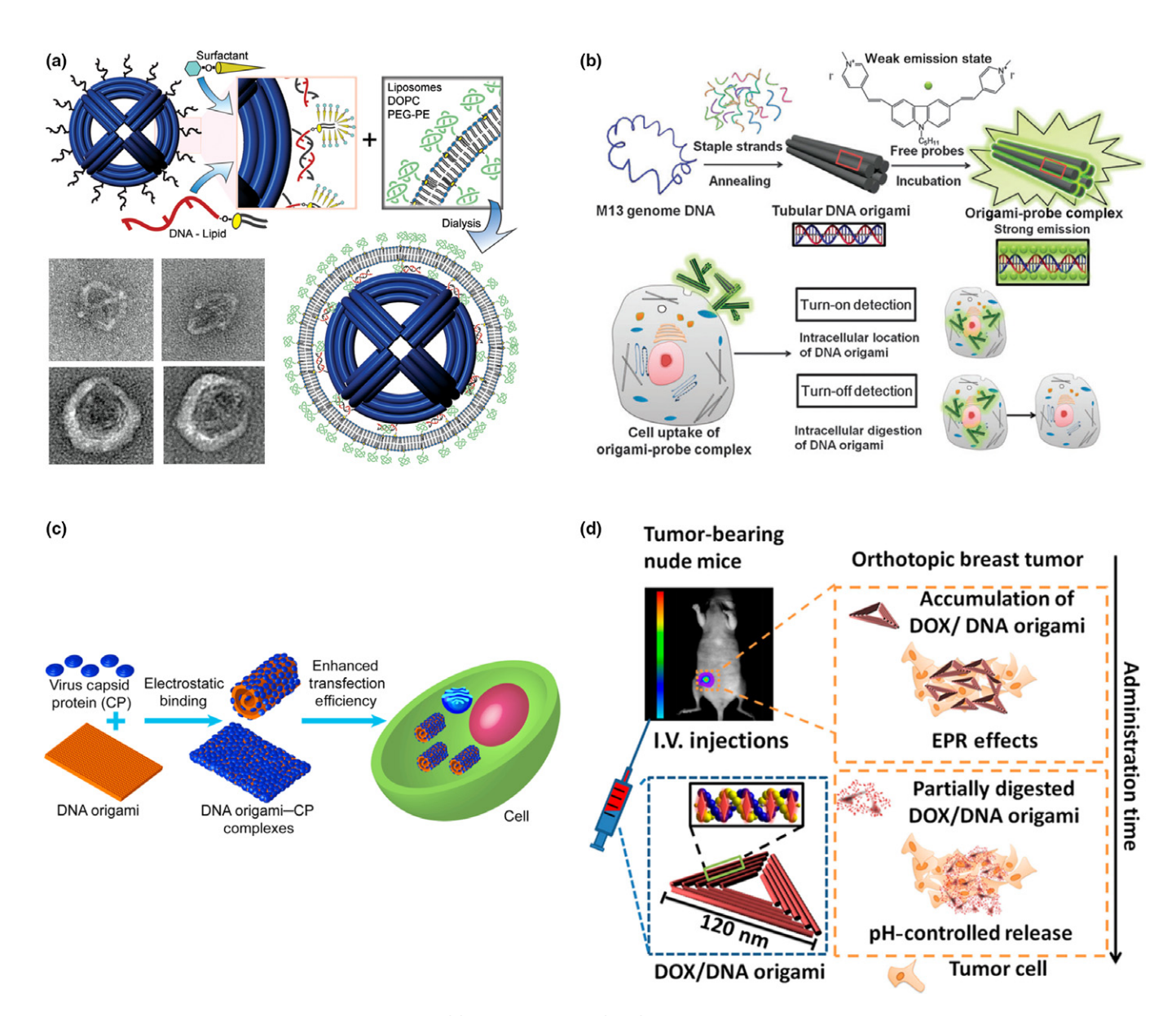


Fig. 3. DNA origami nanostructures as drug carriers. (a) DNA octahedron (blue) encapsulated inside lipid bilayer. Top panels, transmission electron microscopy images of free octahedrons; bottom panels, transmission electron microscopy images of lipid encapsulated octahedrons. Reproduced from Perrault and Shih (2014), with permission from [American Chemical Society]. (49) DOPC, 1,2-dioleoyl-sn-glycero-3- phosphocholine; PEG-PE, polyethylene glycol- phosphatidylethanolamine. (b) Fluorescently labeled DNA origami tubes for cellular tracking. Reproduced from Shen *et al.* (2012), with permission from [American Chemical Society]. (47) (c) Virus capsid protein (CP; blue) covered DNA origami rectangles (orange). Reproduced from Mikkila *et al.* (2014), with permission from [Royal Society of Chemistry]. (d) Doxorubicin (DOX)-containing DNA origami triangles showing enhanced permeability and retention (EPR) effects. Reproduced from Zhang *et al.* (2014), with permission from [American Chemical Society]. (15)

(CpG) sequences, which can trigger immune response, have been used as a model cargo and loaded onto DNA nanocarriers by covalent attachment. (34,55) Encapsulation of a Fab fragment, (6) AuNPs, (6) and active enzymes (56,57) inside a cavity of DNA origami nanostructures have been reported. Data showed that these DNA nanostructures allowed the cargo and enzymes to be more stable, more catalytically active, and more resistant to protease digestion. In addition to internal loading, gold nanorods (AuNRs) were functionalized onto a surface of DNA origami nanostructures and were i.v. injected into mice for photothermal therapy applications. (13,50)

Several DNA origami nanostructures have been used for doxorubicin delivery experiments such as a triangle, (15,45) a tube, (43) and ribbon. Previous reports showed that more drugs could be loaded into 3D DNA origami but released faster from 2D structures. Additionally, Zhao and co-workers reported that DNA nanostructures can be designed to vary in their encapsulation abilities and release rate depending on the amounts of relaxation in the DNA double-helix structures. In addition, other intercalating agents have also been tested with DNA origami, for instance, daunorubicin at 3, 6-bis[2-(1-methylpyridinium) ethynyl]-9-pentyl-carbazole diiodide (BMEPC). (59)

Cellular internalization. Larger size and stronger compactness of DNA origami nanostructures have been shown to allow more efficient internalization than less compact structures or individual ssDNA. Ouyang and colleagues constructed DNA nanoribbons in various sizes and found that the DNA nanostructures with high length-to-width ratio were preferentially internalized by cells. Shen and co-workers used carbazole-based cyanine, which shows a strong fluorescent signal when binding to DNA helices, to visualize DNA nanotubes after internalization into MCF-7 cells (Fig. 3b). Confocal microscopy studies showed that the intact DNA nanotubes were internalized into cells and aggregated in lysosomes. In addition, Chopra and colleagues reported that spermidine-modified DNA nanostructures can be delivered into cells through electroporation.

To improve cellular uptake efficiency, DNA nanostructures have been modified with targeting ligands such as folate, (33) cell-penetrating proteins, (58) and transferrin. (12) It has been shown that after functionalization with viral capsid proteins, the cellular internalization of DNA origami nanostructures was enhanced (Fig. 3c). (35) Recent data for DNA nanoribbons proved that, by using inhibitors of specific internalization pathways, the structures were internalized into the cytoplasm of H460 cells by clathrin- and lipid raft-mediated endocytosis. (60) Moreover, these nanoribbons exhibited endosomal escape abilities after 2 h of incubation.

DNA origami nanostructures also showed enhanced permeability and retention (EPR) effects. Passive accumulation of DNA origami in three different shapes, triangle, rectangle, and tube, have been investigated using QD labelling after i.v. injection into tumor-bearing mice (Fig. 3d). The triangles were shown to accumulate at the tumor site at higher levels than the tubular nanostructures 24 h after injection. Consistent with previous results, AuNR-modified triangles exhibited better internalization into MCF-7 cells than AuNR-modified tubes. These consistent results seem to confirm that the cellular uptake effects are dependent on the size and shape of the nanostructures. However, it remains inconclusive which structural design of DNA origami nanostructures is most preferable for cellular internalization.

Therapeutic efficacy. Nanocarrier properties such as optimal stability, low cytotoxicity, high loading, and releasing capability collectively lead to high efficacy in cancer therapy. Several

studies showed that DNA origami nanostructures enhanced anticancer activities and circumvented drug resistance. Jiang and colleagues reported that triangular and tubular DNA origami nanostructures with doxorubicin resulted in increased apoptosis of doxorubicin-resistant breast cancer cells, (45) dependent on the length of incubation time and drug concentration (Fig. 4a). Interestingly, when loaded in a DNA origami structure, doxorubicin was retained inside DNA nanostructures and gradually diffused out, causing slower cellular elimination rates, whereas free drugs have faster cellular elimination rates. (43) This property resulted in higher numbers of apoptotic cells in the drug–DNA nanotube-treated group compared to the free drug-treated group.

DNA nanocarriers have been reported to reduce the side-effects of chemotherapeutic drugs. Zhang and co-workers showed that doxorubicin-containing DNA triangles effectively decreased tumor size while mice showed no weight loss when compared to those in the free drug group, indicating that doxorubicin-loaded DNA nanocarriers were less toxic. (15) More results showed that DNA nanostructures can enhance therapeutic efficiency. After loaded with doxorubicin, DNA nanoribbons functionalized onto AuNPs exhibited higher antitumor efficiency compared to free doxorubicin. (58) These data indicate that DNA nanoparticles can be internalized by cancer cells and prolong the effects of therapeutic drugs and significantly enhance drug efficacy with fewer side-effects.

Photodynamic therapy. Photodynamic therapy (PDT) is a cancer treatment that uses photosensitizers along with light to kill cancer cells. A number of photosensitizers for PDT exist, including porphyrins, aminolevulinic acid, and silicon phthalocyanine Pc 4. However, some agents suffer from limitations such as weak absorption, rapid clearance, and poor solubility, which consequently result in inadequate therapeutic efficacy. (61) DNA origami nanostructures have also been used as nanocarriers of photosensitizer agents for applications in PDT. For instance, AuNRs have been used as a photosensitizer functionalized onto DNA origami. (50,51) After attachment of AuNRs, these AuNR-modified nanosystems were injected into nude mice and examined for both cellular imaging and photothermal therapy purposes (Fig. 4b). The results indicated that DNA nanocarriers successfully delivered AuNRs into the tumor region and caused tumor-specific damage following near-infrared irradiation laser treatment. Tumor cell viability was significantly lower in mice treated with AuNR-modified DNA nanocarriers compared to those treated with free AuNRs. In addition to AuNRs, the biomedical efficiency of BMEPCloaded DNA triangles as cellular imaging and PDT has been reported. (59) These examples indicate that DNA nanoparticles can also be used in combination with other cancer therapeutic systems and effectively reduce adverse side-effects due to increased specificity and unique carrier properties.

**Detection.** In addition to drug delivery, nanoparticles can be used in cellular and molecular imaging for cancer detection. (62) The development of targeted cancer therapy, as well as the advances of nanomaterials suitable for biomedical sciences, gives rise to the need for powerful imaging tools to probe molecular and microenvironmental changes that are associated with cancer progression. By chemical modification with fluorescent molecules, DNA anostructures could be used as imaging agents for cellular detection. Fluorescent probes such as cyanine dye molecules can be covalently incorporated into the strands of DNA origami and used as a means of direct visualization in live cells. (47,59) DNA origami nanostructures were successfully conjugated with infrared-emitting QDs and

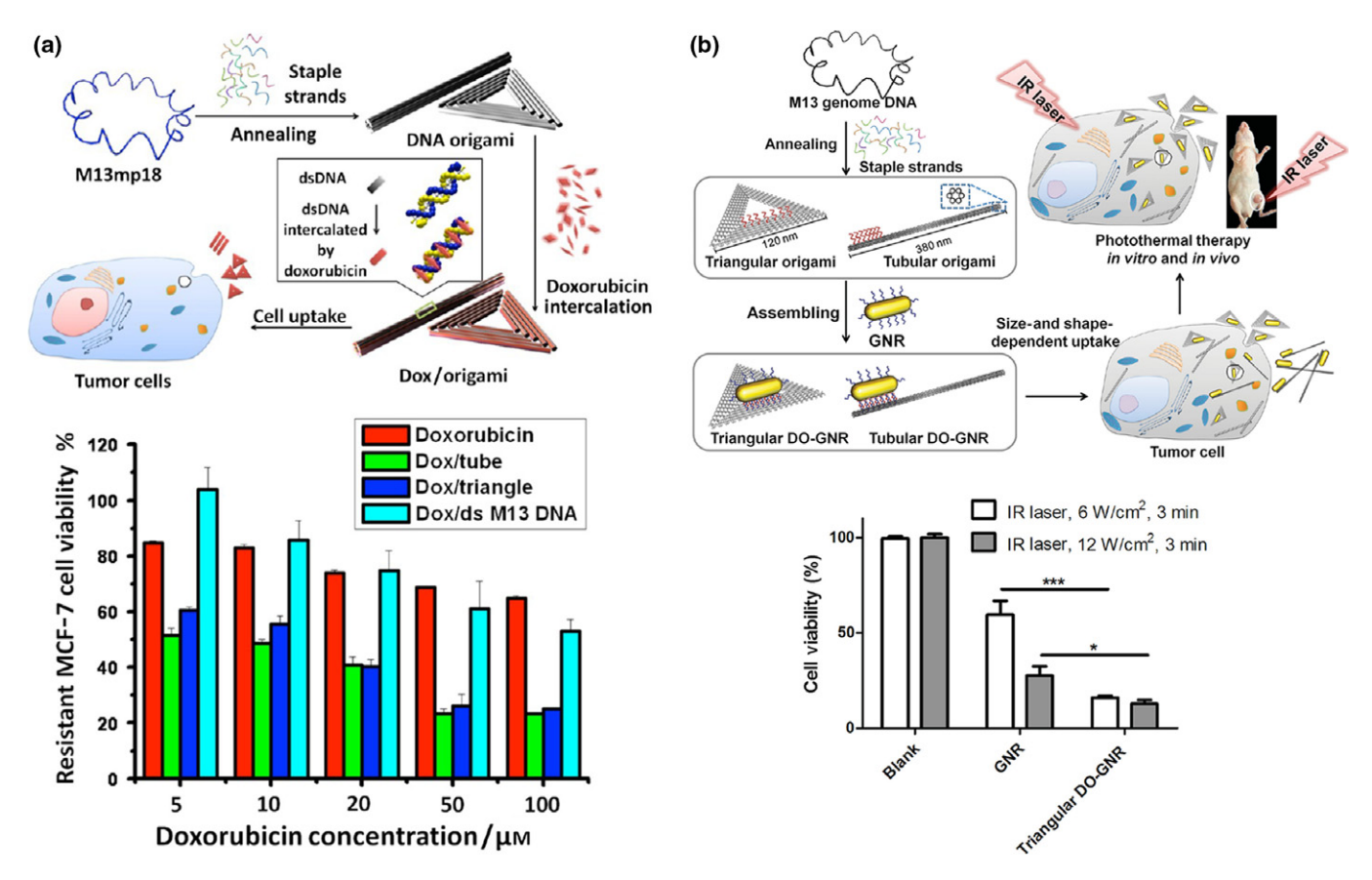


Fig. 4. Additional applications of DNA origami nanocarriers. (a) Doxorubicin (Dox)-loaded DNA origami tubes and triangles exhibited drug resistance circumvention when treated with resistant MCF-7 cells. Reproduced from Jiang (2012), with permission from [American Chemical Society]. (45) (b) Gold nanorod (AuNR)-functionalized DNA origami tubes and triangles used in photothermal dynamic therapy showed lower percentage cell viability of tumor cells in mice. Reproduced from Jiang et al. (2015), with permission from [John Wiley and Sons]. (50) DO-GNR, DNA origami-gold nanorod; dsDNA, double-stranded DNA; GNR, gold nanorod; IR, infrared.

remained stable at high salt concentrations. (14) Moreover, rectangular DNA origami nanostructures have been developed as microRNA analysis tools used for heart failure diagnosis. (63)

#### **Summary and Perspectives**

Over 35 years, tremendous progress in structural DNA nanotechnology has been made, and a wide range of medical applications are now obvious to researchers and clinicians. In addition to DNA origami, other DNA nanostructures have been investigated as nanocarriers for drug delivery systems. For example, DNA hydrogels have been used to deliver drug molecules like camptothecin and insulin, (64) doxorubicin, (65) CpG motifs, (66) and siRNA, (67) which could be loaded inside the porous cavity. Nanopores constructed by a DNA origami technique could be used to regulate the entry of therapeutic drugs into cancer cells. (8,68,69)

The DNA origami technique also plays a key role in accelerating the advances in this research field. Although many challenging tasks have been overcome, it is still too early for DNA origami to be used as a drug carrier system in clinical trials. The stability of these macromolecules in physiological conditions is one of the most essential criteria to be considered. Previous results revealed that DNA nanocarriers can survive long enough to reach the target site and complete their functions. Also, DNA is a biomolecule found in living organisms that should not exhibit any cytotoxic effects; however, pharmacokinetic and

pharmacodynamic studies of these DNA nanostructures in living animals need to be explored further. Long-term cytotoxicity of DNA nanocarrier use is also essential for future clinical trials. In addition, various therapeutic molecules have been tested as cargo for drug loading and releasing capacities of DNA nanocarriers. Some results showed that loading and releasing capabilities could be tuned by structural design. Even though these DNA origami nanostructures show drug resistance circumvention, the internalization pathway of the DNA nanocarriers should be thoroughly investigated. The ultimate goal of targeted drug delivery is to deliver a drug to a specific site in the body, which results in the requirement of small doses and, therefore, minimal sideeffects to normal tissues. In vivo targeted delivery by DNA origami nanostructures using the EPR effect as a passive targeting method has been largely proved, but an active targeting method by targeting ligand modification onto origami nanostructures still remains elusive. To increase the therapeutic efficiency, selectivity, and specificity of the nanocarriers are key parameters that should be carefully designed and further examined.

#### Acknowledgments

This work was supported by Mahidol University (T.K.) and Burapha University (A.U.).

#### **Disclosure Statement**

The authors have no conflict of interest.

#### References

- 1 Zamboni WC. Liposomal, nanoparticle, and conjugated formulations of anticancer agents. Clin Cancer Res 2005; 11: 8230–4.
- 2 Makadia HK, Siegel SJ. Poly lactic-co-glycolic acid (PLGA) as biodegradable controlled drug delivery carrier. *Polymers (Basel)* 2011; 3: 1377–97.
- 3 Jiang W, Kim BYS, Rutka JT, Chan WCW. Nanoparticle-mediated cellular response is size-dependent. *Nat Nanotechnol* 2008; 3: 145–50.
- 4 Chomoucka J, Drbohlavova J, Huska D, Adam V, Kizek R, Hubalek J. Magnetic nanoparticles and targeted drug delivering. *Pharmacol Res* 2010; 62: 144–9.
- 5 Seeman NC. Nucleic acid junctions and lattices. J Theor Biol 1982; 99: 237–47.
- 6 Douglas SM, Bachelet I, Church GM. A logic-gated nanorobot for targeted transport of molecular payloads. *Science* 2012; 335: 831–4.
- 7 Godonoga M, Lin TY, Oshima A et al. A DNA aptamer recognising a malaria protein biomarker can function as part of a DNA origami assembly. Sci Rep 2016; 6: 21266.
- 8 Langecker M, Arnaut V, Martin TG et al. Synthetic lipid membrane channels formed by designed DNA nanostructures. Science 2012; 338: 932-6.
- 9 Czogalla A, Kauert DJ, Franquelim HG et al. Amphipathic DNA origami nanoparticles to scaffold and deform lipid membrane vesicles. Angew Chem Int Ed Engl 2015; 54: 6501–5.
- 10 Pederson RO, Loboa EG, LaBean TH. Sensitization of transforming growth factor-β signaling by multiple peptides patterned on DNA nanostructures. *Biomacromol* 2013; 14: 4157–60.
- 11 Angelin A, Weigel S, Garrecht R et al. Multiscale origami structures as interface for cells. Angew Chem Int Ed 2015; 54: 15813–7.
- 12 Schaffert DH, Okholm AH, Sorensen RS et al. Intracellular delivery of a planar DNA origami structure by the transferrin-receptor internalization pathway. Small 2016; 12: 2634–40.
- 13 Du K, Ko SH, Gallatin GM, Yoon HP, Liddle JA, Berglund AJ. Quantum dot-DNA origami binding: a single particle, 3D, real-time tracking study. *Chem Commun* 2013; 49: 907–9.
- 14 Samanta A, Deng Z, Liu Y. Infrared emitting quantum dots: DNA conjugation and DNA origami directed self-assembly. *Nanoscale* 2014; 6: 4486–90.
- 15 Zhang Q, Jiang Q, Li N et al. DNA origami as an in vivo drug delivery vehicle for cancer therapy. ACS Nano 2014; 8: 6633–43.
- 16 Rothemund PWK. Folding DNA to create nanoscale shapes and patterns. Nature 2006; 440: 297–302.
- 17 Sandersen K. Bioengineering: What to make with DNA origami. *Nature* 2010; **464**: 158–9.
- 2010; **464**: 138–9.

  18 Douglas SM, Dietz H, Liedl T, Hogberg B, Graf F, Shih WM. Self-assembly of DNA into nanoscale three-dimensional shapes. *Nature* 2009;
- 459: 414–8.
  19 Benson E, Mohammed A, Gardell J et al. DNA rendering of polyhedral meshes at the nanoscale. *Nature* 2015; 523: 441–4.
- 20 Marras AE, Zhou L, Su HJ, Castro CE. Programmable motion of DNA origami mechanisms. PNAS 2015; 112: 713–8.
- 21 Douglas SM, Chou JJ, Shih WM. DNA-nanotube-induced alignment of membrane proteins for NMR structure determination. *PNAS* 2007; 104:
- 22 Andersen ES, Dong M, Nielsen MM et al. DNA origami design of dolphin-shaped structures with flexible tails. ACS Nano 2008; 2: 1213–8.
- 23 Ke Y, Sharma J, Liu M, Jahn K, Liu Y, Yan H. Scaffolded DNA origami of a DNA tetrahedron molecular container. *Nano Lett* 2009; 9: 2445–7.
- 24 Han D, Pal S, Nangreave J, Deng Z, Liu Y, Yan H. DNA origami with complex curvatures in three-dimensional space. Science 2011; 332: 342–6.
- 25 Andersen ES, Dong M, Nielsen MM et al. Self-assembly of a nanoscale DNA box with a controllable lid. Nature 2009; 459: 73–6.
- 26 Takenaka T, Endo M, Suzuki Y et al. Photoresponsive DNA nanocapsule having an open/close system for capture and release of nanomaterials. Chemistry 2014; 20: 14951–4.
- 27 Birac JJ, Sherman WB, Kopatsch J, Constantinou PE, Seeman NC. Architecture with GIDEON, a program for design in structural DNA nanotechnology. J Mol Graph Model 2006; 25: 470–80.
- 28 Nanorex Inc. NanoEngineer-1. 2006. Available from: http://www.nanoengineer-1.com/content/.
- 29 Douglas SM, Marblestone AH, Teerapittayanon S, Vazquez A, Church GM, Shih WM. Rapid prototyping of 3D DNA-origami shapes with caDNAno. *Nucleic Acids Res* 2009; 37: 5001–6.
- 30 Castro CE, Kilchherr F, Kim DN et al. A primer to scaffolded DNA origami. Nat Methods 2011; 8: 221–9.
- 31 Veneziano R, Ratanalert S, Zhang K et al. Designer nanoscale DNA assemblies programmed from the top down. Science 2016; 352: 1534.
- 32 Pal S, Deng Z, Ding B, Yan H, Liu Y. DNA-origami-directed self-assembly of discrete silver-nanoparticle architectures. Angew Chem Int Ed 2010; 49: 2700–4.

- 33 Ko SH, Liu H, Chen Y, Mao C. DNA nanotubes as combinatorial vehicles for cellular delivery. *Biomacromol* 2008; 9: 3039–43.
- 34 Schuller VJ, Heidegger S, Sandholzer N et al. Cellular immunostimulation by CpG-sequence-coated DNA origami structures. ACS Nano 2011; 5: 9696–702.
- 35 Mikkila J, Eskelinen AP, Niemela EH et al. Virus-encapsulated DNA origami nanostructures for cellular delivery. Nano Lett 2014; 14: 2196–200.
- 36 Kohman RE, Han X. Light sensitization of DNA nanostructures via incorporation of photo-cleavable spacers. *Chem Commun* 2015; **51**: 5747–50.
- 37 Kohman RE, Cha SS, Man HY, Han X. Light-triggered release of bioactive molecules from DNA nanostructures. *Nano Lett* 2016; 16: 2781–5.
- 38 Voigt NV, Torring T, Rotaru A *et al.* Single-molecule chemical reactions on DNA origami. *Nat Nanotechnol* 2010; 5: 200–3.
- 39 Gu H, Chao J, Xiao SJ, Seeman NC. A proximity-based programmable DNA nanoscale assembly line. *Nature* 2010; 465: 202–5.
- 40 Fu J, Liu M, Liu Y, Woodbury NW, Yan H. Interenzyme substrate diffusion for an enzyme cascade organized on spatially addressable DNA nanostructures. J Am Chem Soc 2012; 134: 5516–9.
- 41 Udomprasert A, Bongiovanni MN, Sha R et al. Amyloid fibrils nucleated and organized by DNA origami constructions. Nat Nanotechnol 2014; 9: 537-41
- 42 Erben CM, Goodman RP, Turberfield AJ. Single-molecule protein encapsulation in a rigid DNA cage. Angew Chem 2006; 118: 7574–7.
- 43 Zhao YX, Shaw A, Zeng X, Benson E, Nystrom AM, Hogberg B. DNA origami delivery system for cancer therapy with tunable release properties. ACS Nano 2012; 6: 8684–91.
- 44 Hahn J, Wickham SFJ, Shih WM, Perrault SD. Addressing the instability of DNA nanostructures in tissue culture. ACS Nano 2014; 8: 8765–75.
- 45 Jiang Q, Song C, Nangreave J et al. DNA origami as a carrier for circumvention of drug resistance. J Am Chem Soc 2012; 134: 13396–403.
- 46 Mei Q, Wei X, Su F et al. Stability of DNA origami nanoarrays in cell lysate. Nano Lett 2011; 11: 1477–82.
- 47 Shen X, Jiang Q, Wang J *et al.* Visualization of the intracellular location and stability of DNA origami with a label-free fluorescent probe. *Chem Commun* 2012; **48**: 11301–3.
- 48 Halley PD, Lucas CR, McWilliams EM *et al.* Daunorubicin-loaded DNA origami nanostructures circumvent drug-resistance mechanisms in a leukemia model. *Small* 2016; **12**: 308–20.
- 49 Perrault SD, Shih WM. Virus-inspired membrane encapsulation of DNA nanostructures to achieve in vivo stability. ACS Nano 2014; 8: 5132–40.
- 50 Jiang Q, Shi Y, Zhang Q et al. A self-assembled DNA origami-gold nanorod complex for cancer theranostics. Small 2015; 11: 5134–41.
- 51 Du Y, Jiang Q, Beziere N et al. DNA-nanostructure-gold-nanorod hybrids for enhanced in vivo optoacoustic imaging and photothermal therapy. Adv Mater 2016; 28: 10000–7.
- 52 Amir Y, Ben-Ishay E, Levner D, Ittah S, Abu-Horowitz A, Bachelet I. Universal computing by DNA origami robots in a living animal. *Nat Nan-otechnol* 2014; 9: 353–7.
- 53 Arnon S, Dahan N, Koren A et al. Thought-controlled nanoscale robots in a living host. PLoS ONE 2016; 11: e0161227.
- 54 Chopra A, Krishnan S, Simmel FC. Electrotransfection of polyamine folded DNA origami structures. *Nano Lett* 2016; 16: 6683–90.
- 55 Ouyang X, Li J, Liu H et al. Rolling circle amplification-based DNA origami nanostructures for intracellular delivery of immunostimulatory drugs. Small 2013; 9: 3082–7.
- 56 Ora A, Jarvihaavisto E, Zhang H et al. Cellular delivery of enzyme-loaded DNA origami. Chem Commun 2016; 52: 14161–4.
- 57 Zhao Z, Fu J, Dhakal S et al. Nanocaged enzymes with enhanced catalytic activity and increased stability against protease digestion. Nat Commun 2016; 7: 10619.
- 58 Yan J, Hu C, Wang P *et al.* Growth and origami folding of DNA on nanoparticles for high efficiency molecular transport in cellular imaging and drug delivery. *Angew Chem Int Ed* 2015; **54**: 2431–5.
- 59 Zhuang X, Ma X, Xue X et al. A photosensitizer-loaded DNA origami nanosystem for photodynamic therapy. ACS Nano 2016; 10: 3486–95.
- 60 Chen G, Liu D, He C, Gannett TR, Lin W, Weizmann Y. Enzymatic synthesis of periodic DNA nanoribbons for intracellular pH sensing and gene silencing. J Am Chem Soc 2015; 137: 3844–51.
- 61 Oleinick NL, Morris RL, Belichenko I. The role of apoptosis in response to photodynamic therapy: what, where, why, and how. *Photochem Photobiol* Sci 2002; 1: 1–21.
- 62 Li C. A targeted approach to cancer imaging and therapy. *Nat Mater* 2014; 13: 110–5.
- 63 Wang D, Fu Y, Yan J et al. Molecular logic gates on DNA origami nanostructures for microRNA diagnostics. Anal Chem 2014; 86: 1932–6.
- 64 Um SH, Lee JB, Park N, Kwon SY, Umbach CC, Luo D. Enzyme-catalysed assembly of DNA hydrogel. *Nat Mater* 2006; 5: 797–801.
- 65 Roh YH, Lee JB, Tan SJ et al. Photocrosslinked DNA nanospheres for drug delivery. Macromol Rapid Commun 2010; 31: 1207–11.

- 66 Nishikawa M, Mizuno Y, Mohri K et al. Biodegradable CpG DNA hydrogels for sustained delivery of doxorubicin and immunostimulatory signals in tumor-bearing mice. Biomaterials 2011; 32: 488–94.
- tumor-bearing mice. *Biomaterials* 2011; **32**: 488–94.

  67 Roh YH, Lee JB, Kiatwuthinon P *et al.* DNAsomes: Multifunctional DNA-based nanocarriers. *Small* 2011; **7**: 74–8.
- 68 Bell NAW, Engst CR, Ablay M et al. DNA origami nanopores. Nano Lett 2012; 12: 512–7.
- 69 Burns JR, Al-Juffali N, Janes SM, Howorka S. Membrane-spanning DNA nanopores with cytotoxic effect. Angew Chem Int Ed 2014; 53: 12466-70